# EFRC *MATERIALS SCIENCE OF ACTINIDES* FINAL REPORT

**Materials Science of Actinides**
**Energy Frontier Research Center**
DE-SC0001089

Lead: University of Notre Dame
Director: Dr. Peter C. Burns

## EXECUTIVE SUMMARY

The Energy Frontier Research Center *Materials Science of Actinides* (MSA) conducted basic research from 2009-2019. The scientific personnel and participating institutes changed several times during the evolution of the Center, and in total included 24 senior investigators, four national laboratories, and ten universities. Workforce development was a motivating goal of the university-led Center, which included many undergraduate, graduate, and post-doctoral researchers. The center focused on the actinide elements, which arise from the sequential filling of the 5*f* electron orbitals. Although the specific themes evolved during the Center's history, the final research themes were: (1) Nanoscale Cage Clusters, (2) Complex Ceramic and Metallic Materials, and (3) Materials Under Extreme Environments. To date, the Center has produced 254 peer-reviewed journal publications and book chapters that acknowledged only the EFRC funding, and an additional 161 journal publications and book chapters that acknowledged funding from the EFRC and additional sources (a few manuscripts are still in preparation). Broad highlights include: (1) Development of an extensive family of actinide nanomaterials that self-assemble in aqueous solution, an understanding of their formation mechanisms and stabilities, and possible uses in nuclear fuel cycles; (2) Establishment of facilities and methodologies to conduct high-temperature calorimetry on transuranium materials, and extensive thermodynamic-based studies of uranium and thorium compounds important to the nuclear fuel cycle; (3) A vastly improved understanding of the behavior of actinide materials in extreme conditions, including high radiation fields, temperatures, and pressures, as well coupled effects of two or more of these; (4) Development of resonance ultrasound spectroscopy and direct measurement of aging of plutonium alloys.

## SUMMARY OF CENTER BACKGROUND, PARTICIPATION, AND MAJOR ACCOMPLISHMENTS

*Materials Science of Actinides* (MSA) was funded initially from 2009-2014 and was renewed through 2018. MSA united researchers to conduct collaborative, novel and transformative research in actinide materials science. Actinides arise from the sequential filling of the 5*f* electron orbitals, are the heaviest natural elements, and are all radioactive. They are unique in their societal importance owing to their roles in energy production, national security, nuclear weapons non-proliferation, medical isotope production, and environmental contamination. The 5*f* electrons, relativistic effects, and redox chemistry complicate the chemistry of actinides. Research in actinide materials has lagged far behind that of most other materials systems, particularly in the synthesis and characterization of new materials, measurement of thermochemical and physical properties, and the design of materials for special applications under extreme conditions, such as may be found in nuclear reactors.

Actinide materials present exceptional scientific challenges because the highly directional nature of 5*f* electron orbitals produces a complex interactive physical and chemical system that is not fully understood. Plutonium, an actinide near the center of the series, sits on the boundary between localized and itinerant electron behavior. Lighter actinides have itinerant electrons, while for heavier actinides the electrons are localized. In ionic compounds, mainly oxides, this transition from itinerant to local behavior results in more variable oxidation states for uranium-plutonium than for the later actinides. In essence, all actinides are structurally and electronically fragile, wherein small changes in pressure, temperature, and composition may have a profound effect on the structures and properties of actinide materials. This fragility (or complex energy landscape) provides an opportunity to modify and probe their underlying complexity and to tailor materials with specific properties.

***Mission:*** The mission of MSA is to conduct collaborative, multidisciplinary, novel and transformative research on actinide materials emphasizing actinide ceramic, metallic, hybrid, and nanoscale materials, effective integration of experimental and computational approaches, and solving research questions that are critical to the energy future of the nation. Workforce development is a fundamental and inherent goal of this university-based center.

Senior Investigators 2009-2014

Thomas Albrecht-Schmitt – University of Notre Dame and then Florida State University
Mark Asta – University of California, Davis
Udo Becker – University of Michigan
Peter C. Burns – University of Notre Dame
Christopher Cahill – George Washington University
William H. Casey – University of California, Davis
Rodney C. Ewing – Stanford University
Jeremy Fein – University of Notre Dame
Laura Gagliardi – University of Minnesota (added to EFRC in 2010)
David Hobbs – Savannah River National Laboratory
Neils Jensen – University of California, Davis (removed from EFRC in 2011)
Jie Lian – Rensselaer Polytechnic Institute
Edward Maginn – University of Notre Dame
Alexandra Navrotsky – University of California, Davis
May Nyman – Sandia National Laboratory and then Oregon State University
Lynda Soderholm – University of Notre Dame (adjunct) (removed from EFRC in 2011)
Tracy Rudisill – Savannah River National Laboratory
Ann Visser – Savannah River National Laboratory
William Weber – Pacific Northwest National Laboratory and then University of Tennessee

Senior Investigators 2014-2018

Mark Asta – University of California, Davis
Peter C. Burns – University of Notre Dame
Christopher Cahill – George Washington University (removed from EFRC in 2016)
William H. Casey – University of California, Davis

Rodney C. Ewing – Stanford University
Jeremy Fein – University of Notre Dame
Laura Gagliardi – University of Minnesota
Amy Hixon – University of Notre Dame
Maik Lang – University of Tennessee
Tianbo Liu – University of Akron
Edward Maginn – University of Notre Dame
Wendy Mao – Stanford University
Albert Migliori – Los Alamos National Laboratory
Alexandra Navrotsky – University of California, Davis
May Nyman – Oregon State University

Scientific Advisory Board (over the lifetime of the Center)

Lynn Boatner – Oak Ridge National Laboratory
Bruce Bursten – University of Tennessee
David Clark – Los Alamos National Laboratory
Sue Clark – Pacific Northwest National Laboratory, Washington State University
Ingmar Grenthe – Professor Emeritus, KTH, Sweden
Richard Haire – Oak Ridge National Laboratory
Joseph Hupp – Northwestern University
Iain May – Chemistry Division, Los Alamos National Lab
Lester Morss – retired from DOE
Mark Peters – Idaho National Laboratory

During 2009-2014, the EFRC had three research themes: (1) Complex Actinide Materials, (2) Nanoscale Actinide Materials, and (3) Actinide Materials Under Extreme Environments. The renewed EFRC in 2014 had four research themes: (1) Nanoscale Cage Clusters, (2) Complex Ceramic and Metallic Materials, (3) Hybrid Materials, and (4) Materials Under Extreme Environments (Fig. 1). In 2016 the research themes of the EFRC were modified following peer review, and were (1) Nanoscale Cage Clusters, (2) Complex Ceramic and Metallic Materials, and (3) Materials Under Extreme Environments. Note that RT1 in 2016 corresponds to RT2 in 2009, RT2 in 2016 corresponds to RT1 in 2009, and RT3 in 2016 corresponds to RT3 in 2009. Summaries of accomplishments will be discussed below organized in the three research themes that existed in 2016.

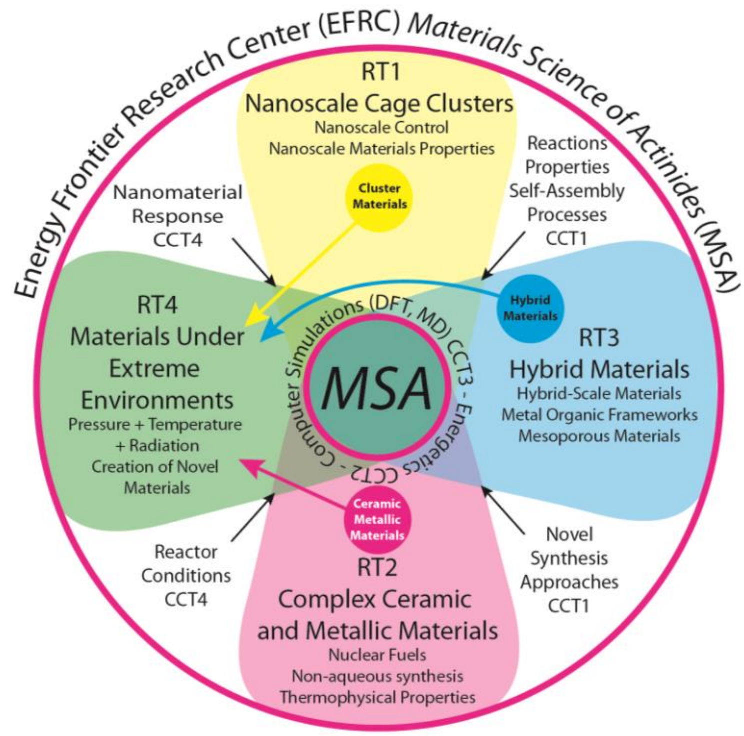

Fig. 1. The intersection between Research Themes (RT) and Cross-Cutting Themes (CCT) defines MSA.

**Research Theme 1: Nanoscale Cage Clusters**

In 2005 Burns and co-workers discovered the spontaneous self-assembly of uranyl peroxide cage clusters in aqueous solutions under ambient conditions, and reported the structures of three of these: U24, U28 and U32 (which contain 24, 28, and 32 uranyl ions, respectively).[1] Upon creation of the EFRC in 2009, uranyl peroxide cage clusters were a major focus of research. The *trans* configuration of the uranyl oxygen atoms provides for stabilization of these clusters on both the inside and outside, and results in a unique class of metal oxide clusters. Research efforts in the EFRC vastly expanded this novel class of nanoscale actinide materials to more than 70 published clusters. In each case clusters were crystallized and single-crystal X-ray diffraction was used to resolve the details of their structures, with neutron diffraction also used for two clusters to provide further detail of H atom and counter cation potions.[2,3] In 2012 we published a very extensive review of the structures and synthesis of uranyl peroxide cage clusters in *Chemical Reviews*[4] in 2013, as well as a comprehensive comparison of uranyl peroxide cage clusters to transition metal polyoxometalates in *Chemical Society Reviews* in 2012.[5] In 2018 we published a Frontier article in *Dalton Transactions* the summarized current understanding and future research directions in uranyl peroxide cluster chemistry.[6] The interested reader is directed to these review articles for details of our studies of uranyl peroxide cage clusters.

In order to achieve our goals in RT1, we applied a variety of experimental techniques to the study of uranyl peroxide cage clusters in solutions. Particularly notable is the application of small-angle X-ray scattering techniques to characterize the size, shape, and aggregation of clusters in solution, electrospray ionization mass spectrometry to characterize the size and charge of cluster species in solution, dynamic and static light scattering to characterize the size and shape of clusters and their aggregates in solution, and cryogenic transmission electron microscopy to image blackberries of uranyl peroxide cage clusters in vitrified solutions.

Broad highlights of the 2009-2018 EFRC research in RT1 include:

- Syntheses, structures and characterization were published for about 60 types of uranyl peroxide cage clusters, producing a library of cluster geometries, compositions, and sizes to support additional research concerning their formation mechanisms, solubilities, stabilities, etc. Each of these was crystallized and single-crystal X-ray diffraction was used to determine their structures. Clusters containing from 16 to 124 uranyl ions were isolated, with diameters extending to 4 nm. In addition to uranyl and peroxide, many ligands were incorporated including hydroxyl, phosphate, pyrophosphate, nitrate, phosphite, oxalate, and etidronic acid.[2,7–25] We also synthesized a series of clusters containing both uranyl and transition metals.[8,14,26]
- We characterized the extremely high solubility of uranyl peroxide cage cluster salts and their use to facilitate dissolution of normally insoluble uranium compounds such as studtite.[27,28] The solubilities of the various salts of clusters exhibit a significant dependence upon the counter cation present, with Li salts being the most soluble.
- Using mass spectrometry, we demonstrated the unexpected stability of uranyl peroxide cage clusters in aqueous solutions over extended periods (many months)[29] and the breakdown mechanisms of clusters[30,31] and their reduction by bacteria.[32]
- We developed a uranium purification and separation process based upon uranyl peroxide cage clusters[33,34] and methods to remove clusters from aqueous solutions using mesoporous materials.[35,36] The former was demonstrated using mass-based filtration of a solution produced by dissolving a surrogate spent nuclear fuel. We also demonstrated high efficiency extraction of uranyl clusters into organic solvents.[37]
- We demonstrated the solubilization of normally insoluble divalent and trivalent metals by encapsulating them in uranyl peroxide cage clusters.[38] We also incorporated lanthanides into the walls of uranyl peroxide cage clusters.[12]
- Computation studies that provided details of uranyl-peroxide interactions and how these favor cluster formation, relative energetics, and cluster formation mechanisms [26,27,39–44].
- Examination of the behavior of uranyl peroxide cage clusters at extremely high pressures in diamond anvil cells, including a mass spectroscopic demonstration of cluster persistence even after the crystals had become X-ray amorphous.[45]
- Determination of the thermodynamic properties of uranyl peroxide cage cluster salts, including the relationship between cluster charge density and enthalpy of formation.[29,46,47]
- Aggregation behavior of uranyl peroxide cage clusters in aqueous solution to form a variety of blackberry structures that were characterized by light scattering[48–55] and transmission electron microscopy.[56]
- Studies of the dynamics of uranyl peroxide cage clusters and their transformations in aqueous solutions, including as a function of pressure, temperature, and pH.[57–60]

- Evaluation of the interaction of uranyl peroxide cage clusters with various mineral surfaces as an evaluation of their significance for the environmental transport of uranium.[61–63]

We summarize the results and impact of some of the more important papers:

- Dembowski, M. *et al.* (2016) *Journal of the American Chemical Society* [2]
  Solution P-31 NMR Study of the Acid-Catalyzed Formation of a Highly Charged $\{U_{24}Pp_{12}\}$ Nanocluster, $[(UO_2)_{24}(O_2)_{24}(P_2O_7)_{12}]^{48-}$, and Its Structural Characterization in the Solid State Using Single-Crystal Neutron Diffraction. The first neutron diffraction study of a single crystal containing uranyl peroxide nanoclusters was reported for a pyrophosphate-functionalized cluster. Relative to earlier X-ray studies, neutron diffraction provides superior information concerning the positions of H atoms and lighter counterions. Hydrogen positions were assigned and reveal an extensive network of H-bonds; notably, most O atoms present in the anionic cluster accept H-bonds from surrounding $H_2O$ molecules, and none of the surface-bound O atoms are protonated. The $D_4h$ symmetry of the cage is consistent with the presence of six encapsulated K cations, which appear to stabilize the lower symmetry variant of this cluster. P-31 NMR measurements demonstrated retention of this symmetry in solution, while *in situ* P-31 NMR studies suggest an acid-catalyzed mechanism for the assembly of 1 across a wide range of pH values.

- Olds, T.A. *et al.* (2017) *Inorganic Chemistry* [15]
  Single-Crystal Time-of-Flight Neutron Diffraction and Magic-Angle-Spinning NMR Spectroscopy Resolve the Structure and H-1 and Li-7 Dynamics of the Uranyl Peroxide Nanocluster U-60. Single-crystal time-of-flight neutron diffraction provided atomic resolution of H atoms of $H_2O$ molecules and hydroxyl groups, as well as Li cations in the uranyl peroxide nanocluster U-60. Solid-state magic-angle-spinning nuclear magnetic resonance (MAS NMR) spectroscopy was used to confirm the dynamics of these constituents, revealing the transportation of Li atoms and $H_2O$ through cluster walls. H atoms of hydroxyl units that are located on the cluster surface are involved in the transfer of $H_2O$ and Li cations from inside to outside and vice versa. This exchange occurs as a concerted motion and happens rapidly even in the solid state.

- Peruski, K. *et al.* (2017) *Inorganic Chemistry* [27]
  Uranyl Peroxide Cage Cluster Solubility in Water and the Role of the Electrical Double Layer. In this study we demonstrated that uranium concentrations as high as $2.94 \times 10^5$ parts per million (1.82 mol of U/1 kg of $H_2O$) occur in water containing nanoscale uranyl cage clusters. The concentration of uranium in these systems is impacted by the countercations (K, Li, Na), and molecular dynamics simulations predicted their distributions in selected cases. Formation of uranyl cages prevents hydrolysis reactions that would result in formation of insoluble uranyl solids under alkaline conditions, and these spherical clusters reach concentrations that require close packing in solution.

- Vlaisavljevich, B. *et al.* (2010) *Journal of the American Chemical Society* [41]
  Understanding the Structure and Formation of Uranyl Peroxide Nanoclusters by Quantum Chemical Calculations. For the first time, density functional theory was applied to

understand the formation of nanoscale uranyl peroxide cage clusters. We investigated the uranyl-peroxide-uranyl interaction and compared the geometries of clusters with and without such interactions. We showed that a covalent interaction along the U-O-peroxo bonds causes the U-$O_2$-U dihedral angle to be bent, and it is this inherent bending of the configuration that encourages curvature and cage cluster formation. The U-$O_2$-U dihedral angle of the peroxo bridge can be tuned to some extent by the size or electronegativity of the counterion present.

- Falaise, C. and Nyman, M. (2016) *Chemistry – A European Journal*[64]
  The Key Role of $U_{28}$ in the Aqueous Self-Assembly of Uranyl Peroxide Nanocages. Here we exploited the high solubility of the $UO_2^{2+}$/$H_2O_2$/LiOH aqueous system to address the effect of the hydroxide concentration. Important techniques of this study are single-crystal X-ray diffraction, small-angle X-ray scattering, and Raman spectroscopy. When the LiOH/U ratio is around three, $U_{28}$ forms rapidly and this cluster can be isolated in high yield and purity. This result was most surprising and challenges the hypothesis that alkali templating is the most important determinant in the cluster geometry. Moreover, analogous experiments with KOH, $NH_4OH$, and TEAOH (TEA=tetraethylammonium) also rapidly yield $U_{28}$, which suggests that $U_{28}$ is the kinetically favored species. Complete mapping of the pH–time phase space reveals only a narrow window of the $U_{28}$ dominance, which is why it was previously overlooked as an important kinetic species in this chemical system, as well as others with different counterions.

## Research Theme 2: Complex Ceramic and Metallic Materials

A wide suite of actinide materials is important for nuclear technology, and a much deeper and more accurate understanding of their properties is critical. From a fundamental perspective, this variety offers exciting opportunities for comparative studies that expand fundamental knowledge of actinide chemistry and physics. The functionality of refractory actinide materials, their phase diagrams, and stability to corrosion and radiation damage all depend on the interplay of structural, chemical, and electronic configurations. The emphasis of this research theme is development of methodologies and measurements of thermodynamic parameters of important actinide materials.

In order to achieve our objectives in this research theme, we developed new calorimetry facilities for measurements of thermodynamic data for transuranium materials.[65,66] We also developed resonant ultrasound spectroscopy to measure aging of plutonium alloys directly for the first time.[67]

Selected highlights of this research effort are:

- Measurement and characterization of the aging of plutonium alloys in real time using spectroscopic techniques.[67–70]
- Measurement of thermodynamic properties of various uranium-based minerals[71–75] and hybrid materials,[73] including coffinite,[71,76–78] which has resisted studies for many years.
- Synthesis and characterization of an extensive family of actinide borates, including examples of cationic frameworks with anion exchange properties.[79–91]

- Determination of thermodynamic properties of a broad range of actinide and lanthanide oxides important as nuclear fuels and nuclear waste forms, often including computational models. [65,71,74,92–111]
- Studies of X-ray amorphous $U_2O_7$ that forms upon heating of the uranyl peroxide studtite and that caused pressurization of drums of yellowcake that resulted in contamination and injuries. [112]
- Determination of formation energetics and order disorder in fluorite oxides.[93,96,98,100–103,107,110]
- Discovery and characterization of complexity of radiation damage and annealing in pyrochlores, including short range weberite structural motifs.[66,95,111,113]
- Developing calorimetric techniques applicable to higher actinides at the University of Notre Dame and at Los Alamos National Laboratory.[65,66]

We summarize the results and impact of some of the more important papers:

- Ennaceur, S. and Migliori, A. (2018) *Philosophical Magazine Letters*[69]
  Toward an understanding of aging in plutonium from direct measurements of stored energy. We present here the first direct measurement of the radiation-damage-induced energy stored in delta-phase plutonium. Each decay imparts about 85 keV of recoil energy to the uranium byproduct, 5.2 Mev to the alpha particle, and a spectrum of mostly low energy gamma rays with the most probable at 51 keV. Most of the decay energy is converted immediately to heat, releasing about 1.9 mW/g. However, some thermally-recoverable energy remains trapped. We report measurements of that stored energy using differential scanning calorimetry (DSC) applied to Pu-239-2.0 at.%Ga delta-phase alloy. Retained energy of similar to 2 J/g saturates at about 5 months and is unchanged after 30 years. The magnitude of the stored energy agrees with a short-bond defect model that that we present. This model treats radiation damage as a Pu impurity with shortened bond lengths. It explains the change in known properties with age and predicts that density increases with age, contrary to current thinking. The short-bond impurities proposed are expected to act like other impurities, affecting strength, phase transitions, grain boundaries and other metallurgical properties.

- Odoh *et al*. (2016) *Inorganic Chemistry*[112]
  Structure and Reactivity of X-ray Amorphous Uranyl Peroxide, $U_2O_7$. Recent accidents resulting in worker injury and radioactive contamination occurred due to pressurization of uranium yellowcake drums produced in the western U.S.A. The drums contained an X-ray amorphous reactive form of uranium oxide that may have contributed to the pressurization. Heating hydrated uranyl peroxides produced during in situ mining can produce an amorphous compound, as shown by X-ray powder diffraction of material from impacted drums. Subsequently, studtite, $[(UO_2)(O_2)(H_2O)_2](H_2O)_2$, was heated in the laboratory. Its thermal decomposition produced a hygroscopic anhydrous uranyl peroxide that reacts with water to release $O_2$ gas and form metaschoepite, a uranyl-oxide hydrate. Quantum chemical calculations indicate that the most stable $U_2O_7$ conformer consists of two bent $(UO_2)^{2+}$ uranyl ions bridged by a peroxide group bidentate and parallel to each uranyl ion, and a $mu_2$-O atom, resulting in charge neutrality. A pair distribution function from neutron total scattering supports this structural model,as do $H^1$ and $O^{17}$ nuclear

magnetic resonance, spectra. The reactivity of $U_2O_7$ in water and with water in air is higher than that of other uranium oxides, and this can be both hazardous and potentially advantageous in the nuclear fuel cycle.

- Zhang *et al*. (2018) *Journal of Nuclear Materials*[65]
  Experimental thermochemistry of neptunium oxides: $Np_2O_5$ and $NpO_2$. Although high temperature oxide melt solution calorimetry has proven very useful in obtaining thermodynamic data for the formation of uranium and thorium oxide materials, it has not yet been applied to transuranium compounds. Continuing a program at Notre Dame to study the thermodynamics of transuranium compounds, we report the first determination of the enthalpies of drop solution of well-characterized neptunium oxides ($Np_2O_5$ and $NpO_2$) using oxide melt solution calorimetry in molten sodium molybdate solvent at 973 K. The calorimetric methodology is straightforward and produces reliable data using milligram quantities of radioactive materials, and can be applied to many other transuranium compounds.

- Alexandrov *et al*. (2011) *Journal of Physical Chemistry Letters*[102]
  Actinide Dioxides in Water: Interactions at the Interface. A comprehensive understanding of chemical interactions between water and actinide dioxide surfaces is critical for safe operation and storage of nuclear fuels. Despite substantial previous research, understanding the nature of these interactions remains incomplete. In this work, we combined accurate calorimetric measurements with first-principles computational studies to characterize surface energies and adsorption enthalpies of water on two fluorite-structured compounds, $ThO_2$ and $CeO_2$. The results show a correlation between the magnitude of the anhydrous surface energy and the water adsorption enthalpy. Further, they suggest a structural model featuring one adsorbed water molecule per one surface cation on the most stable facet that is expected to be a common structural signature of water adsorbed on actinide dioxide compounds.

**Research Theme 3: Materials Under Extreme Environments**

Materials behavior under simultaneous high-irradiation, high-pressure and high-temperature conditions have significant implications for studies in condensed matter physics, materials science, nuclear engineering as well as the geological sciences. The large amount of energy deposited by relativistic heavy ions in materials under high pressure and temperature will have significant influences on the thermodynamics and kinetics of phase-transitions under pressure. Since the ion energy deposition involves extremely short time scales, non-equilibrium processes such as ion-induced pressure/temperature waves may be expected. Their interaction with already applied static pressure and temperature may trigger new phase transitions in solids that are only present under static pressure. In addition, nano-scale materials behave very differently from the bulk material under extreme conditions.

Prior to this research effort there were limited data available on how materials respond to the simultaneous exposure to energetic projectiles, high pressures, and high temperatures as a function of structure, composition, thermodynamic stability and crystallite size. Over the nine year period of this EFRC, researchers in RT3 were able to investigate the behavior of important actinide ceramics, such as $UO_2$, $ThO_2$, actinide-bearing complex ceramics, such as pyrochlore, garnet, and apatite, as well as simple compounds or alloys that have applications in nuclear science, such as ZrN and high entropy metal alloys.

Viewed broadly, the RT3 research team:

- Systematically investigated these coupled processes with high-energy irradiations at elevated pressures and temperatures. We also performed high-pressure/temperature experiments on pre-irradiated samples (to investigate the influence of defects on phase transitions) and irradiation experiments of pre-pressurized/ thermally treated samples (to investigate the stability of high-pressure phases under ion irradiation).
- Sought to understand the response of actinide materials to *combinations of extreme conditions* of temperature, pressure, chemical environments, and high-radiation fields as a function of crystallite size.
- Sought to understand the structures and stabilities of the full range of U:O and Th:O compounds as a function of high pressures and temperatures that were subjected to intense radiation fields in order to determine their response under extreme conditions.
- Investigated the response of actinide materials far from equilibrium using high-energy ion beams and high energy lasers to deposit extremely large amounts of energy into small volumes of actinide materials.
- Synthesized new actinide materials under coupled conditions of high pressures and temperatures in an intensely ionizing radiation field and as a function of crystallite size.

We also successfully addressed a number of fundamental scientific issues specific to actinide compounds

- What are the high-pressure/temperature behaviors of different U:O stoichiometries? How are these related to the much simpler Th:O system?
- What new actinide phases form under extremes of pressure and temperature? What is the effect of grain size on the energetics and dynamics of phase transformations?
- What are the structural responses of different actinide materials to ionization and ballistic collision processes from energetic ion irradiation?
- What are the effects of electronic configuration on the stability and defects of *An*O2 materials?
- How do the microstructures evolve and what are the impacts of nano-grain size and stoichiometry on radiation stability? What is the nature of defects and structures produced by fission products (or similar ions) in *An*O2 materials that do not exhibit track formation?
- What is the structural response of actinide materials to the combined application of relativistic heavy ions, high pressure, and high temperature? Can we predictively model materials behavior under such extreme conditions?
- Can the coupling of extreme conditions result in the formation of novel actinide phases with enhanced performance in harsh environments?
- How is the production and nature of defects affected by ion irradiation at high pressures?

- How does radiation damage from energetic ions affect the thermal and ionic conductivity of *An*$O_2$ materials? What is the relationship of this damage to the underlying nanoscale damage morphology, microstructure evolution, and defect accumulation?
- What is the effect of non-stoichiometry and grain size on these modifications?
- Can very-high-energy ion irradiation be used to tailor nanoscale transport properties?
- How can extremes in high-energy ion irradiation, pressure, and temperature be used to synthesize novel actinide materials? Do these new compounds have useful properties that enhance their use in extreme environments?
- What is the response of different nanoscale uranyl cage topologies to high pressure?

In order to address these issues, new, innovative experimental techniques had to be developed and applied. Much of the effort of the RT3 team was devoted to developing these new techniques. Three broad experimental efforts included:

*1. Coupling of extreme conditions (high-temperature- and high-pressure experiments in intense radiation fields):*

Research on materials exposed to swift heavy ion irradiation, high pressure, and temperature is based on a new experimental approach fulfilling three technical requirements: (*i*) the sample must be enclosed in a high-pressure cell, (*ii*) the ions require sufficient kinetic energy to travel completely through one of the pressure anvils to reach and traverse the sample under investigation, and (*iii*) a heating wire (or heating laser) must be connected with the pressure cell at the irradiation site (Fig. 2). High-pressure techniques have been successfully combined with the use of ion beams by injecting relativistic heavy ions of one of the world's largest accelerator facilities (GSI Helmholtz Center for Heavy Ion Research, in Darmstadt, Germany) through a mm-thick diamond anvil of a high-pressure cell (DAC) into a pressurized target (Fig. 2). During the EFRC project, experimental protocols have been continuously developed to routinely expose samples to controlled extremes of pressure (~1 Mbar) and irradiation (~$1\times10^{13}$ ions/$cm^2$). A wide range of actinide and surrogate materials (nanocrystalline and bulk materials) have been systematically irradiated with swift heavy ions at high pressures to investigate their response to coupled extremes. Material modifications were analyzed by means of *in situ* synchrotron-based X-ray diffraction which requires coordinated beamtimes at large user facilities (characterization at high pressure prior to ion irradiation and afterwards).

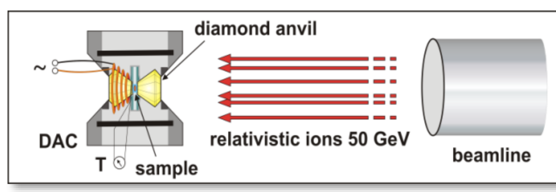

Fig. 2: *Scheme of high-pressure irradiation experiments with relativistic heavy ions. In order to reach the sample pressurized between two diamond anvils (size ~100 μm), the initial beam energy must be ~50 GeV. Temperature can be controlled by heating wires or intense heating lasers (not shown).*

*2. Neutron total scattering characterization of ion irradiation materials:*

The investigation of radiation effects with conventional characterization techniques such as XRD and TEM has two major shortcomings: (*i*) both X-ray and electron probes are insensitive to low-*Z* elements (e.g., oxygen) and (*ii*) diffraction experiments provide no information on the local atomic arrangement and the medium-range structure. To overcome this, we have developed neutron total scattering analysis for ion irradiated materials. Such experiments have not been performed in the past due to the low scattering cross sections and unattainable irradiated sample volumes. The Spallation Neutron Source (SNS) at Oak Ridge National Laboratory – the world's most intense pulsed neutron source – has become operational during the EFRC project for materials research. In a pioneering experiment, we have coupled this unique DOE facility with one of the largest ion accelerators (GSI Helmholtz Center for Heavy Ion Research in Darmstadt, Germany) to characterize radiation damage by means of neutron scattering experiments. With a neutron flux of ~ $1 \times 10^8$ neutrons/$cm^2 \cdot s$ and a large solid angle of detector coverage, the Nanoscale-Ordered Materials Diffractometer (NOMAD) beamline at the SNS requires very little sample mass to produce high-resolution pair distribution functions (PDF). The unique 6-bank detector system at NOMAD together with the wide range of available neutron wavelengths (0.1 - 3 Å) are essential to produce PDFs with very high resolution to resolve subtle structural features within irradiated materials. Key to this experimental procedure is the use of GeV ions to produce sufficient sample material irradiated with a near uniform electronic energy loss. A new holder system was developed for such experiments to facilitate the preparation of ~100 mg sample with precision control of the thickness (Fig. 3). Several of such sample holders were irradiated simultaneously with a ~25 $cm^2$ sized beam of energetic heavy ions (*e.g.*, Au ions, 2.2 GeV). After ion-beam exposure the samples were removed from the irradiation holders, combined, ground into a fine powder, and loaded into sample holders for neutron analysis. The NOMAD instrument has also *in situ* capabilities enabling neutron scattering experiments at high temperatures of up to 1200 °C. We complemented therefore the characterization of radiation effects by studies on damage recovery and defect dynamics at elevated temperatures.

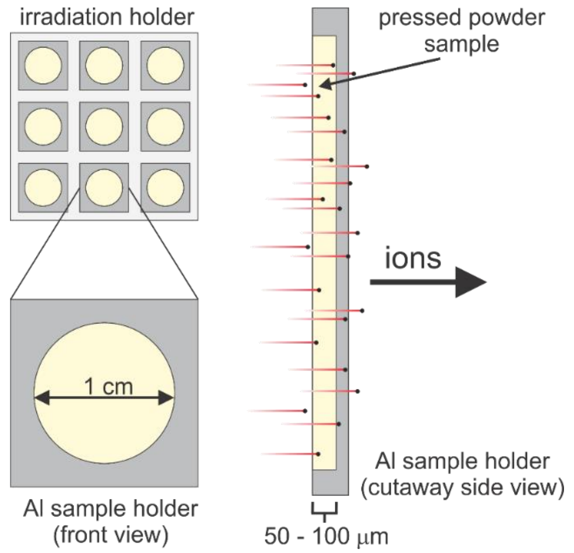

Fig. 3: *Schematic representation of the ion irradiation experimental setup. Sample powders were uniaxially pressed into 50 - 100 µm deep, 1 cm diameter cylindrical indentations that were machined into thin aluminum plates (grey). Nine sample holders were fixed on a 5 x 5 $cm^2$ aluminum plate for ion irradiation (top left). The cutaway side view (right) shows the orientation of the holder during ion irradiation.*

<u>*3. High energy laser irradiations and pump probe experiments:*</u>

One of the challenges of using ion beam irradiation as a source of induced damage was that the volume of material damaged was so small. We solved this problem by using a combination of HRTEM and SAXS experiments, but still the work was tedious. This led us to develop the use of higher energy lasers to move and observe systems far from equilibrium. Ultrafast optical pump-probe experiments were performed using a Ti:sapphire laser with a pulse duration of 50 fs and central wavelength of 800 nm. Probe fluence was over an order of magnitude lower than the pump beam for all measurements, which were collected at elevated pressure using a diamond-anvil cell (DAC) at room temperature. We first demonstrated that the types of phase transitions observed from ion beam irradiations were the same as those induced by high-energy lasers. The ability to temporally resolve ultrafast laser pulses allows one to directly observe the radiation damage process on the relevant timescales by using time-resolved pump-probe spectroscopy. The ultimate goal of this work was to be able to directly observe phase transitions at the atomic-scale.

Over the nine-year period, this research group was remarkably productive. Referring to the tabulated list of publications for the MSA EFRC, RT3 researchers published: 102 papers fully-funded by the EFRC, 46 papers that were completed with collaborators and 4 book chapters. We summarize the results and impact of some of the more important papers below (# indicates the listing in the tabulation of papers from the EFRC:

- Zhang, J.M. *et al.* (2015) *Journal of Materials Research*[114]
  <u>$C_{60}$ and U ion irradiation of $Gd_2Ti_xZr_{2-x}O_7$ pyrochlore.</u> $Gd_2Ti_xZr_{2x}O_7$ (x = 0 to 2) pyrochlore was irradiated by 30 MeV $C_{60}$ clusters, which provide an extremely high ionizing energy density. High-resolution transmission electron microscopy revealed a complex ion-track structure in $Gd_2Ti_2O_7$ and $Gd_2TiZrO_7$, consisting of an amorphous core and a shell of a disordered, defect-fluorite structure. As compared with the irradiation by 1.5 GeV U ions with the highest energy loss, the track structure is consistent with tracks created by monoatomic swift heavy ions, but the diameters (with the entire diameter of 17 nm for $Gd_2Ti_2O_7$ and 15 nm for $Gd_2TiZrO_7$) are significantly larger due to the much smaller velocity and higher energy density of the $C_{60}$ ions. Ion tracks created by monoatomic ions are challenging to describe by HRTEM, as the boundary between disordered fluorite and pyrochlore matrix is less distinct. However, the $C_{60}$ irradiation shows a clearly resolved ion track with completely crystalline, disordered, defect-fluorite structure around an amorphous core. Based on the distinct boundaries of the track morphology, inelastic thermal-spike calculations were used to describe the track size and extract critical energy densities for the interpretation of the complex core–shell morphologies for the different pyrochlore compositions.

- Tracy, C.L. *et al.* (2015) *Nature Communications*[115] and Cureton, W.F. *et al.* (2019) *Journal of Nuclear Materials*[116]
  <u>Redox response of actinide materials to highly ionizing radiation.</u> Energetic radiation can cause dramatic changes in the physical and chemical properties of actinide materials, degrading their performance in fission-based energy systems. Characterization of irradiated actinide oxides by advanced synchrotron techniques (X-ray diffraction and X-ray absorption spectroscopy) showed that the redox behavior of actinides governs the radiation tolerance. The microstructure of the material plays a critical role in this process with a nanoscale grain size reducing significantly the radiation resistance. These findings suggest that by limiting the redox activity of actinide materials through control of composition or microstructure, one can mitigate radiation-induced swelling and microstrain.

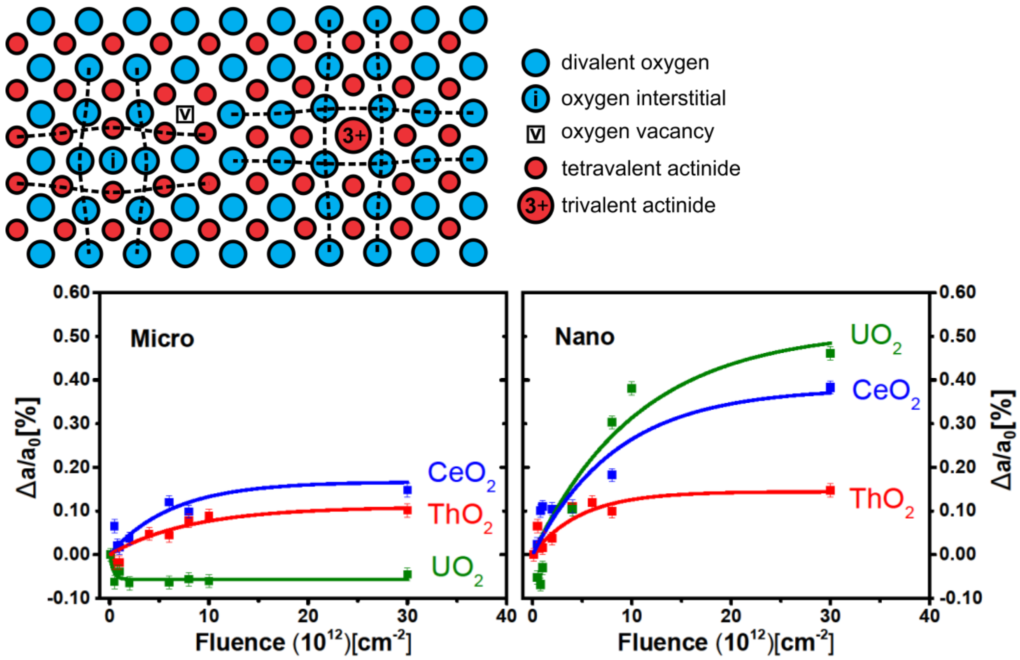


Fig. 4: *(top) Cation reduction causes structural distortion in the actinide oxide lattice that are identical to that caused by Frenkel defects. (bottom) Radiation-induced swelling depends strongly on the electronic structure of the cation and the grain size of the material.*

- Shamblin *et al.* (2016) *Nature Materials*[117]
  Probing disorder in isometric pyrochlore and related complex oxides. Complex oxides are candidate materials for a wide range of energy-related applications, such as solid electrolytes for fuel cells, host materials for actinide immobilization, and thermal barrier coatings for gas turbine jet engines. When subjected to extreme environments, such as high temperatures or highly ionizing radiation, many of these compounds partially lose their ordered structure through, as previously thought, random mixing of their atomic constituents. Neutron total scattering experiments, however, revealed that the cations and oxygen atoms are not randomly arranged at the atomic level, but only appear so when sampling over longer length scales. This discovery indicates that discrepancies may arise when extrapolating the materials structure from the microscale to the atomic scale (or *vice versa*), which has significant implications for modelling properties and degradation phenomena in actinide-bearing materials. Structural heterogeneity across different length scales appears to be a universal phenomenon for both, intrinsically (*e.g.*, chemical doping/substitution) and extrinsically (*e.g.*, irradiation and mechanochemical processing) disordered complex oxides.

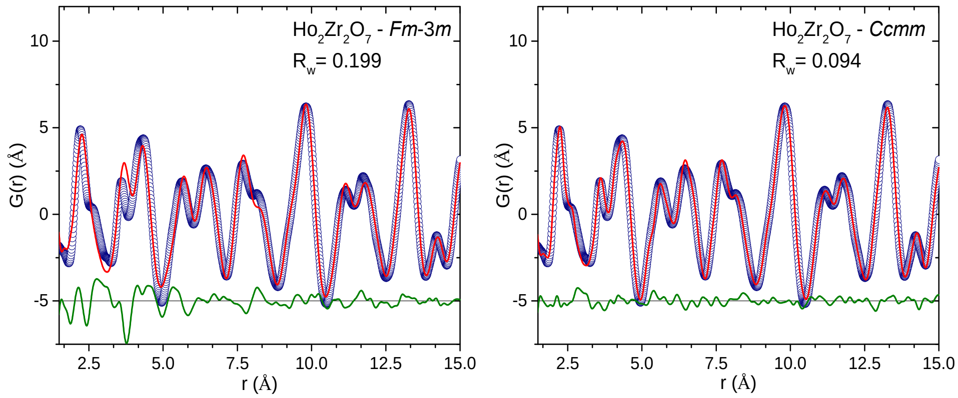


Fig. 5: *(left) The disordered cubic phase does not agree with the neutron scattering data on* $Ho_2Zr_2O_7$*. (right) Despite an average cubic structure, an orthorhombic structure agrees well locally.*

- O'Quinn *et al.* (2017) *Journal of American Chemical Society*[118]
  <u>Inversion in $Mg_{1-x}Ni_xAl_2O_4$ spinel.</u> Given the ubiquity of the spinel structure in many engineering applications, a comprehensive understanding of its structure at the atomic-scale is important, particularly under extreme conditions. The atomic arrangement of the isometric spinel structure is conventionally described by only three degrees of freedom. Of importance is the inversion parameter, which defines the degree of cation exchange and represents a direct measure of intrinsic disorder. Based on neutron total scattering experiments, we have determined that the local structure of spinel cannot be understood as simply being due to cation disorder. Rather, cation inversion creates a local tetragonal symmetry that extends over sub-nanometer domains. Consequently, the simple spinel structure is more complicated than previously thought, as more than three parameters are needed to fully describe the structure. This new insight provides a framework by which the behavior of spinel can be more accurately modeled under the extreme environments important for many geophysics and energy-related applications, including prediction of deep seismic activity and immobilization of nuclear waste in oxides.

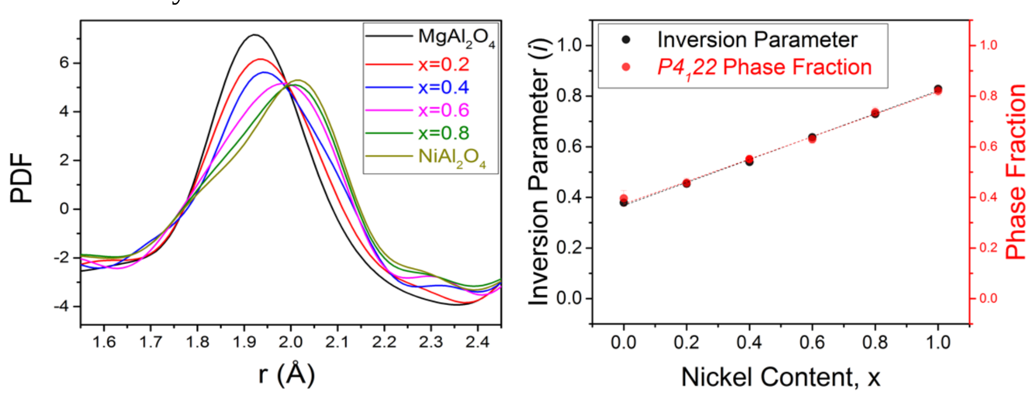


Fig. 6: *(left) Comparison of PDFs for the* $Mg_{1-x}Ni_xAl_2O_4$ *spinel series, highlighting the distances associated with coordination polyhedra in each series member and associated deviation from the isometric structure with increasing Ni-content. (right) The good*

*agreement of inversion parameter, from average structure refinement, and local tetragonal $P4_122$ phase fraction, from PDF refinement indicate that cation inversion can be understood as locally-ordered structural distortion.*

- Tracy *et al.* (2017) *Nature Communications*[119]
  High pressure synthesis of a hexagonal close-packed phase of the high-entropy alloy CrMnFeCoNi. High-entropy alloys, near equi-atomic solid solutions of five or more elements, represent a new strategy for the design of materials with properties superior to those of conventional alloys. However, their phase space remains constrained, with transition metal high-entropy alloys exhibiting only face- or body-centered cubic structures. In this paper, we investigated the high-pressure synthesis of a hexagonal close-packed phase of the prototypical high-entropy alloy CrMnFeCoNi. This martensitic transformation begins at 14GPa and is attributed to suppression of the local magnetic moments, destabilizing the initial fcc structure. Similar to fcc-to-hcp transformations in Al and the noble gases, the transformation is sluggish, occurring over a range of 440 GPa. However, the behavior of CrMnFeCoNi is unique in that the hcp phase is retained following decompression to ambient pressure, yielding metastable fcc-hcp mixtures. This demonstrates a means of tuning the structures and properties of high-entropy alloys in a manner not achievable by conventional processing techniques.

- J. Shamblin *et al.* (2018). *Acta Materialia*[120]
  Similar local order in disordered fluorite and aperiodic pyrochlore structures. A major challenge to understanding the response of materials to extreme environments (e.g., nuclear fuels/waste forms and fusion materials) is to unravel the processes by which a material can incorporate atomic-scale disorder, and at the same time, remain crystalline. Neutron total scattering was utilized to characterize the irradiation response of two pyrochlores, one that is known to disorder and the other to amorphize under ion irradiation. The data demonstrated that in both cases, the local pyrochlore structure is transformed into similar orthorhombic units even though the two compositions have distinctly different structures, aperiodic *vs*. disordered-crystalline, at longer length scales. This suggests that a material's propensity to disorder rather than to amorphize may not be fully determined by its ability to incorporate point defects, but rather on the structure's compatibility with meso-scale modulations of the local order in a way that maintains long-range periodicity. This discovery not only redefines the understanding of radiation resistance, but indicates that discrepancies may arise when extrapolating the material’s structure from the microscale to the atomic scale (or *vice versa*), which has significant implications for modelling properties and degradation phenomena in actinide materials.

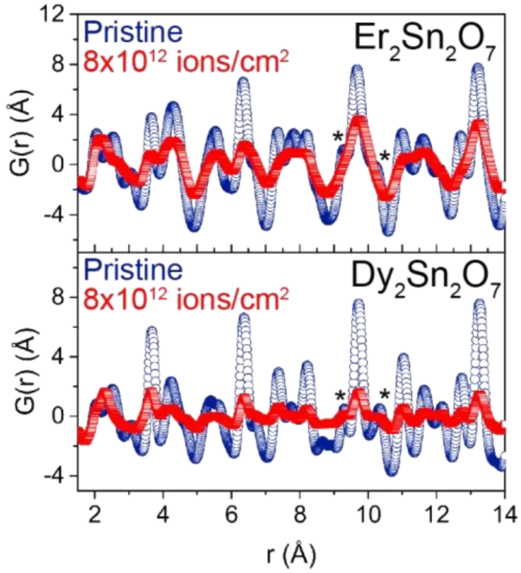


Fig. 7: *Neutron PDFs of pyrochlores before (blue) and after (red) being irradiated with 2.2 GeV Au ions to a fluence of $8\times10^{12}$ ions/cm$^2$. (top) $Er_2Sn_2O_7$, disorder is indicated by broadening and merging of the original pyrochlore peaks. (bottom) $Dy_2Sn_2O_7$, after irradiation the peaks are significantly reduced in area, but do not show pronounced merging, indicative of partial amorphization. The local atomic arrangement changes in both cases from pyrochlore to weberite-type.*

- Rittman *et al.* (2018) *Physical Rev. B*[121]
  Anomalous behavior of nonequilibrium excitations in $UO_2$. Ultrafast optical pump-probe studies of UO2 under pressure were performed in order to better understand the material's response to ionizing radiation. Photoexcitation generates oscillations in the time- resolved reflectivity at two distinct GHz-scale frequencies. The higher-frequency mode is attributed to a coherent longitudinal acoustic mode. The lower-frequency mode does not correspond to any known excitation under equilibrium conditions. The frequency and lifetime of the low-frequency mode are studied as a function of pressure. Abrupt changes in the pressure-dependent slopes of these attributes are observed at ∼10 GPa, which correlates with an electronic transition in UO2. Variation of probe wavelength reveals that the low-*k* dispersion of the low-frequency mode does not fit into either an optical or acoustic framework. Rather, we propose that this mode is related to the dynamical magnetic structure of UO2. The implications of these results help account for the anomalously small volume of damage known to be caused by ionizing radiation in UO2; we propose that the existence of the low-frequency mode enhances the material's transient thermal conductivity, while its long lifetime lengthens the timescale over which energy is dissipated. Both mechanisms enhance damage recovery.

- Palomares, R.I. *et al.* (2019) *Physical Review Materials*[122]
  Oxygen point defect accumulation in single-phase $UO_{2+x}$. Uranium dioxide is of primary technological importance as a nuclear fuel material. A unique feature of the uranium oxide system is the high degree of off-stoichiometry that the material exhibits upon varying oxygen partial pressure and temperature, such as under off-normal operating conditions.

Oxidation of $UO_2$ is an exothermic process that proceeds largely through the incorporation of oxygen atoms into the $UO_2$ matrix. These excess oxygen interstitials are expected to form small defect clusters with morphologies that are not fully understood. Experimental findings from Willis for example, although reproducible, remain at odds with theoretical models, which consistently show that the experimental defect configurations are unstable and decompose into smaller di-interstitial defects upon structural relaxation. Simultaneous modeling of multiple length scales using complementary Reverse Monte Carlo (RMC) and Molecular Dynamics (MD) methods on neutron total scattering data obtained with $UO_{2.07}$ confirm that excess oxygen primarily exists as small defects, such as mono-interstitials and di-interstitials. Employing a combination of analysis methods with varying length-scale sensitivities enabled more accurate assessment of the $UO_{2+x}$ defect structure. These findings provide experimental support for previously predicted di-interstitial defect morphologies in $UO_{2+x}$ that highly influence the accurate prediction of bulk physiochemical properties, such as oxygen diffusivity.

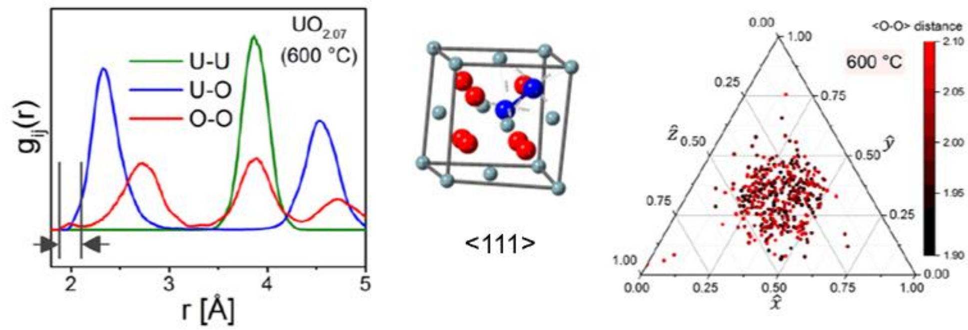


Fig. 8: *Oxygen point defect configurations in $UO_{2.07}$ at 600 and 1000 °C studied by neutron total scattering experiments, Reverse Monte Carlo (RMC) modelling, and Molecular Dynamics (MD) simulations. (left) The oxygen interstitials in the optimized RMC models cause the emergence of a small O-O correlation at ∼2 Å. (middle and right) Bond vector analyses show that these short (1.9–2.1 Å) O-O pairs are oriented primarily along <111> directions.*

## References Cited


(1) Burns, P. C.; Kubatko, K. A.; Sigmon, G.; Fryer, B. J.; Gagnon, J. E.; Antonio, M. R.; Soderholm, L. Actinyl Peroxide Nanospheres. *Angew. Chemie - Int. Ed.* **2005**. https://doi.org/10.1002/anie.200462445.

(2) Dembowski, M.; Olds, T. A.; Pellegrini, K. L.; Hoffmann, C.; Wang, X.; Hickam, S.; He, J.; Oliver, A. G.; Burns, P. C. Solution P-31 NMR Study of the Acid-Catalyzed Formation of a Highly Charged {U(24)Pp(12)} Nanocluster, {[}(UO2)(24)(O-2)(24)(P2O7)(12)](48-), and Its Structural Characterization in the Solid State Using Single-Crystal Neutron Diffraction. *J. Am. Chem. Soc.* **2016**, *138* (27), 8547–8553. https://doi.org/10.1021/jacs.6b04028.

(3) Olds, T. A.; Dembowski, M.; Wang, X.; Hoffman, C.; Alam, T. M.; Hickam, S.; Pellegrini, K. L.; He, J.; Burns, P. C. Single-Crystal Time-of-Flight Neutron Diffraction and Magic-Angle-Spinning NMR Spectroscopy Resolve the Structure and 1H and 7Li Dynamics of the Uranyl Peroxide Nanocluster U60. *Inorg. Chem.* **2017**. https://doi.org/10.1021/acs.inorgchem.7b01174.

(4) Qiu, J.; Burns, P. C. Clusters of Actinides with Oxide, Peroxide, or Hydroxide Bridges. *Chem. Rev.* **2013**, *113* (2), 1097–1120. https://doi.org/10.1021/cr300159x.

(5) Nyman, M.; Burns, P. C. A Comprehensive Comparison of Transition-Metal and Actinyl Polyoxometalates. *Chemical Society Reviews*. 2012. https://doi.org/10.1039/c2cs35136f.

(6) Burns, P. C.; Nyman, M. Captivation with Encapsulation: A Dozen Years of Exploring Uranyl Peroxide Capsules. *Dalt. Trans.* **2018**, *47* (17), 5916–5927. https://doi.org/10.1039/c7dt04245k.

(7) Ling, J.; Qiu, J.; Sigmon, G. E.; Ward, M.; Szymanowski, J. E. S.; Burns, P. C. Uranium Pyrophosphate/Methylenediphosphonate Polyoxometalate Cage Clusters. *J. Am. Chem. Soc.* **2010**, *132* (38), 13395–13402. https://doi.org/10.1021/ja1048219.

(8) Ling, J.; Hobbs, F.; Prendergast, S.; Adelani, P. O.; Babo, J.-M.; Qiu, J.; Weng, Z.; Burns, P. C. Hybrid Uranium-Transition-Metal Oxide Cage Clusters. *Inorg. Chem.* **2014**, *53* (24), 12877–12884. https://doi.org/10.1021/ic5018449.

(9) Qiu, J.; Ling, J.; Sieradzki, C.; Nguyen, K.; Wylie, E. M.; Szymanowski, J. E. S.; Burns, P. C. Expanding the Crystal Chemistry of Uranyl Peroxides: Four Hybrid Uranyl-Peroxide Structures Containing EDTA. *Inorg. Chem.* **2014**, *53* (22), 12084–12091. https://doi.org/10.1021/ic5018906.

(10) McGrail, B. T.; Sigmon, G. E.; Jouffret, L. J.; Andrews, C. R.; Burns, P. C. Raman Spectroscopic and ESI-MS Characterization of Uranyl Peroxide Cage Clusters. *Inorg. Chem.* **2014**, *53* (3), 1562–1569. https://doi.org/10.1021/ic402570b.

(11) Qiu, J.; Ling, J.; Jouffret, L.; Thomas, R.; Szymanowski, J. E. S.; Burns, P. C. Water-Soluble Multi-Cage Super Tetrahedral Uranyl Peroxide Phosphate Clusters. *Chem. Sci.*

**2014**, *5* (1), 303–310. https://doi.org/10.1039/c3sc52357h.

(12) Sigmon, G. E.; Szymanowski, J. E. S.; Carter, K. P.; Cahill, C. L.; Burns, P. C. Hybrid Lanthanide-Actinide Peroxide Cage Clusters. *Inorg. Chem.* **2016**, *55* (6), 2682–2684. https://doi.org/10.1021/acs.inorgchem.6b00207.

(13) Qiu, J.; Dembowski, M.; Szymanowski, J. E. S.; Toh, W. C.; Burns, P. C. Time-Resolved X-Ray Scattering and Raman Spectroscopic Studies of Formation of a Uranium-Vanadium-Phosphorus-Peroxide Cage Cluster. *Inorg. Chem.* **2016**, *55* (14), 7061–7067. https://doi.org/10.1021/acs.inorgchem.6b00918.

(14) Qiu, J.; Dong, S.; Szymanowski, J. E. S.; Dobrowolska, M.; Burns, P. C. Uranyl-Peroxide Clusters Incorporating Iron Trimers and Bridging by Bisphosphonate-and Carboxylate-Containing Ligands. *Inorg. Chem.* **2017**, *56* (7), 3738–3741. https://doi.org/10.1021/acs.inorgchem.7b00389.

(15) Olds, T. A.; Dembowski, M.; Wang, X.; Hoffman, C.; Alam, T. M.; Hickam, S.; Pellegrini, K. L.; He, J.; Burns, P. C. Single-Crystal Time-of-Flight Neutron Diffraction and Magic-Angle-Spinning NMR Spectroscopy Resolve the Structure and H-1 and Li-7 Dynamics of the Uranyl Peroxide Nanocluster U-60. *Inorg. Chem.* **2017**, *56* (16), 9676–9683. https://doi.org/10.1021/acs.inorgchem.7b01174.

(16) Ling, J.; Zhang, H.; Qiu, J.; Stoller, M.; Burgess, D.; Burns, P. C. Pyrophosphate and Methylenediphosphonate Incorporated Uranyl Peroxide Cage Clusters. *Cryst. Growth Des.* **2018**, *18* (12), 7720–7729. https://doi.org/10.1021/acs.cgd.8b01638.

(17) Arteaga, A.; Zhang, L.; Hickam, S.; Dembowski, M.; Burns, P. C.; Nyman, M. Uranyl-Peroxide Capsule Self-Assembly in Slow Motion. *Chem. Eur. J.* **2019**, *25* (24), 6087–6091. https://doi.org/10.1002/chem.201806227.

(18) Unruh, D. K.; Burtner, A.; Pressprich, L.; Sigmon, G. E.; Burns, P. C. Uranyl Peroxide Closed Clusters Containing Topological Squares. *Dalt. Trans.* **2010**, *39* (25), 5807–5813. https://doi.org/10.1039/c0dt00074d.

(19) Ling, J.; Qiu, J.; Szymanowski, J. E. S.; Burns, P. C. Low-Symmetry Uranyl Pyrophosphate Cage Clusters. *Chem. Eur. J.* **2011**, *17* (9), 2571–2574. https://doi.org/10.1002/chem.201003481.

(20) Sigmon, G. E.; Burns, P. C. Rapid Self-Assembly of Uranyl Polyhedra into Crown Clusters. *J. Am. Chem. Soc.* **2011**, *133* (24), 9137–9139. https://doi.org/10.1021/ja2013449.

(21) Unruh, D. K.; Ling, J.; Qiu, J.; Pressprich, L.; Baranay, M.; Ward, M.; Burns, P. C. Complex Nanoscale Cage Clusters Built from Uranyl Polyhedra and Phosphate Tetrahedra. *Inorg. Chem.* **2011**, *50* (12), 5509–5516. https://doi.org/10.1021/ic200065y.

(22) Ling, J.; Ozga, M.; Stoffer, M.; Burns, P. C. Uranyl Peroxide Pyrophosphate Cage Clusters with Oxalate and Nitrate Bridges. *Dalt. Trans.* **2012**, *41* (24), 7278–7284. https://doi.org/10.1039/c2dt30229b.

(23) Ling, J.; Qiu, J.; Burns, P. C. Uranyl Peroxide Oxalate Cage and Core-Shell Clusters Containing 50 and 120 Uranyl Ions. *Inorg. Chem.* **2012**, *51* (4), 2403–2408. https://doi.org/10.1021/ic202380g.

(24) Qiu, J.; Ling, J.; Sui, A.; Szymanowski, J. E. S.; Simonetti, A.; Burns, P. C. Time-Resolved Self-Assembly of a Fullerene-Topology Core-Shell Cluster Containing 68 Uranyl Polyhedra. *J. Am. Chem. Soc.* **2012**, *134* (3), 1810–1816. https://doi.org/10.1021/ja210163b.

(25) Qiu, J.; Nguyen, K.; Jouffret, L.; Szymanowski, J. E. S.; Burns, P. C. Time-Resolved Assembly of Chiral Uranyl Peroxo Cage Clusters Containing Belts of Polyhedra. *Inorg. Chem.* **2013**, *52* (1), 337–345. https://doi.org/10.1021/ic3020817.

(26) Miro, P.; Ling, J.; Qiu, J.; Burns, P. C.; Gagliardi, L.; Cramer, C. J. Experimental and Computational Study of a New Wheel-Shaped \{{[}W5O21](3){[}((UO2)-O-VI)(2)(Mu-O-2)](3)}(30-) Polyoxometalate. *Inorg. Chem.* **2012**, *51* (16), 8784–8790. https://doi.org/10.1021/ic3005536.

(27) Peruski, K. M.; Bernales, V.; Dembowski, M.; Lobeck, H. L.; Pellegrini, K. L.; Sigmon, G. E.; Hickam, S.; Wallace, C. M.; Szymanowski, J. E. S.; Balboni, E.; et al. Uranyl Peroxide Cage Cluster Solubility in Water and the Role of the Electrical Double Layer. *Inorg. Chem.* **2017**, *56* (3), 1333–1339. https://doi.org/10.1021/acs.inorgchem.6b02435.

(28) Lobeck, H. L.; Isner, J. K.; Burns, P. C. Transformation of Uranyl Peroxide Studtite, {[}(UO2)(O-2)(H2O)(2)](H2O)(2), to Soluble Nanoscale Cage Clusters. *Inorg. Chem.* **2019**, *58* (10), 6781–6789. https://doi.org/10.1021/acs.inorgchem.9b00230.

(29) Armstrong, C. R.; Nyman, M.; Shvareva, T.; Sigmon, G. E.; Burns, P. C.; Navrotsky, A. Uranyl Peroxide Enhanced Nuclear Fuel Corrosion in Seawater. *Proc. Natl. Acad. Sci. U. S. A.* **2012**, *109* (6), 1874–1877. https://doi.org/10.1073/pnas.1119758109.

(30) Flynn, S. L.; Szymanowski, J. E. S.; Dembowski, M.; Burns, P. C.; Fein, J. B. Experimental Measurements of U24Py Nanocluster Behavior in Aqueous Solution. *Radiochim. ACTA* **2016**, *104* (12), 853–864. https://doi.org/10.1515/ract-2015-2493.

(31) Flynn, S. L.; Szymanowski, J. E. S.; Gao, Y.; Liu, T.; Burns, P. C.; Fein, J. B. Experimental Measurements of U60 Nanocluster Stability in Aqueous Solution. *Geochim. Cosmochim. Acta* **2015**, *156*, 94–105. https://doi.org/10.1016/j.gca.2015.02.021.

(32) Yu, Q.; Fein, J. B. Enzymatic Reduction of U60 Nanoclusters by Shewanella Oneidensis MR-1. *Radiochim. ACTA* **2018**, *106* (1), 21–30. https://doi.org/10.1515/ract-2017-2759.

(33) Wylie, E. M.; Peruski, K. M.; Prizio, S. E.; Bridges, A. N. A.; Rudisill, T. S.; Hobbs, D. T.; Phillip, W. A.; Burns, P. C. Processing Used Nuclear Fuel with Nanoscale Control of Uranium and Ultrafiltration. *J. Nucl. Mater.* **2016**, *473*, 125–130. https://doi.org/10.1016/j.jnucmat.2016.02.013.

(34) Wylie, E. M.; Peruski, K. M.; Weidman, J. L.; Phillip, W. A.; Burns, P. C. Ultrafiltration of Uranyl Peroxide Nanoclusters for the Separation of Uranium from Aqueous Solution.

*ACS Appl. Mater. Interfaces* **2014**, *6* (1), 473–479. https://doi.org/10.1021/am404520b.

(35) Liu, Y.; Czarnecki, A.; Szymanowski, J. E. S.; Sigmon, G. E.; Burns, P. C. Extraction of Uranyl Peroxo Clusters from Aqueous Solution by Mesoporous Silica SBA-15. *J. Radioanal. Nucl. Chem.* **2015**, *303* (3), 2257–2262. https://doi.org/10.1007/s10967-014-3740-7.

(36) Liu, Y.; Czarnecki, A.; Szymanowski, J. E. S.; Sigmon, G. E.; Burns, P. C. Extraction Behaviors of Uranyl Peroxo Cage Clusters by Mesoporous Silica SBA-15. *J. Radioanal. Nucl. Chem.* **2016**, *310* (1), 453–462. https://doi.org/10.1007/s10967-016-4801-x.

(37) Neal, H. A.; Szymanowski, J.; Fein, J. B.; Burns, P. C.; Nyman, M. Benchmarking Uranyl Peroxide Capsule Chemistry in Organic Media. *Eur. J. Inorg. Chem.* **2017**, *2017* (1), 39–46. https://doi.org/10.1002/ejic.201601219.

(38) Renier, O.; Falaise, C.; Neal, H.; Kozma, K.; Nyman, M. Closing Uranyl Polyoxometalate Capsules with Bismuth and Lead Polyoxocations. *Angew. Chemie - Int. Ed.* **2016**. https://doi.org/10.1002/anie.201607151.

(39) Xie, J. s; Neal, H. A.; Szymanowski, J.; Burns, P. C.; Alam, T. M.; Nyman, M.; Gagliardi, L. Resolving Confined Li-7 Dynamics of Uranyl Peroxide Capsule U-24. *Inorg. Chem.* **2018**, *57* (9), 5514–5525. https://doi.org/10.1021/acs.inorgchem.8b00474.

(40) Qiu, J.; Vlaisavljevich, B.; Jouffret, L.; Nguyen, K.; Szymanowski, J. E. S.; Gagliardi, L.; Burns, P. C. Cation Templating and Electronic Structure Effects in Uranyl Cage Clusters Probed by the Isolation of Peroxide-Bridged Uranyl Dimers. *Inorg. Chem.* **2015**, *54* (9), 4445–4455. https://doi.org/10.1021/acs.inorgchem.5b00248.

(41) Vlaisavljevich, B.; Gagliardi, L.; Burns, P. C. Understanding the Structure and Formation of Uranyl Peroxide Nanoclusters by Quantum Chemical Calculations. *J. Am. Chem. Soc.* **2010**, *132* (41), 14503–14508. https://doi.org/10.1021/ja104964x.

(42) Miro, P.; Vlaisavljevich, B.; Gil, A.; Burns, P. C.; Nyman, M.; Bo, C. Self-Assembly of Uranyl-Peroxide Nanocapsules in Basic Peroxidic Environments. *Chem. Eur. J.* **2016**, *22* (25), 8571–8578. https://doi.org/10.1002/chem.201600390.

(43) Dembowski, M.; Bernales, V.; Qiu, J.; Hickam, S.; Gaspar, G.; Gagliardi, L.; Burns, P. C. Computationally-Guided Assignment of Unexpected Signals in the Raman Spectra of Uranyl Triperoxide Complexes. *Inorg. Chem.* **2017**, *56* (3), 1574–1580. https://doi.org/10.1021/acs.inorgchem.6b02666.

(44) Miro, P.; Vlaisavljevich, B.; Dzubak, A. L.; Hu, S.; Burns, P. C.; Cramer, C. J.; Spezia, R.; Gagliardi, L. Uranyl-Peroxide Nanocapsules in Aqueous Solution: Force Field Development and First Applications. *J. Phys. Chem. C* **2014**, *118* (42), 24730–24740. https://doi.org/10.1021/jp504147s.

(45) Turner, K. M.; Szymanowski, J. E. S.; Zhang, F.; Lin, Y.; McGrail, B. T.; Mao, W. L.; Burns, P. C.; Ewing, R. C. Uranyl Peroxide Nanoclusters at High-Pressure. *J. Mater. Res.* **2017**, *32* (19), 3679–3688. https://doi.org/10.1557/jmr.2017.301.

(46) Sharifironizi, M.; Szymanowski, J. E. S.; Qiu, J.; Castillo, S.; Hickam, S.; Burns, P. C. Charge Density Influence on Enthalpy of Formation of Uranyl Peroxide Cage Cluster Salts. *Inorg. Chem.* **2018**, *57* (18), 11456–11462. https://doi.org/10.1021/acs.inorgchem.8b01300.

(47) Zhang, L.; Dembowski, M.; Arteaga, A.; Hickam, S.; Martin, N. P.; Zakharov, L. N.; Nyman, M.; Burns, P. C. Energetic Trends in Monomer Building Blocks for Uranyl Peroxide Clusters. *Inorg. Chem.* **2019**, *58* (1), 439–445. https://doi.org/10.1021/acs.inorgchem.8b02661.

(48) Liu, Z.; Liu, T.; Tsige, M. Elucidating the Origin of the Attractive Force among Hydrophilic Macroions. *Sci. Rep.* **2016**, *6*. https://doi.org/10.1038/srep26595.

(49) Li, H.; Shen, Y.; Yang, P.; Szymanowski, J. E. S.; Chen, J.; Gao, Y.; Burns, P. C.; Kortz, U.; Liu, T. Isotope and Hydrogen-Bond Effects on the Self-Assembly of Macroions in Dilute Solution. *Chem. Eur. J.* https://doi.org/10.1002/chem.201902444.

(50) Liu, Z.; Liu, T.; Tsige, M. Unique Symmetry-Breaking Phenomenon during the Self-Assembly of Macroions Elucidated by Simulation. *Sci. Rep.* **2018**, *8*. https://doi.org/10.1038/s41598-018-31533-z.

(51) Li, D.; Liu, Z.; Song, J.; Li, H.; Zhang, B.; Yin, P.; Zheng, Z. N.; Roberts, J. E.; Tsige, M.; Hill, C. L.; et al. Cation Translocation around Single Polyoxometalate-Organic Hybrid Cluster Regulated by Electrostatic and Cation-Pi Interactions. *Angew. CHEMIE-INTERNATIONAL Ed.* **2017**, *56* (12), 3294–3298. https://doi.org/10.1002/anie.201612008.

(52) Gao, Y.; Chen, J.; Zhang, T.; Szymanowski, J. E. S.; Burns, P. C.; Liu, T. Inhomogeneous Distribution of Cationic Surfactants around Anionic Molecular Clusters. *Chem. Eur. J.* https://doi.org/10.1002/chem.201903544.

(53) Chu, Y.; Chen, J.; Haso, F.; Gao, Y.; Szymanowski, J. E. S.; Burns, P. C.; Liu, T. Expanding the Schulze-Hardy Rule and the Hofmeister Series to Nanometer-Scaled Hydrophilic Macroions. *Chem. Eur. J.* **2018**, *24* (21), 5479–5483. https://doi.org/10.1002/chem.201706101.

(54) Gao, Y.; Haso, F.; Szymanowski, J. E. S.; Zhou, J.; Hu, L.; Burns, P. C.; Liu, T. Selective Permeability of Uranyl Peroxide Nanocages to Different Alkali Ions: Influences from Surface Pores and Hydration Shells. *Chem. Eur. J.* **2015**, *21* (51), 18785–18790. https://doi.org/10.1002/chem.201503773.

(55) Gao, Y.; Szymanowski, J. E. S.; Sun, X.; Burns, P. C.; Liu, T. Thermal Responsive Ion Selectivity of Uranyl Peroxide Nanocages: An Inorganic Mimic of K+ Ion Channels. *Angew. CHEMIE-INTERNATIONAL Ed.* **2016**, *55* (24), 6887–6891. https://doi.org/10.1002/anie.201601852.

(56) Soltis, J. A.; Wallace, C. M.; Penn, R. L.; Burns, P. C. Cation-Dependent Hierarchical Assembly of U60 Nanoclusters into Macro-Ion Assemblies Imaged via Cryogenic Transmission Electron Microscopy. *J. Am. Chem. Soc.* **2016**, *138* (1), 191–198.

https://doi.org/10.1021/jacs.5b09802.

(57) Oliveri, A. F.; Pilgrim, C. D.; Qiu, J.; Colla, C. A.; Burns, P. C.; Casey, W. H. Dynamic Phosphonic Bridges in Aqueous Uranyl Clusters. *Eur. J. Inorg. Chem.* **2016**, No. 6, 797–801. https://doi.org/10.1002/ejic.201600036.

(58) Dembowski, M.; Colla, C. A.; Hickam, S.; Oliveri, A. F.; Szymanowski, J. E. S.; Oliver, A. G.; Casey, W. H.; Burns, P. C. Hierarchy of Pyrophosphate-Functionalized Uranyl Peroxide Nanocluster Synthesis. *Inorg. Chem.* **2017**, *56* (9), 5478–5487. https://doi.org/10.1021/acs.inorgchem.7b00649.

(59) Johnson, R. L.; Ohlin, C. A.; Pellegrini, K.; Burns, P. C.; Casey, W. H. Dynamics of a Nanometer-Sized Uranyl Cluster in Solution. *Angew. CHEMIE-INTERNATIONAL Ed.* **2013**, *52* (29), 7464–7467. https://doi.org/10.1002/anie.201301973.

(60) Oliveri, A. F.; Colla, C. A.; Callahan, J. R.; Bogard, G.; Qiu, J.; Dembowski, M.; Burns, P. C.; Casey, W. H. Cation-Directed Isomerization of the U-28 Uranyl-Peroxide Cluster. *Eur. J. Inorg. Chem.* **2017**, No. 46, 5429–5433. https://doi.org/10.1002/ejic.201701074.

(61) Sadergaski, L. R.; Said, M.; Hixon, A. E. Calcium-Facilitated Aggregation and Precipitation of the Uranyl Peroxide Nanocluster U-60 in the Presence of Na-Montmorillonite. *Environ. Sci. Technol.* **2019**, *53* (9), 4922–4930. https://doi.org/10.1021/acs.est.8b06731.

(62) Sadergaski, L. R.; Stoxen, W.; Hixon, A. E. Uranyl Peroxide Nanocluster (U-60) Persistence and Sorption in the Presence of Hematite. *Environ. Sci. Technol.* **2018**, *52* (5), 3304–3311. https://doi.org/10.1021/acs.est.7b06510.

(63) Sadergaski, L. R.; Hixon, A. E. Kinetics of Uranyl Peroxide Nanocluster (U-60) Sorption to Goethite. *Environ. Sci. Technol.* **2018**, *52* (17), 9818–9826. https://doi.org/10.1021/acs.est.8b02716.

(64) Falaise, C.; Nyman, M. The Key Role of U28in the Aqueous Self-Assembly of Uranyl Peroxide Nanocages. *Chem. - A Eur. J.* **2016**. https://doi.org/10.1002/chem.201602130.

(65) Zhang, L.; Dzik, E. A.; Sigmon, G. E.; Szymanowski, J. E. S.; Navrotsky, A.; Burns, P. C. Experimental Thermochemistry of Neptunium Oxides: Np2O5 and NpO2. *J. Nucl. Mater.* **2018**, *501*, 398–403. https://doi.org/10.1016/j.jnucmat.2017.10.034.

(66) Guo, X.; Boukhalfa, H.; Mitchell, J. N.; Ramos, M.; Gaunt, A. J.; Migliori, A.; Roback, R. C.; Navrotsky, A.; Xu, H. Sample Seal-and-Drop Device and Methodology for High Temperature Oxide Melt Solution Calorimetric Measurements of PuO2. *Rev. Sci. Instrum.* **2019**, *90* (4). https://doi.org/10.1063/1.5093567.

(67) Maiorov, B.; Betts, J. B.; Soderlind, P.; Landa, A.; Hernandez, S. C.; Saleh, T. A.; Freibert, F. J.; Migliori, A. Elastic Moduli of Delta-Pu-239 Reveal Aging in Real Time. *J. Appl. Phys.* **2017**, *121* (12). https://doi.org/10.1063/1.4978509.

(68) Migliori, A.; Soderlind, P.; Landa, A.; Freibert, F. J.; Maiorov, B.; Ramshaw, B. J.; Betts, J. B. The Excited Delta-Phase of Plutonium. *Proc. Natl. Acad. Sci. U. S. A.* **2017**, *114* (3),

E269. https://doi.org/10.1073/pnas.1619207114.

(69) Ennaceur, S. M.; Migliori, A. Toward an Understanding of Aging in Plutonium from Direct Measurements of Stored Energy. *Philos. Mag. Lett.* **2018**, *98* (11), 502–510. https://doi.org/10.1080/09500839.2019.1583392.

(70) Migliori, A.; Soderlind, P.; Landa, A.; Freibert, F. J.; Maiorov, B.; Ramshaw, B. J.; Betts, J. B. Origin of the Multiple Configurations That Drive the Response of Delta-Plutonium's Elastic Moduli to Temperature. *Proc. Natl. Acad. Sci. U. S. A.* **2016**, *113* (40), 11158–11161. https://doi.org/10.1073/pnas.1609215113.

(71) Guo, X.; Szenknect, S.; Mesbah, A.; Clavier, N.; Poinssot, C.; Wu, D.; Xu, H.; Dacheux, N.; Ewing, R. C.; Navrotsky, A. Energetics of a Uranothorite (Th1-XUxSiO4) Solid Solution. *Chem. Mater.* **2016**, *28* (19), 7117–7124. https://doi.org/10.1021/acs.chemmater.6b03346.

(72) Shvareva, T. Y.; Fein, J. B.; Navrotsky, A. Thermodynamic Properties of Uranyl Minerals: Constraints from Calorimetry and Solubility Measurements. *Ind. Eng. Chem. Res.* **2012**, *51* (2), 607–613. https://doi.org/10.1021/ie2002582.

(73) Cahill, C. L.; Deifel, N. P.; Reusser, D.; Zhang, L.; Navrotsky, A. Thermochemical Properties of U(VI) Hybrid Materials Containing Uranyl Tetrachloride Anions. *J. Chem. Thermodyn.* **2017**, *114* (SI), 66–70. https://doi.org/10.1016/j.jct.2017.05.009.

(74) Hanken, B. E.; Shvareva, T. Y.; Gronbech-Jensen, N.; Stanek, C. R.; Asta, M.; Navrotsky, A. Energetics of Cation Mixing in Urania-Ceria Solid Solutions with Stoichiometric Oxygen Concentrations. *Phys. Chem. Chem. Phys.* **2012**, *14* (16), 5680–5685. https://doi.org/10.1039/c2cp40295e.

(75) Shvareva, T. Y.; Mazeina, L.; Gorman-Lewis, D.; Burns, P. C.; Szymanowski, J. E. S.; Fein, J. B.; Navrotsky, A. Thermodynamic Characterization of Boltwoodite and Uranophane: Enthalpy of Formation and Aqueous Solubility. *Geochim. Cosmochim. Acta* **2011**, *75* (18), 5269–5282. https://doi.org/10.1016/j.gca.2011.06.041.

(76) Szenknect, S.; Mesbah, A.; Cordara, T.; Clavier, N.; Brau, H.-P.; Le Goff, X.; Poinssot, C.; Ewing, R. C.; Dacheux, N. First Experimental Determination of the Solubility Constant of Coffinite. *Geochim. Cosmochim. Acta* **2016**, *181*, 36–53. https://doi.org/10.1016/j.gca.2016.02.010.

(77) Mesbah, A.; Szenknect, S.; Clavier, N.; Lozano-Rodriguez, J.; Poinssot, C.; Den Auwer, C.; Ewing, R. C.; Dacheux, N. Coffinite, USiO4, Is Abundant in Nature: So Why Is It So Difficult To Synthesize? *Inorg. Chem.* **2015**, *54* (14), 6687–6696. https://doi.org/10.1021/ic502808n.

(78) Deditius, A. P.; Pointeau, V.; Zhang, J. M.; Ewing, R. C. Formation of Nanoscale Th-Coffinite. *Am. Mineral.* **2012**, *97* (4), 681–693. https://doi.org/10.2138/am.2012.3951.

(79) Wang, S.; Alekseev, E. V; Stritzinger, J. T.; Depmeier, W.; Albrecht-Schmitt, T. E. How Are Centrosymmetric and Noncentrosymmetric Structures Achieved in Uranyl Borates?

*Inorg. Chem.* **2010**, *49* (6), 2948–2953. https://doi.org/10.1021/ic902480n.

(80) Wang, S.; Alekseev, E. V; Stritzinger, J. T.; Liu, G.; Depmeier, W.; Albrecht-Schmitt, T. E. Structure-Property Relationships in Lithium, Silver, and Cesium Uranyl Borates. *Chem. Mater.* **2010**, *22* (21), 5983–5991. https://doi.org/10.1021/cm1022135.

(81) Wang, S.; Alekseev, E. V; Depmeier, W.; Albrecht-Schmitt, T. E. Surprising Coordination for Plutonium in the First Plutonium(III) Borate. *Inorg. Chem.* **2011**, *50* (6), 2079–2081. https://doi.org/10.1021/ic200064n.

(82) Wang, S.; Yu, P.; Purse, B. A.; Orta, M. J.; Diwu, J.; Casey, W. H.; Phillips, B. L.; Alekseev, E. V; Depmeier, W.; Hobbs, D. T.; et al. Selectivity, Kinetics, and Efficiency of Reversible Anion Exchange with TcO4- in a Supertetrahedral Cationic Framework. *Adv. Funct. Mater.* **2012**, *22* (11), 2241–2250. https://doi.org/10.1002/adfm.201103081.

(83) Polinski, M. J.; Grant, D. J.; Wang, S.; Alekseev, E. V; Cross, J. N.; Villa, E. M.; Depmeier, W.; Gagliardi, L.; Albrecht-Schmitt, T. E. Differentiating between Trivalent Lanthanides and Actinides. *J. Am. Chem. Soc.* **2012**, *134* (25), 10682–10692. https://doi.org/10.1021/ja303804r.

(84) Polinski, M. J.; Cross, J. N.; Villa, E. M.; Lin, J.; Alekseev, E. V; Depmeier, W.; Albrecht-Schmitt, T. E. Synthesis of Divalent Europium Borate via in Situ Reductive Techniques. *Inorg. Chem.* **2013**, *52* (14), 8099–8105. https://doi.org/10.1021/ic400781x.

(85) Wang, S.; Alekseev, E. V; Diwu, J.; Miller, H. M.; Oliver, A. G.; Liu, G.; Depmeier, W.; Albrecht-Schmitt, T. E. Functionalization of Borate Networks by the Incorporation of Fluoride: Syntheses, Crystal Structures, and Nonlinear Optical Properties of Novel Actinide Fluoroborates. *Chem. Mater.* **2011**, *23* (11), 2931–2939. https://doi.org/10.1021/cm2004984.

(86) Wang, S.; Alekseev, E. V; Ling, J.; Skanthakumar, S.; Soderholm, L.; Depmeier, W.; Albrecht-Schmitt, T. E. Neptunium Diverges Sharply from Uranium and Plutonium in Crystalline Borate Matrixes: Insights into the Complex Behavior of the Early Actinides Relevant to Nuclear Waste Storage. *Angew. CHEMIE-INTERNATIONAL Ed.* **2010**, *49* (7), 1263–1266. https://doi.org/10.1002/anie.200906127.

(87) Wang, S.; Villa, E. M.; Diwu, J.; Alekseev, E. V; Depmeier, W.; Albrecht-Schmitt, T. E. Role of Anions and Reaction Conditions in the Preparation of Uranium(VI), Neptunium(VI), and Plutonium(VI) Borates. *Inorg. Chem.* **2011**, *50* (6), 2527–2533. https://doi.org/10.1021/ic102356d.

(88) Wang, S.; Alekseev, E. V; Depmeier, W.; Albrecht-Schmitt, T. E. Recent Progress in Actinide Borate Chemistry. *Chem. Commun.* **2011**, *47* (39), 10874–10885. https://doi.org/10.1039/c1cc14023j.

(89) Polinski, M. J.; Alekseev, E. V; Depmeier, W.; Albrecht-Schmitt, T. E. Recent Advances in Trivalent F-Element Borate Chemistry. *ZEITSCHRIFT FUR Krist. Mater.* **2013**, *228* (10, 2), 489–498. https://doi.org/10.1524/zkri.2013.1613.

(90) Wang, S.; Alekseev, E. V; Miller, H. M.; Depmeier, W.; Albrecht-Schmitt, T. E. Boronic Acid Flux Synthesis and Crystal Growth of Uranium and Neptunium Boronates and Borates: A Low-Temperature Route to the First Neptunium(V) Borate. *Inorg. Chem.* **2010**, *49* (21), 9755–9757. https://doi.org/10.1021/ic101678d.

(91) Rowland, C. E.; Cahill, C. L.; Post, J. E. The Structure of Braitschite, a Calcium Rare Earth Borate. *Am. Mineral.* **2011**, *96* (1), 197–201. https://doi.org/10.2138/am.2011.3592.

(92) Zhao, M.; Xu, Y.; Shuller-Nickles, L.; Amoroso, J.; Frenkel, A. I.; Li, Y.; Gong, W.; Lilova, K.; Navrotsky, A.; Brinkman, K. S. Compositional Control of Radionuclide Retention in Hollandite-Based Ceramic Waste Forms for Cs-Immobilization. *J. Am. Ceram. Soc.* **2019**, *102* (7), 4314–4324. https://doi.org/10.1111/jace.16258.

(93) Zhang, L.; Solomon, J. M.; Asta, M.; Navrotsky, A. A Combined Calorimetric and Computational Study of the Energetics of Rare Earth Substituted UO2 Systems. *ACTA Mater.* **2015**, *97*, 191–198. https://doi.org/10.1016/j.actamat.2015.06.048.

(94) Grote, R.; Zhao, M.; Shuller-Nickles, L.; Amoroso, J.; Gong, W.; Lilova, K.; Navrotsky, A.; Tang, M.; Brinkman, K. S. Compositional Control of Tunnel Features in Hollandite-Based Ceramics: Structure and Stability of (Ba,Cs)(1.33)(Zn,Ti)(8)O-16. *J. Mater. Sci.* **2019**, *54* (2), 1112–1125. https://doi.org/10.1007/s10853-018-2904-1.

(95) Chung, C.-K.; Shamblin, J.; O’Quinn, E. C.; Shelyug, A.; Gussev, I.; Lang, M.; Navrotsky, A. Thermodynamic and Structural Evolution of Dy2Ti2O7 Pyrochlore after Swift Heavy Ion Irradiation. *ACTA Mater.* **2018**, *145*, 227–234. https://doi.org/10.1016/j.actamat.2017.12.044.

(96) Alexandrov, V.; Gronbech-Jensen, N.; Navrotsky, A.; Asta, M. Theoretical Study of Mixing Energetics in Homovalent Fluorite-Structured Oxide Solid Solutions. *J. Nucl. Mater.* **2014**, *444* (1–3), 292–297. https://doi.org/10.1016/j.jnucmat.2013.10.001.

(97) Aizenshtein, M.; Shvareva, T. Y.; Navrotsky, A. Thermochemistry of Lanthana- and Yttria-Doped Thoria. *J. Am. Ceram. Soc.* **2010**, *93* (12), 4142–4147. https://doi.org/10.1111/j.1551-2916.2010.04001.x.

(98) Shvareva, T. Y.; Alexandrov, V.; Asta, M.; Navrotsky, A. Energetics of Mixing in ThO(2)-CeO(2) Fluorite Solid Solutions. *J. Nucl. Mater.* **2011**, *419* (1–3), 72–75. https://doi.org/10.1016/j.jnucmat.2011.08.002.

(99) Solomon, J. M.; Alexandrov, V.; Sadigh, B.; Navrotsky, A.; Asta, M. Computational Study of the Energetics and Defect Clustering Tendencies for Y- and La-Doped UO2. *ACTA Mater.* **2014**, *78*, 282–289. https://doi.org/10.1016/j.actamat.2014.06.052.

(100) Navrotsky, A. Thermodynamics of Solid Electrolytes and Related Oxide Ceramics Based on the Fluorite Structure. *J. Mater. Chem.* **2010**, *20* (47), 10577–10587. https://doi.org/10.1039/c0jm01521k.

(101) Alexandrov, V.; Gronbech-Jensen, N.; Navrotsky, A.; Asta, M. First-Principles Computational Study of Defect Clustering in Solid Solutions of ThO2 with Trivalent

Oxides. *Phys. Rev. B* **2010**, *82* (17). https://doi.org/10.1103/PhysRevB.82.174115.

(102) Alexandrov, V.; Shvareva, T. Y.; Hayun, S.; Asta, M.; Navrotsky, A. Actinide Dioxides in Water: Interactions at the Interface. *J. Phys. Chem. Lett.* **2011**, *2* (24), 3130–3134. https://doi.org/10.1021/jz201458x.

(103) Shelyug, A.; Navrotsky, A. Thermodynamic Stability of the Fluorite Phase in the CeO2 - CaO - ZrO2 System. *J. Nucl. Mater.* **2019**, *517*, 80–85. https://doi.org/10.1016/j.jnucmat.2019.01.043.

(104) Shelyug, A.; Palomares I, R.; Lang, M.; Navrotsky, A. Energetics of Defect Production in Fluorite-Structured CeO2 Induced by Highly Ionizing Radiation. *Phys. Rev. Mater.* **2018**, *2* (9). https://doi.org/10.1103/PhysRevMaterials.2.093607.

(105) Rittman, D. R.; Park, S.; Tracy, C. L.; Zhang, L.; Palomares, R. I.; Lang, M.; Navrotsky, A.; Mao, W. L.; Ewing, R. C. Structure and Bulk Modulus of Ln-Doped UO2 (Ln = La, Nd) at High Pressure. *J. Nucl. Mater.* **2017**, *490*, 28–33. https://doi.org/10.1016/j.jnucmat.2017.04.007.

(106) Shelyug, A.; Mesbah, A.; Szenknect, S.; Clavier, N.; Dacheux, N.; Navrotsky, A. Thermodynamics and Stability of Rhabdophanes, Hydrated Rare Earth Phosphates REPO4 Center Dot n H2O. *Front. Chem.* **2018**, *6*. https://doi.org/10.3389/fchem.2018.00604.

(107) Zhang, L.; Shelyug, A.; Navrotsky, A. Thermochemistry of UO2 - ThO2 and UO2 - ZrO2 Fluorite Solid Solutions. *J. Chem. Thermodyn.* **2017**, *114* (SI), 48–54. https://doi.org/10.1016/j.jct.2017.05.026.

(108) Solomon, J. M.; Shamblin, J.; Lang, M.; Navrotsky, A.; Asta, M. Chemical Ordering in Substituted Fluorite Oxides: A Computational Investigation of Ho2Zr2O7 and RE2Th2O7 (RE=Ho, Y, Gd, Nd, La). *Sci. Rep.* **2016**, *6*. https://doi.org/10.1038/srep38772.

(109) Solomon, J. M.; Navrotsky, A.; Asta, M. Energetics and Defect Clustering Trends for Trivalent Rare Earth Cations Substituted in UO2. *J. Nucl. Mater.* **2015**, *457*, 252–255. https://doi.org/10.1016/j.jnucmat.2014.11.089.

(110) Zhang, L.; Navrotsky, A. Thermochemistry of Rare Earth Doped Uranium Oxides Ln(x)U(1-x)O(2-0.5x+y) (Ln = La, Y, Nd). *J. Nucl. Mater.* **2015**, *465*, 682–691. https://doi.org/10.1016/j.jnucmat.2015.06.059.

(111) Chung, C.-K.; O'Quinn, E. C.; Neuefeind, J. C.; Fuentes, A. F.; Xu, H.; Lang, M.; Navrotsky, A. Thermodynamic and Structural Evolution of Mechanically Milled and Swift Heavy Ion Irradiated Er2Ti2O7 Pyrochlore. *ACTA Mater.* **2019**, *181*, 309–317. https://doi.org/10.1016/j.actamat.2019.09.022.

(112) Odoh, S. O.; Shamblin, J.; Colla, C. A.; Hickam, S.; Lobeck, H. L.; Lopez, R. A. K.; Olds, T.; Szymanowski, J. E. S.; Sigmon, G. E.; Neuefeind, J.; et al. Structure and Reactivity of X-Ray Amorphous Uranyl Peroxide, U2O7. *Inorg. Chem.* **2016**, *55* (7), 3541–3546. https://doi.org/10.1021/acs.inorgchem.6b00017.

(113) Chung, C.-K.; Lang, M.; Xu, H.; Navrotsky, A. Thermodynamics of Radiation Induced Amorphization and Thermal Annealing of Dy2Sn2O7 Pyrochlore. *ACTA Mater.* **2018**, *155*, 386–392. https://doi.org/10.1016/j.actamat.2018.06.003.

(114) Zhang, J.; Toulemonde, M.; Lang, M.; Costantini, J. M.; Della-Negra, S.; Ewing, R. C. C-60 and U Ion Irradiation of Gd2TixZr2-XO7 Pyrochlore. *J. Mater. Res.* **2015**, *30* (16), 2456–2466. https://doi.org/10.1557/jmr.2015.230.

(115) Tracy, C. L.; Lang, M.; Pray, J. M.; Zhang, F.; Popov, D.; Park, C.; Trautmann, C.; Bender, M.; Severin, D.; Skuratov, V. A.; et al. Redox Response of Actinide Materials to Highly Ionizing Radiation. *Nat. Commun.* **2015**, *6*. https://doi.org/10.1038/ncomms7133.

(116) Cureton, W. E.; Palomares I, R.; Tracy, C. L.; O'Quinn, E. C.; Walters, J.; Zdorovets, M.; Ewing, R. C.; Toulemonde, M.; Lang, M. Effects of Irradiation Temperature on the Response of CeO2, ThO2, and UO2 to Highly Ionizing Radiation. *J. Nucl. Mater.* **2019**, *525*, 83–91. https://doi.org/10.1016/j.jnucmat.2019.07.029.

(117) Shamblin, J.; Feygenson, M.; Neuefeind, J.; Tracy, C. L.; Zhang, F.; Finkeldei, S.; Bosbach, D.; Zhou, H.; Ewing, R. C.; Lang, M. Probing Disorder in Isometric Pyrochlore and Related Complex Oxides. *Nat. Mater.* **2016**, *15* (5), 507+. https://doi.org/10.1038/NMAT4581.

(118) O'Quinn, E. C.; Shamblin, J.; Perlov, B.; Ewing, R. C.; Neuefeind, J.; Feygenson, M.; Gussev, I.; Lang, M. Inversion in Mg1-XNixAl2O4 Spinel: New Insight into Local Structure. *J. Am. Chem. Soc.* **2017**, *139* (30), 10395–10402. https://doi.org/10.1021/jacs.7b04370.

(119) Tracy, C. L.; Park, S.; Rittman, D. R.; Zinkle, S. J.; Bei, H.; Lang, M.; Ewing, R. C.; Mao, W. L. High Pressure Synthesis of a Hexagonal Close-Packed Phase of the High-Entropy Alloy CrMnFeCoNi. *Nat. Commun.* **2017**, *8*. https://doi.org/10.1038/ncomms15634.

(120) Shamblin, J.; Tracy, C. L.; Palomares, R. I.; O'Quinn, E. C.; Ewing, R. C.; Neuefeind, J.; Feygenson, M.; Behrens, J.; Trautmann, C.; Lang, M. Similar Local Order in Disordered Fluorite and Aperiodic Pyrochlore Structures. *ACTA Mater.* **2018**, *144*, 60–67. https://doi.org/10.1016/j.actamat.2017.10.044.

(121) Rittman, D. R.; Teitelbaum, S. W.; Reis, D. A.; Mao, W. L.; Ewing, R. C. Anomalous Behavior of Nonequilibrium Excitations in UO2. *Phys. Rev. B* **2019**, *99* (13). https://doi.org/10.1103/PhysRevB.99.134307.

(122) Palomares I, R.; McDonnell, M. T.; Yang, L.; Yao, T.; Szymanowski, J. E. S.; Neuefeind, J.; Sigmon, G. E.; Lian, J.; Tucker, M. G.; Wirth, B. D.; et al. Oxygen Point Defect Accumulation in Single-Phase UO2+x. *Phys. Rev. Mater.* **2019**, *3* (5). https://doi.org/10.1103/PhysRevMaterials.3.053611.

## Archival Journal and Book Publications of EFRC

## Solely EFRC Papers


*1.* Unruh, D.K.; Burtner, A.; Pressprich, L.; Sigmon, G.E.; and Burns, P.C. Uranyl peroxide closed clusters containing topological squares. *Dalton Transactions*, **39**, 5807-5814 (2010).

*2.* Sigmon, G.E. and Burns, P.C. Crystal chemistry of new thorium nitrates and chromates. *Journal of Solid State Chemistry*, **183**, 1604-1608 (2010).

*3.* Ling, J.; Wallace, C.M.; Szymanowski, J.E.S.; and Burns, P.C. Hybrid uranium-oxalate fullerene topology cage clusters. *Angewandte Chem. International Edition*, **49**, 7271-7273 (2010). Rated Very Important Paper by journal.

*4.* Ling, J.; Qiu, J.; Sigmon, G.E.; Ward, M.; Szymanowski, J.E.S.; and Burns, P.C. Uranium pyrophosphate / methylenediphosphonate polyoxometalate cage clusters. *Journal of the American Chemical Society*, **38**, 13395-13402 (2010).

*5.* Aizenshtein, M.; Shvareva, T. Y.; and Navrotsky, A. Thermochemistry of lanthana and yttria doped thoria. *Journal of the American Ceramic Society*, **93**, 4142-4147 (2010).

*6.* Alexandrov, V.; Grønbech-Jensen, N.; Navrotsky, A.; and Asta, M. First-principles computational study of defect clustering in solid solutions of $ThO_2$ with trivalent oxides. *Physical Review B*, **82**. 174115, 1-8 (2010).

*7.* Nyman, M.; Rodriquez, M.A.; and Campana, C.F. Self-assembly of alkali-uranyl-peroxide clusters. *Inorganic Chemistry*, **49**, 7748-7755 (2010).

*8.* Navrotsky, A. Thermodynamics of solid electrolytes and related oxide ceramics based on the fluorite structure. *Journal of Materials Chemistry*, **20**, 10577-10587 (2010).

*9.* Lu, F.Y.; Zhang, J.; Navrotsky, A.; Ewing, R.C.; and Lian, J. Temperature and size effects on radiation-induced phase transformation in monoclinic nano-sized zirconia. *Microscopy and Microanalysis*, **16**, 1624-1625 (2010).

*10.* Lian, J.; Dong, Z.; Zhang, J.; Wang, L.; White, T.; and Ewing, R.C. Ion irradiation-induced amorphization in vanadate-phosphate apatites. *Microscopy and Microanalysis*, **16**, 1634-1635 (2010).

*11.* Unruh, D.K.; Ling. J.; Qiu, J.; Pressprich, L.; Baranay, M.; Ward, M.; and Burns, P.C. Complex nanoscale cage clusters built from uranyl polyhedra and phosphate tetrahedra. *Inorganic Chemistry*, **50**, 5509-5516 (2011).

*12.* Sigmon, G.E. and Burns, P.C. Rapid self-assembly of uranyl polyhedra into crown clusters. *Journal of the American Chemical Society*, **133**, 9137-9139 (2011).

*13.* Rák, Z.; Ewing, R.C.; and Becker, U. First-principles investigation of $Ca_3(Ti,Zr,Hf,Sn)_2Fe_2SiO_{12}$ garnet structure for incorporation of actinides. *Physical Review B*, **83**, 155123 (2011).

*14.* Harley, S. J.; Ohlin, C. A.; Johnson, R. L.; Panasci, A. F.; and Casey, W. H. The pressure dependence of oxygen-isotope-exchange rates between solution and apical oxygens on the $UO_2(OH)_4^{2-}$ ion. *Angewandte Chem. International Edition*, **50**, 4467-4469 (2011).

*15.* Gou, H.; Zhang, J.; Li, Z.; Wang, G.; Gao, F.; Ewing, R.C.; and Lian, J. Energetic stability, structural transition and electronic properties of $ZnSnO_3$. *Applied Physics Letters*, **98**, 091914 (2011).

*16.* Ling, J.; Qiu, J.; Szymanowski, J.E.S.; and Burns, P.C. Low-symmetry uranyl pyrophosphate cage clusters. *Chemistry – A European Journal*, **17**, 2571-2574 (2011).

*17.* Nyman, M.; Rodriquez, M.A.; and Alam, T.M. The $U_{28}$ Nanosphere: What's inside? *European Journal of Inorganic Chemistry*, **14**, 2197-2205 (2011). Web release March 3 2011 (cover) and was featured in Chem Views (European equivalent of C&E News).

*18.* Johnson, R.L; Harley, S.J.; Ohlin, C.A.; Panasci, A.F.; and Casey, W.H. Multinuclear NMR study of the pressure dependence for carbonate exchange in the $UO_2(CO_3)_3^{4-}$ (aq) ion. *ChemPhysChem*, **12**, 2903-2906 (2011).

*19.* Shvareva, T.; Alexandrov, V.; Asta, M.; and Navrotsky, A. Energetics of $ThO_2$ – $CeO_2$ fluorite solid solutions. *Journal of Nuclear Materials*, **419**, 72-75 (2011).

*20.* Ewing, R.C. Actinides and radiation effects: Impact on the back-end of the nuclear fuel cycle. *Mineralogical Magazine*, **75**, 2359-2377 (2011).

*21.* Villa, E.M.; Wang, S.; Alekseev, E.V.; Depmeier, W.; and Albrecht-Schmitt, T.E. Facile routes to Th(IV), U(IV), and Np(IV) phosphites and phosphates. *European Journal of Inorganic Chemistry*, **25**, 3749-3754 (2011).

*22.* Xiao, H. Y. and Weber, W. J. Pressure induced structural transformation in $Gd_2Ti_2O_7$ and $Gd_2Zr_2O_7$. *Journal of Physics: Condensed Matter*, **23**, 035501 (2011).

*23.* Xiao, H.Y. and Weber, W.J. Oxygen vacancy formation and migration in $Ce_xTh_{1-x}O_2$ ($0 \leq x \leq 1$) solid solution. *Journal of Physical Chemistry B*, **115**, 6524-6533 (2011).

*24.* Xiao, H.Y.; Zhang, Y.; and Weber, W.J. Trapping and diffusion of fission products in $ThO_2$ and $CeO_2$. *Journal of Nuclear Materials*, **414**, 464-470 (2011).

*25.* Zhang, Y.; Edmondson, P.D.; Varga, T.; Moll, S.; Namavar, F.; Lan, C.; and Weber, W.J. Structural modification of nanocrystalline ceria by ion beams. *Physical Chemistry Chemical Physics*, **13**, 11946-11950 (2011).

*26.* Edmondson, P.D.; Weber, W.J.; Namavar, F.; and Zhang, Y. Lattice distortions and oxygen vacancies produced in $Au^+$-irradiated nanocrystalline cubic zirconia. *Scripta Materialia*, **65**, 675-678 (2011).

*27.* Wang, J.; Zhang, F.X.; Lian, J.; Ewing, R.C.; and Becker, U. Energetics and concentration of defects in $Gd_2Ti_2O_7$ and $Gd_2Zr_2O_7$ pyrochlore at high-pressure. *Acta Materialia*, **59**, 1607-1618 (2011).

*28.* Ewing, R.C. Actinides in the nuclear fuel cycle: Role of mineralogy and geochemistry. Hallimond Lecture of the Mineralogical Society of Great Britain and Ireland. *Mineralogical Magazine*, **75**, 1-19 (2011).

*29.* Ewing, R.C. Safe management of actinides in the nuclear fuel cycle: Role of mineralogy. *Comptes Rendus Geoscience*, **343**, 219-229 (2011).

*30.* Zhang, F.X.; Lang. M.; Zhang, J.M.; Ewing, R.C. and Nyman, M. Structural changes of $(K,Gd)_2(Ta_2O_7)$ pyrochlore at high pressure. *Journal of Solid State Chemistry*, **184**, 2329-2332 (2011).

*31*. Rák, Z.; Ewing, R.C.; and Becker U. The role of Fe in the incorporation of actinides in ferric garnet matrices. *Physical Review B*, **84**, 155128 (2011).

*32.* Zhang, F.X.; Lang, M.; Liu, Zhenxian; Ewing, R.C. Phase stability of some actinides with brannerite structure at high pressures. *Journal of Solid State Chemistry*, **184**, 2834-2839 (2011).

*33.* Kerr, A.T. and Cahill, C.L. Crystal engineering with the uranyl cations III. Mixed aliphatic dicarboxylate/aromatic dipyridyl coordination polymers: Synthesis, structures, and speciation. *Crystal Growth and Design*, **11**, 5634-5641 (2011).

*34.* Alexandrov, V.; Shvareva, T.; Hayun, S.; Asta, M.; and Navrotsky, A. Actinide dioxides in water: Interactions at the interface. *Journal of Physical Chemistry Letters*, **2**, 3130-3134 (2011).

*35.* Burns, P.C. Nanoscale uranium-based cage clusters inspired by uranium mineralogy. *Mineralogical Magazine*, **75**, 1-25 (2011). (Invited, available online).

*36.* Shvareva, T.Y.; Mazeina, L.; Gorman-Lewis, D.; Burns, P.C.; Szymanowski, J.E.S.; Fein, J.B.; and Navrotsky, A. Thermodynamic characterization of boltwoodite and uranophane: Enthalpy of formation and aqueous solubility. *Geochimica et Cosmochimica Acta*, **75**, 5269-5282 (2011).

*37.* Jouffret, L.J.; Krivovichev, S.V.; and Burns, P.C. Polymorphism in alkali metal uranyl nitrates: Synthesis and crystal structure of gamma-$K(UO_2)(NO_3)_3$. *Zeitschrift Fur Anorganishe Allegemene Chemie*, **637**, 1475-1480 (2011).

*38.* Shvareva, T.Y.; Fein, J.B.; and Navrotsky, A. Thermodynamic properties of uranyl minerals: Constraints from calorimetry and solubility measurements. *Industrial & Engineering Chemistry Research*, **51**, 605-611 (2012).

*39.* Lu, F.; Lang, M.K.; Huang, M.; Namavar, F.; Trautmann, C.; Ewing, R.C.; and Lian, J. ZrSi formation at ZrN/Si interface induced by ballistic and ionizing radiations. *Nuclear Instruments and Methods in Physics Research B*, **286**, 266-270 (2012).

*40.* Edmondson, P.D.; Weber, W.J.; Namavar, F.; and Zhang, Y. Determination of the displacement energy of O, Si, and Zr under electron beam irradiation. *Journal of Nuclear Materials*, **422**, 86-91 (2012).

*41.* Deditius, A.P.; Pointeau, V.; Zhang, J.M.; and Ewing, R.C. Formation of nanoscale Th-coffinite. *American Mineralogist*, **97**, 681-683 (2012).

*42.* Lang, M.K.; Zhang, F.; Li, W.; Severin, D.; Bender, M.; Klaumunzer, S.; Trautmann, C.; and Ewing, R.C. Swift heavy ion-induced amorphization of $CaZrO_3$ perovskite. *Nuclear Instruments and Methods in Physics Research B*, **286**, 271-276 (2012).

*43.* Li, W.; Lang, M.K.;Gleadow, A.J.W.; Zdorovets, M.V.; and Ewing, R.C. Thermal annealing of unetched fission tracks in apatite. *Earth and Planetary Science Letters*, **321-322**, 121-127 (2012).

*44.* Armstrong, C.R.; Nyman, M.; Shvareva, T.; Sigmon, G.E.; Burns, P.C.; and Navrotsky, A. Uranyl peroxide enhanced nuclear fuel corrosion in seawater. *Proceedings of the National Academy of Sciences of the United States of America*, **109**, 1874-1877 (2012).

*45.* Burns, P.C.; Ewing, R.C.; and Navrotsky, A. Nuclear fuel in a reactor accident. *Science*, **335**, 1184-1188 (2012).

*46.* Ling, J.; Qiu, J.; and Burns, P.C. Uranyl peroxide oxalate cage and core-shell clusters containing 50 and 120 uranyl ions. *Inorganic Chemistry*, **51**, 2403-2408 (2012).

*47.* Qiu, J.; Ling, J.; Sui, A.; Szymanowski, J.E.S.; Simonetti, A.; and Burns, P.C. Time-resolved self-assembly of a fullerene-topology core-shell cluster containing 68 uranyl polyhedra. *Journal of the American Chemical Society*, **134**, 1810-1816 (2012).

*48.* Wang, S.; Yu, P.; Purse, B.A.; Orta, M.J.; Diwu, J.; Casey, W.H.; Phillips, B.L.; Alekseev, E.V.; Depmeier, W.; Hobbs, D.T.; and Albrecht-Schmitt, T.E. Selectivity, kinetics, and efficiency of reversible anion exchange with $TcO_4^-$ in a supertetrahedral cationic framework. *Advanced Functional Materials*, **22**, 2241-2250 (2012). DOI: 10.1002/adfm.201103081. The

press release went viral and resulted in a series of interviews by various popular science magazines, newspaper articles around the world (India and Belgium for example), and radio talk show interviews.

*49.* Laverov, N.P.; Yudintsev, S.V.; Stefanovsky, S.V.; and Ewing, R.C. Phase composition and radiation stability of matrices for isolation of REE-actinide waste. *Doklady Akademii Nauk*, **443**(6), pp. 726-731 [in Russian]; *Doklady Earth Sciences – Geochemistry*, **443** (2) 526-531 [English] (2012).

*50.* Nelson, A.G.D.; Alekseev, E.; Ewing, R.C.; and Albrecht-Schmitt, T.E. Barium uranyl diphosphonates. *Journal of Solid State Chemistry*, **192**, 153-160 (2012).

*51.* Ling, J.; Ozga, M.; Stoffer, M.; and Burns, P.C. Uranyl peroxide pyrophosphate cage clusters with oxalate and nitrate bridges. *Dalton Transactions*, **41**, 7278-7284 (2012).

*52.* Edmondson, P.D.; Zhang, Y.; Moll, S.; Varga, T.; Namavar, F.; and Weber, W.J. Anomalous grain growth in the surface region of a nanocrystalline $CeO_2$ film under low-temperature heavy ion irradiation. *Physical Review B,* **85**, 214113 (2012).

*53.* Zhang, F.X.; Lang, M.; Zhang, J.M.; Cheng, Z.Q.; Liu, Z.X.; Lian, J.; and Ewing, R.C. Phase transition and abnormal compressibility of lanthanide silicate with the apatite structure. *Physical Review B*, **85**, 214116 (2012).

*54.* Xiao, H.Y.; Zhang, Y.; and Weber, W.J. *Ab initio* molecular dynamics simulations of low-energy recoil events in $ThO_2$, $CeO_2$, and $ZrO_2$. *Physical Review B*, **86**, 054109 (2012).

*55.* Edmondson, P.D.; Zhang, Y.; Moll, S.; Namavar, F.; and Weber, W.J. Irradiation effects on microstructure change in nanocrystalline ceria – Phase, lattice stress, grain size and boundaries. *Acta Materialla*, **60**, 5408-5416 (2012).

*56.* Rai, N.; Tiwari, S.P.; and Maginn, E.J. Force field development for actinyl ions via quantum mechanical calculations: An approach to account for many body solvation effects. *Journal of Physical Chemistry B*, **116**, 10885-10897 (2012).

*57.* Lu, F.Y.; Huang, M.B.; Yaqoob, F.; Lang, M.; Namavar, F.; Trautmann, C.; Sun, H.T.; Ewing, R.C.; and Lian, J. Displacive radiation-induced structural contraction in nanocrystalline ZrN. *Applied Physics Letters*, **101**, 041904 (2012).

*58.* Nyman, M. and Burns, P.C. A comprehensive comparison of transition-metal and actinyl polyoxometalates. *Chemical Society Reviews*, **41**, 7354-7367 (2012).

*59.* Tracy, C.L.; Lang, M.; Zhang, J.M.; Zhang, F.X.; Wang Z.W.; and Ewing, R.C. Structural response of $A_2TiO_5$ (A = La, Nd, Sm, Gd) to swift heavy ion irradiation. *Acta Materialia*, **60**, 4477-4486 (2012).

*60.* Zhang, F.X.; Lang, M.; Zhang, J.M.; and Ewing, R.C. Swift heavy ion irradiation of diamond powder. *Nuclear Instruments and Methods in Physics Research B*, **286**, 262-265 (2012).

*61.* Grant, D.J.; Weng, Z.H.; Jouffret, L.J.; Burns, P.C.; and Gagliardi, L. Synthesis of a uranyl persulfide complex and quantum chemical studies of formation and topologies of hypothetical uranyl persulfide cage clusters. *Inorganic Chemistry*, **51**, 7801-7809 (2012).

*62.* Cross, J.N.; Villa, E.M.; Wang, S.A.; Diwu, J.; Polinski, M.J.; and Albrecht-Schmitt, T.E. Syntheses, structures, and spectroscopic properties of plutonium and americium phosphites and the redetermination of the ionic radii of Pu(III) and Am(III). *Inorganic Chemistry*, **51**, 8419-8424 (2012).

*63.* Jouffret, L.J.; Wylie, E.M.; and Burns, P.C. Influence of the organic species and oxoanion in the synthesis of two uranyl sulfate hydrates, $(H_3O)_2[(UO_2)_2(SO_4)_3(H_2O)]\cdot 7\ H_2O$ and $(H_3O)_2[(UO_2)_2(SO_4)_3(H_2O)]\cdot 4\ H_2O$, and a uranyl selenate-selenite $[C_5H_6N][(UO_2)(SeO_4)(HSeO_3)]$. *Zeitschrift Fur Anorganische Und Allegemeine Chemie*, **638**, 1796-1803 (2012).

*64.* Lin, J.; Diwu, J.; Cross, J.N.; Villa, E.M.; and Albrecht-Schmitt, T.E. Cerium (IV) tellurite halides $[Ce_2Te_7O_{17}]X_2$, X = $Cl^-$ or $Br^-$): The first cerium-containing cationic frameworks. *Inorganic Chemistry*, **51**, 10083-10085 (2012).

*65.* Lin, J.; Cross, J.N.; Diwu, J.; Polinski, M.J.; Villa, E.M.; and Albrecht-Schmitt, T.E. Unusual coordination for plutonium (IV), cerium (IV), and zirconium (IV) in the cationic layered materials $[M_2Te_4O_{11}]X_2$ (M = Pu, Ce, Zr; X = Cl, Br). *Inorganic Chemistry*, **51**, 11949-11954 (2012).

*66.* Nyman, M. and Alam, T.M. Dynamics of uranyl peroxide nanocapsules. *Journal of the American Chemical Society*, **134**, 20131-20138 (2012).

*67.* Rák, Z.; Ewing, R.C.; and Becker, U. Hydroxylation-induced surface stability of $AnO_2$ (An = U, Np, Pu) from first-principles. *Surface Science*, **608**, 180-187 (2012).

*68.* Villa, E.M.; Marr, C.J.; Jouffret, L.J.; Alekseev, E.V.; Depmeier, W.; and Albrecht-Schmitt, T.E. Systematic evolution from uranyl (VI) phosphites to uranium (VI) phosphates. *Inorganic Chemistry*, **51**, 6548-6558 (2012).

*69.* Jouffret, L.; Wylie, E.M.; and Burns, P.C. Amine templating effect absent in uranyl sulfates synthesized with 1,4-diaminobutane. *Journal of Solid State Chemistry*, **197**, 160-165 (2013).

*70.* Qiu, J. and Burns, P.C. Clusters of actinides with oxide, peroxide, or hydroxide bridges. *Chemical Reviews*, **113**, 1097-1120 (2013). DOI: 10.1021/cr300159x.

*71.* Qiu, J.; Nguyen, K.; Jouffret, L.J.; Szymanowski, J.E.S.; and Burns, P.C. Time resolved assembly of chiral uranyl peroxo cage clusters containing belts of polyhedra. *Inorganic Chemistry*, **52**, 337-345 (2013). DOI**:** 10.1021/ic3020817.

*72.* Xiao, H.Y.; Zhang, Y.; and Weber, W.J. Thermodynamic properties of $Ce_xTh_{1-x}O_2$ solid solution from first-principles calculations. *Acta Materialia*, **61**, 467-476 (2013).

*73.* Nelson, A-G. D.; Alekseev, E.V.; Albrecht-Schmitt, T.E.; and Ewing, R.C. Uranium diphosphonates template by interlayer organic amines. *Journal of Solid State Chemistry*, **198**, 270-278 (2013).

*74.* Villa, E.M.; Marr, C.J.; Diwu, J.; Alekseev, E.V.; Depmeier, W.; and Albrecht-Schmitt, T.E. From order to disorder and back again: *In situ* hydrothermal redox reactions of uranium phosphites and phosphates. *Inorganic Chemistry*, **52**, 965-973 (2013). DOI: 10.1021/ic302198w.

*75.* Polinski, M.J.; Alekseev, E.V.; Depmeier, W.; and Albrecht-Schmitt. Recent Advances in Trivalent *f*-element borate chemistry. *Z. Kristallogr*., **228**, 489-498 (2013). DOI: 10.1524/zkri.2013.1613.

*76.* Wang, J.W.; Lang, M.; Ewing, R.C.; and Becker, U. Multi-scale simulation of structural heterogeneity of swift-heavy ion tracks in complex oxides. *Journal of Physics: Condensed Matter*, **25**, 135001 (2013).

*77.* Rák, Z.; Ewing, R.C.; and Becker, U. Ferric garnet matrices for immobilization of actinides. *Journal of Nuclear Materials*, **436,** 1-7 (2013).

*78.* Zhang, J.M.; Zhang, F.X.; Lang, M; Lu, F.; Lian, J.; and Ewing, R.C. Ion irradiation-induced structural transitions in orthorhombic $Ln_2TiO_5$. *Acta Materialia*, **61**, 4191-4199 (2013).

*79.* Villa, E.M.; Alekseev, E.V.; Depmeier, W.; and Albrecht-Schmitt, T.E. Syntheses, structures, and comparisons of thallium uranium phosphites, mixed phosphate-phosphite, and phosphate. *Crystal Growth and Design*, **13**, 1721-1729 (2013).

*80.* Liao, Z.; Reinke, L.R.; Szymanowski, J.E.S.; Sigmon, G.E.; and Burns, P.C. Cage clusters built from uranyl ions bridged through peroxo and 1-hydroxyethane-1,1-diphosphonic acid ligands. *Dalton Transactions*, **42**, 6793-6802 (2013). DOI: 10.1039/C3DT33025G.

*81.* Alessi, D.S.; Szymanowksi, J.E.S.; Forbes, T.Z.; Quicksall, A.N.; Sigmon, G.E.; Burns, P.C.; and Fein, F.B. Mineralogic controls on aqueous neptunium (V) concentrations in silicate systems. *Journal of Nuclear Materials*, **433**, 233-239 (2013).

*82.* Lu, F.; Shen, Y.; Dong, Z.; Navrotsky, A.; Ewing, R.C.; and Lian, J. Size dependence of radiation-induced amorphization and recrystallization of synthetic nanostructured $CePO_4$ monazite. *Acta Materialia*, **61**, 2984-2992 (2013). (Highlighted by DOE EFRC Frontiers in Energy Research addressing the Fifth Grand Challenge for Science in the $21^{st}$ Century "Mastering Materials Far from Equilibrium).

*83.* Hughes, J.T.; Bennett, T.D.; Cheetham, A.K.; and Navrotsky, A. Thermochemistry of zeolitic imidazolate frameworks (ZIF) with varying porosity. *Journal of the American Chemical Society*, **135**, 598-601 (2013).

*84.* Thangavelu, S.G.; Andrews, M.B.; Pope, S.J.A.; and Cahill, C.L. Synthesis, structures, and luminescent properties of uranyl terpyridine aromatic carboxylate coordination polymers. *Inorganic Chemistry*, **52**, 2060-2069 (2013). DOI: 10.1021/ic3024698.

*85.* Edmondson, P.D.; Young, N.P.; Parish, C.M.; Moll, S.; Namavar, F.; Weber, W.J.; and Zhang, Y. Ion-beam-induced chemical mixing at a nanocrystalline $CeO_2$-Si interface. *Journal of the American Ceramic Society*, **96**, 1666-1672 (2013).

*86.* Moll, S.; Zhang, Y.; Zhu, Z.; Edmondson, P.D.; Namavar, F.; and Weber, W.J. Comparison between simulated and experimental Au-ion profiles implanted in nanocrystalline ceria. *Nuclear Instruments and Methods in Physics Research B*, **307**, 93-97 (2013).

*87.* Adelani, P.O.; Ozga, M.; Wallace, C.M.; Qiu, J.; Szymanowski, J.E.S.; Sigmon, G.E.; and Burns, P.C. Hybrid uranyl-carboxyphosphonate cage clusters. *Inorganic Chemistry*, **52**, 7673-7679 (2013).

*88.* Wang, J.W.; Ewing, R.C.; and Becker, U. Electronic structure and stability of hyperstoichiometric $UO_{2+x}$ under pressure. *Physical Review B*, **88**, 024109 (2013).

*89.* Villa, E.M.; Diwu, J.; Alekseev, E.V.; Depmeier, W.; and Albrecht-Schmitt, T.E. Structural changes within the alkaline earth uranyl phosphites. *Dalton Transactions*, **13**, 9637-9644 (2013).

*90.* Cantos, P.M.; Jouffret, L.J.; Wilson, R.E.; Burns, P.C.; and Cahill, C.L. Series of uranyl-4,4'-biphenyldicarboxylates and an occurrence of a cation-cation interaction: Hydrothermal synthesis and *in situ* Raman studies. *Inorganic Chemistry*, **52**, 9487-9495 (2013).

*91.* Johnson, R.L.; Ohlin, C.A.; Pellegrini, K.; Burns, P.C.; and Casey, W.H. A nanometer-size uranyl cluster equilibrates with other metastable structures in solution. *Angewandte Chem. International Edition*, **52**, 7464-7467 (2013).

*92.* Rák, Z.; Ewing, R.C.; and Becker, U. Electronic structure and thermodynamic stability of uranium-doped yttrium iron garnet (YIG). *Journal of Physics: Condensed Matter*, **25**, 495502 (2013).

*93.* Aidhy, D.; Zhang, Y.; and Weber, W.J. Stabilizing nanocrystalline grains in ceramic-oxides. *Physical Chemistry Chemical Physics*, **15**, 18915-18920 (2013).

*94.* Zhang, F.X.; Xiao, H.Y.; Lang, M.; and Ewing, R.C. Structure and properties of rare earth silicates with the apatite structure at high pressure. *Physics and Chemistry of Minerals*, **40**, 817-825 (2013).

*95.* Liu, B.; Xiao, H.Y.; Zhang, Y.; and Weber, W.J. *Ab initio* molecular dynamics simulations of overlapping recoil events in $ThO_2$. *Journal of Physics: Condensed Matter*, **25**, 395004 (2013).

*96.* Xiao, H.Y.; Zhang, Y.; and Weber, W.J. Stability and migration of charged oxygen interstitials in $ThO_2$ and $CeO_2$. *Acta Materialia*, **61**, 7639-7645 (2013).

*97.* Hughes, J.T.; Sava, D.F.; Nenoff, T.M.; and Navrotsky, A. Thermochemical evidence for strong iodine chemisorption by ZIF-8. *Journal of the American Chemical Society*, **135**, 16256-16259 (2013).

*98.* Bhunia, M.K.; Hughes, J.T.; Fettinger, J.C.; and Navrotsky, A. Thermochemistry of paddle wheel MOFs: Cu-HKUST-1 and Zn-HKUST-1. *Langmuir*, **29**, 8140-8145 (2013).

*99.* Lin, J.; Cross, J.N.; Diwu, J.; Meredith, N.; Albrecht-Schmitt, T.E. Comparisons of plutonium, thorium, and cerium tellurite sulfates. *Inorganic Chemistry*, **52**, 4277-4281 (2013).

*100.* Lin, J.; Diefenbach, K.; Cross, J.N.; Babo, J.M.; and Albrecht-Schmitt, T.E. Thermochromism, the alexandrite effect, and dynamic Jahn-Teller distortions in $Ho_2Cu(TeO_3)_2(SO_4)_2$. *Inorganic Chemistry*, **52**, 13278-13281 (2013).

*101.* Cantos, P.M.; Pope, S.J.A.; and Cahill, C.L. An exploration of homo- and heterometallic $UO_2^{2+}$ hybrid materials containing chelidamic acid: Synthesis, structure, and luminescence studies. *CrystEngComm*, **15**, 9039-9051 (2013).

*102*. Wang, J.W. and Becker, U. Activation energetics of actinide diffusion in $UO_2$ from first-principles calculations. *Journal of Nuclear Materials*, **433**, 424-430 (2013).

*103*. Guo, X.; Tavakoli, A.H.; Sutton, S.; Kukkadapu, R.; Qi, L.; Lanzirotti, A.; Newville, M.; Asta, M.; and Navrotsky, A. Cerium substitution in yttrium iron garnet: Valence state, structure, and energetics. *Chemistry of Materials*, **26**, 1133-1143 (2014*)*. DOI: 10.1021/cm403444f.

*104*. Wylie, E.M.; Peruski, K.M.; Weidman, J.L.; Phillip, W.A.; and Burns, P.C. Ultrafiltration of uranyl peroxide nanoclusters for the separation of uranium from aqueous solution. *ACS Applied Materials and Interfaces*, **6**, 473-479 (2014). DOI: 10.1021/am404520b.

*105*. Alexandrov, V.; Gronbech-Jensen, N.; Navrotsky, A.; and Asta, M. Theoretical study of mixing energetics in homovalent fluorite-structured oxide solid solutions. *Journal of Nuclear Materials*, **444**, 292-297 (2014).

*106*. McGrail, B.; Sigmon, G.E.; Jouffret, L.J.; Andrews, C.; and Burns, P.C. Raman spectroscopic and ESI-MS characterization of uranyl peroxide cage clusters. *Inorganic Chemistry*, **53**, 1562-1569 (2014).

*107*. Qiu, J.; Ling, J.; Jouffret, L.J.; Thomas, R.; Szymanowski, J.E.S.; and Burns, P.C. Water-soluble multi-cage super tetrahedral uranyl peroxide phosphate clusters. *Chemical Science*, **5**, 303-310 (2014). DOI: 10.1039/C3SC52357H.

*108*. Tracy, C.L.; Pray, J.M.; Lang, M.; Popov, D.; Park, C.; Trautmann, C.; and Ewing, R.C. Defect accumulation in $ThO_2$ irradiated with swift heavy ions. *Nuclear Instruments and Methods B*, **326**, 169-173 (2014). DOI: 10.1016/j.nimb.2013.08.070.

*109*. Park, S.; Lang, M.; Tracy, C.L.; Zhang, J.; Zhang, F.; Trautmann, C.; Kluth, P.; Rodriguez, M.D.; and Ewing, R.C. Swift heavy ion irradiation-induced amorphization of $La_2Ti_2O_7$. *Nuclear Instruments and Methods B*, **326**, 145-149 (2014). DOI: 10.1016/j.nimb.2013.10.088.

*110*. Aidhy, D.S.; Zhang, Y.; and Weber, W.J. Strained ionic interfaces: Effect on oxygen diffusivity from atomistic simulations. *Journal of Physical Chemistry C*, **118**, 4207-4212 (2014).

*111*. Aidhy, D.S.; Zhang, Y.; and Weber, W.J. Impact of segregation energetics on oxygen conductivity at ionic grain boundaries. *Journal of Materials Chemistry A*, **2**, 1704-1709 (2014).

*112*. Lin, J.; Chai, P.; Diefenbach, K.; Shatruk, M.; and Albrecht-Schmitt, T.E. Challenges in the search for magnetic coupling in 3*d*-4*f* materials: Syntheses, structures, and magnetic properties of the lanthanide copper heterobimetallic compounds, $RE_2Cu(TeO_3)_2(SO_4)_2$. *Chemical Materials*, **26**, 2187-2194 (2014).

*113*. Eaton, T.; Lin, J.; Cross, J.N.; Stritzinger, J.T.; and Albrecht-Schmitt, T.E. $Th(VO_3)_2(SeO_3)$ and $Ln(VO_3)_2(IO_3)$ (Ln = Ce, Pr, Nd, Sm, and Eu): Unusual cases of aliovalent substitution. *Chemical Communications*, **50**, 3668-3670 (2014).

*114*. Cross, J.N.; Cary, S.K.; Stritzinger, J.T.; Polinski, M.J.; and Albrecht-Schmitt, T.E. Synthesis and spectroscopy of new plutonium (III) and -(IV) molybdates: Comparisons of electronic characteristics. *Inorganic Chemistry*, **53**, 3148-3152 (2014).

*115*. Kerr, A.T. and Cahill, C.L. Post synthetic rearrangement/metalation as a route to bimetallic uranyl coordination polymers: Syntheses, structures, and luminescence. *Crystal Growth and Design*, **14**, 1914-1921 (2014). DOI: 10.1021/cg500050q.

*116*. Carter, K.P.; Pope, S.J.A.; and Cahill, C.L. A series of Ln-p-chlorobenzoic acid-terpyridine complexes: Lanthanide contraction effects, supramolecular interactions and luminescent behavior. *CrystEngComm*, **16**, 1873-1884 (2014).

*117*. Cantos, P.M. and Cahill, C.L. Poly[diammonium [diaqua([mu]7-benzene-1,2,3,4,5,6-hexacarboxylato)tetraoxidodiuranium(VI)]]. *Acta Crystallograhic, Section E: Structural Rep. Online*, **70**, m142-m143 (2014). DOI: 10.1107/S1600536814006047.

*118*. Wang, J.; Ewing, R.C.; and Becker, U. Average structure and local configuration of excess oxygen in $UO_{2+x}$. *Scientific Reports*, **4**, 4216 (2014). DOI: 10.1038/srep04216. Open-access journal supported by Nature (www.nature.com/scientificreports).

*119*. Zhang, F.X.; Lang, M.; Wang, J.M.; Li, W.X.; Sun, K.; Prakapenka, V.; and Ewing, R.C. High-pressure $U_3O_8$ with the fluorite-type structure. *Journal of Solid State Chemistry*, **213**, 110-115 (2014).

*120*. Tiwari, S.P.; Rai, N.; Maginn, E.J. Dynamics of actinyl ionic in water: A molecular dynamics simulation study. *Physical Chemistry Chemical Physics*, **16**, 8060-8069 (2014). DOI: 10.1039/c3cp54556c.

*121*. Zhang, Y.; Aidhy, D.S.; Varga, T.; Moll, S.; Edmondson, P.D.; Namavar, F.; Jin, K.; Ostrouchov, C. N.; and Weber, W.J. The effect of electronic energy loss on irradiation-induced grain growth in nanocrystalline oxides. *Physical Chemistry Chemical Physics*, **16**, 8051-8059 (2014). DOI: 10.1039/c4cp00392f.

*122*. Oh, G. and Burns, P.C. Solid-state actinide acid phosphites from phosphorous acid melts. *Journal of Solid State Chemistry*, **215**, 50-56 (2014).

*123*. Alam, T.M.; Liao, Z.; Zakhavor, L.N.; and Nyman, M. Solid-state dynamics of uranyl polyoxometalates. *Chemistry – A European Journal*, **20**, 8302-8307 (2014). DOI: 10.1002/chem.201402351.

*124*. Aidhy, D.S.; Zhang, Y.; and Weber, W.J. A fast grain-growth mechanism revealed in nanocrystalline ceramic oxides. *Scripta Materialia*, **83**, 9-12 (2014). DOI: 10.1016/j.scriptamat.2014.03.020.

*125*. Cross, J.N.; Villa, E.M.; Darling, V.R.; Polinski, M.J.; Lin, J.; Tan, X.; Kikugawa, N.; Shatruk, J.; Baumbach, R.E.; and Albrecht-Schmitt, T.E. Straightforward reductive routes to air-stable uranium (III) and neptunium (III) materials. *Inorganic Chemistry*, **53**, 7455-7466 (2014). DOI: 10.1021/ic500771t.

*126*. Cantos, P.M. and Cahill, C.L. A family of $UO_2^{2+}$-5-Nitro-1,3-dicarboxylate hybrid materials: Structural variation as a function of pH and structure directing species. *Crystal Growth and Design*, **14**, 3044-3053 (2014). DOI: 10.1021/cg500304d.

*127*. Kerr, A.T. and Cahill, C.L. CuPYDC metalloligands and postsynthetic rearrangement/metalation as routes to bimetallic uranyl containing hybrid materials: Syntheses, structures, and fluorescence. *Crystal Growth and Design*, **14**, 4094-4103 (2014). DOI: 10.1021/cg5007132.

*128*. Wang, J.W.; Ewing, R.C.; Becker, U. Defect formation energy in pyrochlore: The effect of crystal size. *Materials Research Express*, **1**, 035501 (2014) DOI: 10.1088/2053-1591/1/3/035501.

*129*. Carter, K.P.; Zulato, C.; and Cahill, C.L. Exploring supramolecular assembly and luminescent behavior in a series of RE-p-chlorobenzoic acid-1,10-phenanthroline complexes. *CrystEngComm*, **16**, 10189 (2014). DOI: 10.1039/c4ce01806k.

*130*. Liao, Z.L.; Deb, T.; and Nyman, M. Elucidating self-assembly mechanisms of uranyl peroxide capsules from monomers. *Inorganic Chemistry*, **53**, 10506-10513 (2014). DOI: 10.1021/ic501587g.

*131*. Lang, M.; Toulemonde, M.; Zhang, J.M.; Zhang, F.X.; Tracy, C.L.; Lian J.; Wang, Z.W.; Weber, W.J.; Severin, D.; Bender, M.; Trautmann, C.; Ewing, R.C. Swift heavy ion track formation in $Gd_2Zr_{2-x}Ti_xO_7$ pyrochlore: Effect of electronic energy loss. *Nuclear instruments and Methods in Physics Research B*, **336**, 102-115 (2014). DOI: 10.1016/j.nimb.2014.06.019.

*132*. Qiu, J.; Ling, J.; Sieradzki, C.; Nguyen, K.; Wylie, E.M.; Szymanowski, J.E.S.; and Burns, P.C. Expanding the crystal chemistry of uranyl peroxides: Four hybrid uranyl-peroxide structures containing EDTA. *Inorganic Chemistry*, **53**, 12084-12091 (2014). DOI: 10.1021/ic5018906.

*133*. Ling, J.; Hobbs, F.; Prendergast, S.; Adelani, P.O.; Babo, J.M.; Qiu, J.; Weng, Z.; and Burns, P.C. Hybrid uranium-transition-metal oxide cage clusters. *Inorganic Chemistry*, **53**, 12877-12884. (2015). DOI: 10.1021/ic5018449.

*134*. Solomon, J.M.; Navrotsky, A.; and Asta, M. Energetics and defect clustering trends for trivalent rare earth cations substituted in $UO_2$. *Journal of Nuclear Materials*, **457**, 252-255 (2015). DOI: 10.1016/j.jnucmat.2014.11.089.

*135*. Solomon, J.M.; Alexandrov, V.; Sadigh, B. ; Navrotsky, A.; and Asta, M. Computational study of the energetics and defect clustering tendencies for Y and La-doped $UO_2$. *Acta Materialia*, **78**, 282-289 (2014). DOI: 10.1016/j.actamat.2014.06.052.

*136*. Thangavelu, S.G. and Cahill, C.L. Uranyl promoted peroxide generation: Synthesis and characterization of three uranyl peroxo $[(UO_2)_2(O_2)]$ complexes. *Inorganic Chemistry*, **54**, 4208-4221 (2015). DOI: 10.1021/ic502767k.

*137*. Guo, X.; Kukkadapu, R.; Lanzirotti, A.; Newville, M.; Engelhard, M.; Sutton, S.; and Navrotsky, A. Charge-coupled substituted garnets $(Y_{3-x}Ca_{0.5x}M_{0.5x})Fe_5O_{12}$ (M=Ce, Th): Structure and stability as crystalline nuclear waste forms. *Inorganic Chemistry*, **54**, 4156-4166 (2015). DOI: 10.1021/acs.inorgchem.5b00444.

*138*. Lang, M.; Devanathan, R.; Toulemonde, M.; Trautmann, C. Advances in understanding of swift heavy ion tracks in complex ceramics. *Current Opinion in Solid State and Materials Science*, **19**, 39-48 (2015). DOI: 10.1016/j.cossms.2014.10.002.

*139*. Tracy, C.L; Lang, M; Pray, J.M.; Zhang, F.X.; Popov, D.; Park C.Y.; Trautmann, C.; Bender, M.; Severin, D.; Skuratov, V.A.; Ewing, R.C. Redox response of actinide materials to highly ionizing radiation. *Nature Communications*, **6**, 6133 (9 pages) (2015). DOI: 10.1038/ncomms7133.

*140*. Ewing, R.C. Long-term storage of spent nuclear fuel. *Nature Materials*, **14**, 252-257 (2015). DOI: 10.1038/nmat4226.

*141*. Lang, M.; Tracy, C.L.; Palomares, R.I.; Zhang, F.X.; Severin, D.; Bender, M.; Trautmann, C.; Park, C.; Prakapenka, V.B.; Skuratov, V.A.; and Ewing R.C. Characterization of ion-induced radiation effects in nuclear materials using synchrotron X-ray techniques. *Journal of Materials Research*, **30**, 1366-1379 (2015). DOI: 10.1557/jmr.2015.6.

*142*. Palomares, R.I.; Tracy, C.L.; Zhang, F.X.; Park, C.; Popov, D.; Trautmann, C.; Ewing, R.C. and Lang, M. *In situ* defect annealing of swift heavy ion irradiated $CeO_2$ and $ThO_2$ using synchrotron X-ray diffraction and a hydrothermal diamond anvil cell. *Journal of Applied Crystallography*, **48** 711-718 (2015). DOI: 10.1107/s160057671500477X.

*143.* Flynn, S.L.; Szymanowski, J.E.S.; Gao, Y.; Liu, T.; Burns, P.C.; and Fein, J.B. Experimental measurements of U60 nanocluster stability in aqueous solution. *Geochimica et Cosmochimica Acta*, **156**, 94-105 (2015). DOI: 10.1016/j.gca/2015.02.021.

*144.* Qiu, J.; Vlaisavljevich, B.; Jouffret, L.; Nguyen, K.; Szymanowski, J.E.S.; Gagliardi, L; and Burns, P.C. Cation templating and electronic structure effects in uranyl cage clusters probed by the isolation of peroxide-bridged uranyl dimers. *Inorganic Chemistry*, **54**, 4445-4455 (2015). DOI: 10.1021/acs.inorgchem.5b00248.

*145.* Liu, Y.; Czarnecki, A.; Szymanowski, J.E.S.; Sigmon, G.E.; and Burns, P.C. Extraction of uranyl peroxo clusters from aqueous solution by mesoporous silica SBA-15. *Journal of Radioanalytical and Nuclear Chemistry*, **303**, 2257-2262 (2015). DOI: 10.1007/s10967-014-3740-7.

*146.* Gao, Y.; Haso, F.; Szymanowski, J.E.S.; Zhou, J.; Hu, L.; Burns, P.C.; and Liu T. Selective permeability of uranyl peroxide nanocages to different alkali ions: Influences from surface pores and hydration shells. *Chemistry – A European Journal*, **21**, 18785-18790 (2015). DOI: 10.1002/chem.201503773.

*147.* Guo, X.; Rák, Zs.; Tavakoli, A.H.; Becker, Udo; Ewing, R.C.; and Navrotsky, A. Thermodynamics of thorium substitution in yttrium iron garnet: Comparison of experimental and theoretical results. *Journal of Materials Chemistry A*, **2**, 16945-16954. (2014) DOI: 10.1039/C4TA03683B.

*148.* Park, S.; Lang, M.; Tracy, C.L.; Zhang, J.; Zhang, F.; Trautmann, C.; Rodriguez, M.D.; Kluth, P.; and Ewing, R.C. Response of $Gd_2Ti_2O_7$ and $La_2Ti_2O_7$ to swift-heavy ion irradiation and annealing. *Acta Materialia*, **93**, (2015) DOI: 10.1016/j.actamat.2015.04.010.

*149.* Thangavelu, S.; Butcher, R.J.; and Cahill, C.L. Role of N-Donor sterics on the coordination environment and dimensionality of uranyl thiophenedicarboxylate coordinated polymers. *Crystal Growth and Design*, **15**, 3481-3492 (2015). DOI: 10.1021/acs.cgd.5b00549.

*150.* Thangavelu, S.; Pope S.J.; and Cahill C.L. Synthetic, structural, and luminescence study of uranyl coordination polymers containing chelating terpyridine and trispyridyltriazine ligands. *CrystEngComm*, **17**, 6236-6247 (2015). DOI: 10.1039/C5CE00984G.

*151.* Carter, K.P.; Zulato, C.; Rodriguez, E.M.; Pope.S. J.A.; Sigoli, F.A.; and Cahill, C.L. Controlling dimensionality via a dual ligand strategy in Ln-Thiophene-2,5-dicarboxylic acid – terpyridine corrdination polymers, *Dalton Transactions*, **44**, 15843-15854 (2015). DOI: 10.1039/c5dt02596f.

*152.* Zhang, J.; Toulemonde, M.; Lang, M.; Constantini, J.M.; Della-Negra, S.; and Ewing, R.C. $C_{60}$ and U ion irradiation of $Gd_2Ti_xZr_{2-x}O_7$ pyrochlore, *Journal of Materials Research*, **30**, 2456-2466 (2015) DOI: 10.1557/jmr.2015.230.

*153.* Tracy, C.L.; Lang, M.; Zhang, F.; Trautmann, C.; and Ewing, R.C. Phase transformations in $Ln_2O_3$ materials irradiated with swift heavy ions. *Physical Review B*, **92**, 174101 (2015). DOI: 10.1103/PhysRevB.92.174101.

*154.* Tracy, C.L.; Lang, M.; Severin, D.; Bender, M.; Trautmann, C.; and Ewing, R.C. Anisotropic expansion and amorphization of $Ga_2O_3$ irradiated with 946 MeV Au ions. *Nuclear Instruments and Methods in Physics Research B*, **374**, 40-44 (2015). 10.1016/j.nimb.2015.08.059.

*155.* Zhang, L. and Navrotsky, A. Thermochemistry of rare earth doped uranium oxides $Ln_xU_{1-x}O_{2-0.5x+y}$. *Journal of Nuclear Materials*, **465**, 682-691 (2015). DOI: 10.1016/j.jnucmat.2015.06.059.

*156.* Zhang, L.; Solomon, J. M.; Asta, M.D.; and Navrotsky, A. A combined calorimetric and computational study of the energetics of rare earth substituted $UO_2$ systems. *Acta Materialia*, **97**, 191-198 (2015). DOI: 10.1016/j.actamat.2015.06.048.

*157.* Thangavelu, S. and Cahill, C.L. A family of uranyl coordination polymers containing O-donor dicarboxylates and trispyridyltraizine guests. *Crystal Growth and Design*, **16**, 42-50 (2015). DOI: 10.1021/acs.cgd.5b00778.

*158.* Deb, T.; Zakharov, L.; Falaise, C.; Nyman, M. Structure and solution speciation of $U^{IV}$-linked phosphomolybdate ($Mo^{V}$) clusters. *Inorganic Chemistry*, **55**, 755-761 (2015). DOI:10.1021/acs.inorgchem.5b02229.

*159.* Soltis, J.A.; Wallace, C.M.; Penn, R.L.; and Burns, P.C. Cation-dependent hierarchical assembly of U60 nanoclusters into macro-ion assemblies images via cryogenic transmission electron microscopy. *Journal of the American Chemical Society*, **138**, 191-198 (2016). DOI: 10.1021/jacs.5b09802.

*160.* Shamblin, J.; Feygenson, M.; Neuefeind, J.; Tracy, C.L.; Zhang, F.; Finkeldei, S.; Bosbach, D.; Zhou, H.; Ewing, R.C.; and Lang, M. Probing disorder in isometric pyrochlore and related complex oxides. *Nature Materials*, **15**, 507-511 (2016). DOI: 10.1038/nmat4581.

*161.* Sigmon, G.E.; Szymanowski, J.E.S.; Carter, K.P.; Cahill, C.L.; and Burns, P.C. Hybrid lanthanide-actinide peroxide cage clusters. *Inorganic Chemistry*, **55**, 2682-2684 (2016) DOI: 10.1021/acs.inorgchem.6b00207.

*162.* Oliveri, A.F.; Pilgrim, C.D.; Qiu, J.; Colla, C.A.; Burns, P.C.; and Casey, W.H. Dynamic phosphonic bridges in aqueous uranyl clusters. *European Journal of Inorganic Chemistry*, 2016 (6), 797-801 (2016). DOI: 10.1002/ejic.201600036.

*163.* Odoh, S.; Shamblin, J.; Colla, C.A.; Hickam, S.; Lobeck, H.L.; Lopez, R.A.K.; Olds, T.; Szymanowski, J.E.S.; Sigmon, G.E.; Neuefeind, J.; Casey, W.H.; Lang, M.K.; Gagliardi, L.; and Burns, P.C. Structure and reactivity of X-ray amorphous uranyl peroxide, $U_2O_7$, *Inorganic Chemistry*, **55**, 3541-3546 (2016). DOI: 10.1021/acs.inorgchem.6b00017.

*164.* Wylie, E.M.; Peruski, K.M.; Prizio, S.E.; Bridges, A.N.A.; Rudisill, T.S.; Hobbs, D.T.; Phillip, W.A.; and Burns, P.C. Processing used nuclear fuel with nanoscale control of uranium and ultrafiltration. *Journal of Nuclear Materials*, **473**, 125-130 (2016). DOI: 10.1016/j.jnucmat.2016.02.013.

*165.* Liu, Y.; Czarneki, A.; Sigmon, G.E.; Szymanowski, J.E.S.; and Burns, P.C. Extraction behaviors of uranyl peroxo cage clusters by mesoporous silica SBA-15. *Journal of Radioanalytical and Nuclear Chemistry*, **310**, 453-462 (2016). DOI: 10.1007/s10967-016-4801-x.

*166.* Gao, Y.; Szymanowski, J.E.S.; Sun, X.; Burns, P.C.; and Liu, T. Thermal responsive ion selectivity of uranyl peroxide nanocages: An inorganic mimic of $K^+$ ion channels. *Angewante Chem. International Edition*, **55**, 6887-6891 (2016). DOI: 10.1002/anie.201601852.

*167.* Liu, Z.; Liu, T.; and Tsige, M. Elucidating the origin of the attractive force among hydrophilic macroions. *Scientific Reports*, **6**, Article number 26595 (2016). DOI: 10.1038/srep26595.

*168.* Alam, T.M.; Liao, Z.; Nyman, M.; and Yates, J. Insight into hydrogen bonding of uranyl hydroxide layers and capsules by use of H-1 Magic-Angle Spinning NMR spectroscopy. *Journal of Physical Chemistry C*, **120**, 10675-10685 (2016). DOI: 10.1021/acs.jpcc.6b02692.

*169.* Shamblin, J.; Calder, S.; Dun, Z.; Lee, M.; Choi, E.S.; Neuefeind, J.; Zhou, H.; Lang, M. Crystal structure and partical lsing-like magnectic ordering of orthorhombic $Dy_2TiO_5$. *Physical Review B*, **94**, 024413 (2016). DOI: 10.1103/PhysRevB.94.024413.

*170.* Dembowski, M.; Olds, T.A.; Pellegrini, K.L.; Hoffman, C.; Wang, X.; Hickam, S.; He, J.; Oliver, A.G.; Burns, P.C. Solution P-31 NMR study of the acid-catalyzed formation of a highly charged {U(24)Pp(12)} Nanocluster, $[(UO_2)_{24}(O_2)_{24}(P_2O_7)_{12}]^{48-}$, and its structural characterization in the solid state using single-crystal neutron diffraction. *Journal of the American Chemical Society*, **138**, 8547-8553 (2016). DOI: 10.1021/jacs.6b04028.

*171.* Qiu, J.; Dembowski, M.; Szymanowski, J.E.S.; Toh, W.C.; Burns, P.C. Time-resolved X-ray scattering and Raman spectroscopic studies of formation of a uranium-vanadium-phosphorus-peroxide cage cluster. *Inorganic Chemistry*, **55**, 7061-7067 (2016). DOI: 10.1021/acs.inorgchem.6b00918.

*172.* Carter, K.P.; Thomas, K.E.; Pope, S.J.; Holmberg, R.J.; Butcher ,R.J.; Murugesu, M.; Cahill, C.L. Supramolecular assembly of molecular rare-earth-3,5-dichlorobenzoic acid-2,2’: 6’,2’’-terpyridine materials: Structural systematics, luminescence properties, and magnetic behavior. *Inorganic Chemistry*, **55**, 6902-6915 (2016). DOI:10.1021/acs.inorgchem.6b00408.

*173.* Tracy, C.L.; Shamblin, J.; Park, S.; Zhang, F.; Trautmann, C.; Lang, M.; Ewing, R.C. Role of composition, bond covalency, and short-range order in the disordering of stannate pyrochlores by swift heavy ion irradiation. *Physical Review B*, **94**, 064102 (2016). DOI:

10.1103/PhysRevB.94.064102.

*174.* Tracy, C.L.; Lang, M.; Zhang, F.; Park, S.; Palomares, R.I.; and Ewing, R.C. Review of recent experimental results on the behavior of actinide-bearing oxides and related materials in extreme environments. *Progress in Nuclear Energy*, **104**, 342-358 (2018). DOI: 10.1016/j.pnucene.2016.09.012.

*175.* Shamblin, J.; Tracy, C.L.; Ewing, R.C.; Zhang, F.X.; Li, W.; Trautmann, C.; and Lang. M. Structural response of titanate pyrochlores to swift heavy ion irradiation. *Acta Materialia*, **117**, 207-215 (2016). DOI: 10.1016/j.actamat.2016.07.017.

*176.* Falaise, C. and Nyman, M. The key role of U-28 in the aqueous self-assembly of uranyl peroxide nanocages. *Chemistry – A European Journal*, **22**, 14678-14687 (2016). DOI: 10.1002/chem.201602130.

*177.* Migliori, A.; Soderlind, P.; Landa, A.; Freibert, F.J.; Maiorov, B.; Ramshaw, B.J.; Betts, J.B. Origin of the multiple configurations that drive the response of delta-plutonium's elastic moduli to temperature. *Proceedings of the National Academy of Sciences of the United States of America*, **113**, 11158-11161 (2016). DOI: 10.1073/pnas.1609215113.

*178.* Spano, T.; Dzik, E.A.; Sharifironizi, M.; Dustin, M.K., Turner, M.; and Burns, P.C. Thermodynamic investigation of uranyl vanadate minerals: Implications for structural stability, *American Mineralogist*, **102**, 1149-1153 (2017). DOI: 10.2138/am-2017-5894.

*179.* Sharifironizi, M.; Szymanowski, J.E.S.; Sigmon, G.E.; Navrotsky, A.; Fein, J.B. and Burns, P.C. Thermodyanmaic studies of zippeite, a uranyl sulfate common in mine wastes. *Chemical Geology*, **447**, 54-58 (2016). DOI: 10.1016/j.chemgeo.2016.10.022.

*180.* Peruski, K.; Bernales, V.; Dembowski, M.; Lobeck, H.L.; Pellegrini, K.L.; Sigmon, G.E.; Hickam, S.; Wallace, C.M.; Szymanowski, J.E.S.; Balboni, E.; Gagliardi, L.; and Burns, P.C. Uranyl peroxide cage cluster solubility in water and the role of the electrical double layer. *Inorganic Chemistry*, **56**, 1333-1339 (2017). DOI:10.1021/acs.inorgchem.6b02435.

*181.* Flynn, S.L., Szymanowski, J.E.S., Burns, P.C., and Fein, J.B. Experimental measurements of U24Py nanocluster behavior in aqueous solution. *Radiochimica Acta*, **104**, 853-864 (2016). DOI: 10.1515/ract-2015-2493.

*182.* Dembowski, M.; Bernales, V.; Qiu, J.; Hickam, S.; Gaspar, G.; Gaglardi, L.; and Burns, P.C. Computationally-guided assignment of unexpected signals in the Raman spectra of uranyl triperoxide complexes. *Inorganic Chemistry*, **56**, 1574-1580 (2017). DOI: 10.1021/acs.inorgchem.6b02666.

*183.* Guo, X., Wu, D., Xu, H., Burns, P.C. and Navrotsky, A. Thermodynamics of studtite thermal decomposition pathways via amorphous intermediates $UO_3$, $U_2O_7$, and $UO_4$. *Journal of Nuclear Materials*, **478**, 158-163 (2016). DOI: 10.1016/j.jnucmat.2016.06.014.

*184.* Guo, X., Lipp, C., Tiferet, E.; Lanzirotti, A., Newville, M.; Engelhard, M.H.; Wu, D.; Ilton, E.S.; Sutton, S.R.; Xu, H.; Burns, P.C.; and Navrotsky, A. Structure and thermodynamic stability of $UTa_3O_{10}$, a U(V)-bearing compound. *Dalton Transactions*, **45**, 18892-18899 (2016). DOI: 10.1039/C6DT02843H.

*185.* Neal, H.A.; Szymanowski, J.E.S.; Fein, J.B.; Burns, P.C. and Nyman, M. Benchmarking uranyl peroxide capsule chemistry in organic media. *European Journal of Inorganic Chemistry*, **2017**, 39-46 (2016). DOI: 10.1002/ejic.201601219.

*186.* Qiu, J.; Spano, T.; Dembowski, M.; Kokot, A.; Szymanowski, J.E.S., and Burns, P.C. Sulfate-centered sodium-ocosahedron-templated uranyl peroxide phosphate cages with uranyl bridged by n-$m_1$:$m_2$ peroxide. *Inorganic Chemistry*, **56**, 1874-1880 (2017). DOI: 10.1021/acs.inorgchem.6b02429.

*187.* Renier, O.; Falaise, C.; Neal, H.; Kozma, K.; and Nyman, M. Closing uranyl polyoxometalate capsules with bismuth and lead polyoxocations. *Angewandte Chem. International Edition*, **55**, 13480-13484 (2016). DOI: 10.1002/anie.201607151.

*188.* Solomon, J.M.; Shamblin, J.; Lang, M.; Navrotsky, A.; and Asta, M. Chemical ordering in substituted fluorite oxides: A computational investigation of $Ho_2Zr_2O_7$ and $RE_2Th_2O_7$ (RE=Ho, Y, Gd, Nd, La). *Scientific Reports*, **6**, 38722 (2016). DOI: 10.1038/srep38772.

*189.* Migliori, A.; Soderlind, P.; Landa, A.; Freibert, F.J.; Maiorov, B.; Ramshaw, B.J.; Betts, J.B. The excited delta-phase of plutonium. *Proceedings of the National Academy of Sciences of the United States of America*, **114**, E269-E269 (2017). DOI: 10.1073/pnas.1619207114.

*190.* Tracy, C.L.; Lang, M.; Severin, D.; Bender, M.; Trautmann, C.; Ewing, R.C. Anisotropic expansion and amorphization of $Ga_2O_3$ irradiated with 946 MeV Au ions. *Nuclear Instruments and Methods in Physics Research Section B*, **374**, 40-44 (2016). DOI: 10.1016/j.nimb.2015.08.059.

*191.* Rittman, D.R.; Turner, K.M.; Park, S.; Fuentes, A.F.; Yan, J.; Ewing, R.C. and Mao, W.L. High-pressure behavior of $A_2B_2O_7$ pyrochlore (A=Eu, By; B=Ti, Zr). *Journal of Applied Physics*, **121**, 045902 (2017). DOI: 10.1063/1.4974871.

*192.* Ridenour, J.A.; Carter, K.P.; Butcher, R.J.; and Cahill, C.L. Re-p-halobenzoic acid-terpyridine complexes, Part II: Structural diversity, supramolecular assembly, and luminescence properties in a series of p-bromobenzoic acid rare-earth hybrid materials. *CrystEngComm*, **19**, 1172 (2017). DOI: 10.1039/c6ce02355J.

*193.* Ridenour, J.A.; Carter, K.P.; and Cahill, C.L. Re-p-halobenzoic acid-terpyridine complexes, part III: Structural and supramolecular trends in a series of p-iodobenzoic acid rare-earth hybrid materials. *CrystEngComm*, **19**, 1190 (2017). DOI: 10.1039/c6ce02356H.

*194.* Maiorov, B.; Betts, J.B.; Soderlind, P.; Landa, A.; Hernandez, S.C.; Saleh, T.A.; Freibert, F.J.; and Migliori, A. Elastic moduli of delta-Pu-239 reveal aging in real time. *Journal of Applied Physics*, **121**, 125107 (2017). DOI: 10.1063/1.4978509.

*195.* Rittman, D.R.; Park, S.; Tracy, C.L.; Palomares, R.I.; Lang, M.; Navrotsky, A.; Mao, W.L.; and Ewing, R.C. Structure and bulk modulus of Ln-doped $UO_2$ (Ln=La, Nd) at high pressure. *Journal of Nuclear Materials*, **490**, 28-33 (April 2017). DOI: 10.1016/j.jnucmat.2017.04.007.

*196.* Cahill, C.L.; Deifel, N.P.; Reusser, D.; Zhang, L.; and Navrotsky, A. Thermochemical properties of U(VI) hybrid materials containing uranyl tetrachloride anions. *Journal of Chemical Thermodynamics*, **114**, 66-70 (2017). DOI: 10.1016/j.jct.2017.05.009.

*197.* Falaise, C.; Neal, H.A.; and Nyman, M. U(IV) aqueous speciation from the monomer to $UO_2$ nanoparticles: Two levels of control from Zwitterionic glycine ligands. *Inorganic Chemistry*, **56**, 6591-6598 (2017). DOI: 10.1021/acs.inorgchem.7b00616.

*198.* Rittman, D. R., Turner, K. M., Park, S., Fuentes A. F., Park C. Y., Ewing R. C., Mao W. L. Strain engineered pyrochlore at high pressure. *Scientific Reports*, **7**, 2236-2246 (2017). DOI: 10.1038/s41598-017-02637-9.

*199.* Tracy, C. L., Park, S., Rittman, D. R., Zinkle, S. J., Bei, H., Lang, M., Ewing, R. C., Mao, W. L., High pressure synthesis of a hexagonal close-packed phase of the high-entropy alloy CrMnFeCoNi. *Nature Communications*, **8**, 15634 (2017) DOI: 10.1038/ncomms15634.

*200.* Palomares, R.I.; Tracy, C.L.; Neuefeind, J.; Ewing, R.C.; Trautmann, C.; and Lang, M. Thermal defect annealing of swift heavy ion irradiated $ThO_2$. *Nuclear Instruments and Methods in Physics Research Section B: Beam Interactions with Materials and Atoms*, **405**, 15-21 (2017). DOI: 10.1016/j.nimb.2017.05.007.

*201.* Zhang, L.; Shelyug, A.; and Navrotsky, A. Thermochemistry of $UO_2$-$ThO_2$ and $UO_2$-$ZrO_2$ fluorite solid solutions. *Journal of Chemical Thermodynamics*, **114**, 48-54 (2017). DOI: 10.1016/j.jct.2017.05.026.

*202.* Turner, K.M.; Rittman, D.R.; Heymach, R.A.; Tracy, C.L.; Turner, M.L.; Fuentes, A.F.; Mao, W.L.; and Ewing, R.C. Pressure-induced structural modifications of rare-earth hafnate pyrochlore. *Journal of Physics: Condensed Matter*, **29**, 255401 (2017). DOI: 10.1088/1361-648X/aa7148.

*203.* Ridenour, J.A and Cahill, C.L. Synthesis, crystal structure, and topological analysis of a La-p-brombenzoic acid-terpyridine 1D-coordination polymer with repeating decameric units and a new 3,3,3,5,5 pentanodal net topology with a novel point symbol. *Inorganica Chimica Acta*, **466**, 78-85 (2017). DOI: 10.1016/j.ica.2017.05.062.

*204.* Palomares, R.I.; Shamblin, J.; Tracy, C.L.; Neuefeind, J.; Ewing, R.C.; Trautmann, C., and Lang, M. Defect accumulation in swift heavy ion-irradiated $CeO_2$ and $ThO_2$. *Journal of Materials Chemistry A*, **5**, 12193-12201 (2017). DOI: 10.1039/c7ta02640d.

*205.* Yu, Q. and Fein, J.B. Enzymatic reduction of U60 nanoclusters by Shewanella oneidensis MR-1. *Radiochimica Acta*, **106**, 21-30 (2017). DOI: 10.1515/ract-2017-2759.

*206.* Dzik, E.A.; Lobeck, H.L.; Zhang, L.; and Burns, P.C. Thermodynamic properties of phosphate members of the meta-autunite group: A high-temperature calorimetric study. *Journal of Chemical Thermodynamics*, **114**, 165-171 (2017). DOI: 10.1016/j.jct.2017.07.007.

*207.* Ridenour, J.A; Pyrch, M.M.; Manning, Z.J.; Bertke, J.A.; and Cahill, C.L. Two novel bimetallic transition metal-uranyl one-dimensional coordination polymers with manganese(II) and cobalt(II) incorporating bridging diglycolate (2,2'-oxydiacetate) ligands. *Acta Crystallographica C,* **73**, 588-592 (2017). DOI: 10.1107/S2053229617009263.

*208.* O'Quinn, E.C.; Shamblin, J.; Perlov, B.; Ewing, R.C.; Neuefeind, J.; Feygenson, M.; Gussev, I.; and Lang, M. Inversion in $Mg_{1-x}Ni_xAl_2O_4$ spinel: New insight into local structure. *Journal of the American Chemical Society*, **139**, 10395-10402 (2017). DOI: 10.1021/jacs.7b04370.

*209.* Kalaj, M.; Carter, K.P.; Savchenkov, A.V.; Pyrch, M.M.; and Cahill, C.L. Syntheses, structures, and comparisons of heterometallic uranyl iodobenzoates with monovalent cations. *Inorganic Chemistry*, **56**, 9156-9168 (2017). DOI: 10.1021/acs.inorgchem.7b01208.

*210.* Olds, T.A.; Dembowski, M.; Wang, X.; Hoffman, C.; Alam, T.M.; Hickam, S.; Pellegrini, K.L.; He, J.; and Burns, P.C. Single-crystal time-of-flight neutron diffraction and magic-angle-spinning NMR spectroscopy resolve the structure of 1H and 7Li dynamics of the uranyl peroxide nanocluster U60. *Inorganic Chemistry*, **56**, 9676-9683 (2017). DOI: 10.1021/acs.inorgchem.7b01174.

*211.* Turner, K.M.; Szymanowski, J.E.S.; Zhang, F., Lin, Y.; McGrail, B.T.; Mao, W.L.; Burns, P.C.; and Ewing, R.C. Uranyl peroxide nanoclusters at high-pressure. *Journal of Materials Research*, **32**, 3679-3688 (2017). DOI: 10.1557/jmr.2017.301.

*212.* Falaise, C.; Hickam, S.M.; Burns, P.C.; and Nyman, M. From aqueous speciation to supramolecular assembly in alkaline earth-uranyl polyoxometalates. *Chemical Communications*, **53**, 9550-9553 (2017). DOI: 10.1039/c7cc05357F.

*213.* Dzik, E.A.; Lobeck, H.L.; Zhang, L.; and Burns, P.C. Thermodynamic characterization of synthetic autunite. *American Mineralogist*, **102**, 1977-1982 (2017). DOI: 10.2138/am-2017-6109.

*214.* Carter, K.P.; Pope, S.J.A.; Kalaj, M.; Holmberg, R.J.; Murugesu, M.; and Cahill, C.L. Exploring the promotion of synthons of choice: Halogen bonding in molecular lanthanide complexes characterized via X-ray diffraction, luminescence spectroscopy, and magnetic measurements. *Zeitschrift fur anorganische und allgemeine chemie* (ZAAC), **643**, 1948-1955 (2017). DOI: 10.1002/zaac.201700341.

*215.* Oliveri, A.F.; Colla, C.A.; Callahan, J.R.; Bogard, G.; Qiu, J.; Dembowski, M.; Burns, P.C.; and Casey, W.H. Cation-directed isomerization of the U28 uranyl-peroxide cluster. *European Journal of Inorganic Chemistry*, **2017**, 5429-5433 (2017). DOI: 10.1002/ejic.201701074.

*216.* Park, S.; Tracy, C.L.; Zhang, F.; Palomares, R.I.; Park, C.; Trautman, C.; Lang, M.; Mao, W.L.; and Ewing, R.C. Swift-heavy ion irradiation response and annealing behavior of $A_2TiO_5$ (A = Nd, Gd, and Yb). *Journal of Solid State Chemistry*, **258**, 108-116 (2018). DOI: 10.1016/j.jssc.2017.09.028.

*217.* Zhang, L.; Dzik, E.A.; Sigmon, G.E.; Szymanowski, J.E.S.; Navrotsky, A.; and Burns, P.C. Experimental thermochemistry of neptunium oxides: $Np_2O_5$ and $NpO_2$. *Journal of Nuclear Materials*, **501**, 398-403 (2017). DOI: 10.1016/j.jnucmat.2017.10.034.

*218.* Luo, Y.; Lin, S.; Leroux, M.; Wakeham, N.; Fobes, D.M.; Bauer, E.D.; Betts, J.B.; Thompson, J.D.; Migliori, A.; Janoschek, M.; and Maiorov, B.. Elasticity in the skyrmion phase unveils depinning at ultra-low current densities. Condensed Matter (2017). arXiv:1711.08873 [cond-mat.str-el].

*219.* Carter, K.P.; Kerr, A.T.; Taydakov, I.V.; and Cahill, C.L. Molecular and polymeric uranyl and thorium hybrid materials featuring methyl substituted pyrazole dicarboxylates and heterocyclic 1,3-diketones. *Solid State Sciences*, **76**, 20-32 (2018). DOI: 10.1016/j.solidstatesciences.2017.12.002.

*220.* Liu, Y.; Szymanowski, J.E.S.; Sigmon, G.E.; Morris, D.E.; Hixon, A.E.; Migliori, A.; and Burns, P.C. Measurement of the effective capacitance of solutions containing nanoscale uranyl peroxide cage clusters (U60) reveals cluster effects. *Journal of Radioanalytical and Nuclear Chemistry*, **315**, 341-346 (2017). DOI: 10.1007/s10967-017-5659-2.

*221.* Ridenour, J.A. and Cahill, C.L. Synthesis, structural analysis, and supramolecular assembly of a series of in-situ generated uranyl-peroxide complexes with functionalized 2,2'-bipyridine and varied carboxylic acid ligands. *New Journal of Chemistry*, **42**, 1816-1831 (2018). DOI: 10.1039/C7NJ03828C.

*222.* Shamblin, J.; Tracy, C.L.; Palomares, R.I.; O'Quinn, E.C.; Ewing, R.C.; Neuefeind, J.; Feygenson, M.; Behrens, J.; Trautmann, C.; and Lang, M. Similar local order in disordered fluorite and aperiodic pyrochlore structures. *Acta Materialia*, **144**, 60-67 (2018). DOI: 10.1016/j.actamat.2017.10.044.

*223.* Chung, C.K.; Shamblin, J.; O'Quinn, E.C.; Shelyug, A.; Gussev, I.; Lang, M.; and Navrotsky, A. Thermodynamic and structural evolution of $Dy_2Ti_2O_7$ pyrochlore after swift heavy ion irradiation. *Acta Materialia*, **145**, 227-237 (2018). DOI: 10.1016/j.actamat.2017.12.044.

*224.* Turner, K. M., Tracy, C. L., Mao, W.L., Ewing R. C., Lanthanide stannate pyrochlores ($Ln_2Sn_2O_7$: Ln = Nd, Gd, Er) at high pressure. *Journal of Physics: Condensed Matter*, **29**, 504005 (2017). DOI: 10.1088/1361-648X/aa9960.

*225.* Dal Bo, F.; Aksenov, S.M.; Hatert, F.; Burns, P.C. Synthesis, IR spectroscopy and crystal structure of $[(UO_2)_2\{Be(H_2O)_2(PO_4)_2\}](H_2O)$, the first compound with a trimer beryllophosphate anion. *Zeitschrift fur Kristallographie – Crystalline Materials*, **233**, 391-398 (2018). DOI: 10.1515/zkri-2017-2113.

*226.* Tracy, C.L.; Chen, C.H.; Park, S.; Davisson, M.L.; and Ewing, R.C. Measurement of $UO_2$ surface oxidation using grazing-incidence X-ray diffraction: Implications for nuclear forensics. *Journal of Nuclear Materials*, **502**, 68-75. (2018). DOI: 10.1016/j.jnucmat.2018.01.052.

*227.* O'Quinn, E.C.; Biship, J.L.; Sherrod, R.; Neuefeind, J.; Montemayor, S.M.; Fuentes, A.F.; and Lang, M. Advanced characterization technique for mechanochemically synthesized materials: Neutron total scattering analysis. *Journal of Materials Science*, **53**, 13400-13410 (2018). DOI: 10.1007/s10853-018-2212-9.

*228.* Burns, P.C. and Nyman, M. Captivation with encapsulation: A dozen years of exploring uranyl peroxide capsules. *Dalton Transactions*, **47**, 5916-5927 (2018). DOI: 10.1039/C7DT04245K.

*229.* Lang, M.; O'Quinn, E.C.; Shamblin, J.; and Neuefeind, J. Advanced experimental technique for radiation damage effects in nuclear waste forms: Neutron total scattering analysis. *MRS Advances*, **3**, 1735-1747 (2018). DOI: 10.1557/adv.2018.199.

*230.* Park S., Rittman, D. R., Tracy, C. L., Chapman, K. W., Zhang, F. X., Park, C., Tkachev, S. N., O'Quinn E. C., Shamblin, J., Lang, M., Mao, W. L., Ewing, R. C. $A_2TiO_5$ (A= Dy, Gd, Er, and Yb) at high pressure. *Inorganic Chemistry*, **57**, 4, 2269-2277 (2018). DOI: 10.1021/acs.inorgchem.7b03106

*231*. Pilgrim, C.P.; Mason, H.E.; Zavarin, M.; Casey, W.H. Rates of ligand exchange around the bis-oxalato complex $[NpO_2(C_2O_4)_2]^{3-}$ measured by using multinuclear NMR spectroscopy under neutral to semi-alkaline conditions. *ChemPlusChem*, **83**, 590-596 (2018). DOI: 10.1002/cplu.201800025.

*232*. Chen, C-H., Tracy, C. K., Wang, C., Lang, M., Ewing, R. C. Initial stages of ion beam-induced phase transformation in $Gd_2O_3$ and $Lu_2O_3$. *Applied Physics Letters*, **112**, 073904-073909 (2018). DOI: 10.1063/1.5023018.

*233.* Park, S.; Tracy, C.L.; Zhang, F.; Park, C.; Trautmann, C., Tkachev, S.N.; Lang, M.; Mao, W.L.; and Ewing, R.C. Radiation-induced disorder in compressed lanthanide zirconates. *Phys. Chem. Chem. Phys*., **20**, 6187-6197 (2018). DOI: 10.1039/C7CP08664D.

*234.* Rittman, D.R.; Tracy, C.L.; Chen, C.H.; Solomon, J.; Asta, M.; Mao, W.L.; Yalisove, S.M.; and Ewing, R.C. Phase transformation pathways of ultrafast-laser-irradiated $Ln_2O_3$ (Ln = Er-Lu). *Physical Review B*, **97**, 024104 (2018). DOI: 10.1103/PhysRevB.97.024104.

*235.* Xie, J.; Neal, Ha.A.; Szymanowski, J.E.S.; Burns, P.C.; Alam, T.M.; Nyman, M.; and Gagliardi, L.. Resolving Confined $^7Li$ Dynamics or Uranyl Peroxide Capsule U24, *Inorganic* Chem*istry*, **57**, 5514-5525, (2018). DOI: 10.1021/acs.inorgchem.8b00474.

*236.* Sadergaski, L.R.; Stoxen, W.; Hixon, A.E. Uranyl peroxide nanocluster (U60) persistence and sorption in the presence of hematite. *Environmental Science and Technology*, **52**, 3304-3311 (2018). DOI: 10.1021/acs.est.7b06510.

*237.* Gao, Y.; Dembowski, M.; Szymanowski, J.E. S.; Yin, W.; Chuang, S.S.C.; Burns, P.C. and Liu, T. A spontaneous Structural transition of {U24pp12} clusters triggered by alkali counterion replacement in dilute solution." *Chemistry – A European Journal*, **23**, 7915-19. (2017) DOI: 10.1002/chem.201701972.

*238.* Newcomb, K.; Tiwari, S.P.; Rai, N.; and Maginn, E.J. A molecular dynamics investigation of actinyl-ligand speciation in aqueous solution. *Physical Chemistry Chemical Physics*, **20**, 15753-15763 (2018). DOI: 10.1039/C8CP01944D.

*239.* Chung, C.K.; Lang, M.; Xu, H., and Navrotsky, A. Thermodynamics of raidation induced amorphization and thermal annealing of $Dy_2Sn_2O_7$ pyrochlore. *Acta Materialia*, **155**, 386-392 (2018). DOI: 10.1016/j.actamat.2018.06.003.

*240.* Dzik, E.A.; Lobeck, H.L.; Zhang, L.; and Burns, P.C. High-temperature calorimetric measurements of thermodynamic properties of uranyl arsenates of the meta-autunite group. *Chemical Geology*, **493**, 353-358 (2018). DOI: 10.1016/j.chemgeo.2018.06.009.

*241*. Falaise, C.; Kozma, K.; and Nyman, M. Thorium oxo-clusters as building blocks for open frameworks. *Chemistry – A European Journal*, **24**, 1-8 (2018). DOI: 10.1002/chem.201802671.

*242.* Sadergaski, L.R. and Hixon, A.E. Kinetics of uranyl peroxide nanocluster (U60) sorption to goethite. *Environmental Science and Technology*, **52**, 9818-9826 (2018). DOI: 10.1021/acs.est.8b02716.

*243.* Sharifironizi, M.; Szymanowski, J.E.S.; Qui, J.; Castillo, Sarah; Hickam, S.; and Burns, P.C. Charge density influence on ethanply of formation of uranyl peroxide cage cluster salts. *Inorganic Chemistry*, **57**, 11456-11462 (2018). DOI: 10.1021/acs.inorgchem.8b01300.

*244.* Dal Bo, F.; Kohlgruber, T.; Szymanowski, J.E.S.; Aksenov, S.M.; and Burns, P.C. $Rb_2[Ca(NpO_2)_2(PO_4)_2]$, the first mixed alkali-alkaline earth metals neptunyl(V) phosphate: Crystal chemistry and sheet stereoisomerism. *Crystal Growth and Design*, **18**, 7254-7258 (2018). DOI: 10.1021/acs.cgd.8b01627.

*245.* Dal Bo, F.; Aksenov, S.M.; and Burns, P.C. A novel family of microporous uranyl germanates: Framework topology and complexity of the crystal structures. *Journal of Solid State Chemistry*, **271**, 126-134 (2019). DOI: 10.1016/j.jssc.2018.12.044.

*246.* Shelyug, A. and Navrotsky, A. Thermodynamic stability of the fluorite phase in the $CeO_2$ – CaO – $ZrO_2$ system. *Journal of Nuclear Materials*, **517**, 80-85 (2019). DOI: 10.1016/j.jnucmat.2019.01.043.

*247.* Dal Bo, F.; Aksenvo, S.M. and Burns, P.C. $Mg[(UO_2)_2(Ge_2O_6(OH)_2](H_2O)_{4.4}$, a novel compound with mixed germanium coordination: Cation disordering and topological features of β-$U_3O_8$ type sheets. *Zeitschrift fur Kristallographie – Crystalline Materials*, **234**, 383-393 (2019). DOI: 10.1515/zkri-2018-2156.

*248.* Sadergaski, L.R.; Said, M.; and Hixon, A.E. Calcium-facilitated aggregation and precipitation of the uranyl peroxide nanocluster U in the presence of Na-montmorillonite. *Environmental Science and Technology*, **53**, 4922-4930 (2019). DOI: 10.1021/acs.est.8b06731.

*249.* Guo, X.; Boukhalfa, H.; Mitchell, J.N.; Ramos, M.; Gaunt, A.J.; Migliori, A.; Robeck, R.C.; Navrotsky, A.; and Xu, H.. Sample seal-and-drop device and methodology for high temperature oxide melt solution calorimetric measurements of $PuO_2$. *Review of Scientific Instruments*, **90**, 044101 (2019). DOI: 10.1063/1.5093567.

*250.* Guo, X.; Wu, D.; Ushakov, S.V.; Shvareva, T.; Xu, H.; and Navrotsky, A. Energetics of hydration on uranium oxide and peroxide surfaces. *Journal of Materials Research*, **34**, 3319-3325 (2019). DOI: 10.1557/jmr.2019.192.

*251*. Cureton, W.F.; Palomares, R.I.; Tracy, C.L.; O'Quinn, E.C.; Walters, J.; Zdorovets, M.; Ewing, R.C.; Toulemonde, M.; and Lang, M. Effects of irradiation temperature on the response of $CeO_2$, $ThO_2$, and $UO_2$ to highly ionizing radiation. *Journal of Nuclear Materials*, **525**, 83-91 (2019). DOI: 10.1016/j.jnucmat.2019.07.029.

*252*. Gao, Y.; Chen, J.; Zhang, T.; Szymanowski, J.E.S.; Burns, P.C.; and Liu, T. Inhomogeneous distribution of cationic surfactants around anionic molecular clusters. *Chemistry – A European Journal*, **25**, 1-6 (2019). DOI: 10.1002/chem.201903544.

*253*. Newcomb, Ken; Bernales, Varinia; Tiwari, Surya Prakash; Gagliardi, Laura; and Maginn, Edward J. The role of cations in uranyl nanocluster association: A molecular dynamics study. Phys. Chem. Chem. Phys. Online December 2019. DOI: 10.1039/C9CP05138D.

*254*. Rittman, Dylan R.; Teitelbaum, Samuel W.; Reis, David A.; Mao, Wendy L.; and Ewing, R.C. Anomalous behavior of nonequilibrium excitations in UO2. Physical Review B, 99, 134307 (2019). DOI: 10.1103/PhysRevB.99.134307.

**<u>Collaborative Papers</u>**

*255.* Zhang, J.M.; Salje, E.K.H.; and Ewing, R.C. OH species, U ions, and $CO/CO_2$ in thermally annealed metamict zircon ($ZrSiO_4$). *American Mineralogist*, **95**, 1717-1724 (2010).

*256.* Alsobrook, A. N.; Hauser, B. G.; Hupp, J. T.; Alekseev, E. V.; Depmeier, W.; and Albrecht Schmitt, T. E. Cubic and rhombohedral heterobimetallic networks constructed from uranium, transition metals, and phosphonoacetate: New methods for constructing porous materials. *Chemical Communications*, **46, 9167-9169 (2010).**

*257.* Wang, S.; Alekseev, E. V.; Miller, H. M.; Depmeier, W.; and Albrecht-Schmitt, T. E. Boronic acid flux synthesis and crystal growth of uranium and neptunium noronates and borates: A low temperature route to the first neptunium (V) borate. *Inorganic Chemistry*, **49**, 9755-9757 (2010).

*258.* Wang, S.; Alekseev, E. V.; Stritzinger, J. T.; Liu, G.; Depmeier, W.; and Albrecht-Schmitt, T. E. Structure-property relationships in lithium, silver, and cesium uranyl borates. *Chemistry of Materials*, **22**, 5983-5991 (2010).

*259.* Adelani, P. O. and Albrecht-Schmitt, T. E. Differential ion exchange in elliptical uranyl diphosphonate nanotubules. *Angewandte Chemie*, *International Edition*, **49**, 8909-8911 (2010).

*260.* Yu, P.; Wang, S.; Alekseev, E.V.; Depmeier, W.; Hobb, D.T.; Albrecht-Schmitt, T. E.; Phillips, B. L.; and Casey, W. H. Technetium-99 MAS NMR spectroscopy of a cationic framework material that traps $TcO_4^-$ ions. *Angewandte Chem*. *International Edition*, **49**, 5975-5977 (2010).

*261.* Wang, S.; Alekseev, E.V.; Stritzinger, J. T.; Depmeier, W.; and Albrecht-Schmitt, T. E. Crystal chemistry of the potassium and rubidium uranyl borate families derived from boric acid fluxes. *Inorganic Chemistry*, ***49****, 6690-6696 (2010).*

*262.* Wang, S.; Alekseev, E. V.; Depmeier, W.; and Albrecht-Schmitt, T. E. Further insights into intermediate- and mixed-valency in neptunium oxoanion compounds: Structure and absorption spectroscopy of $K_2[(NpO_2)_3B_{10}O_{16}(OH)_2(NO_3)_2]$. *Chemical Communications*, **46**, 3955-3957 (2010). *Invited Article.*

*263.* Vlaisavljevich, B.; Gagliardi, L.; and Burns, P. C. Understanding the structure and formation of uranyl peroxide nanoclusters by quantum chemical calculations. *Journal of the American Chemical Society*, **132**, 14503-14508 (2010).

*264.* Ewing, R.C.; Runde, W.; and Albrecht-Schmitt, T.E. Environmental impact of the nuclear fuel cycle: Fate of actinides. *MRS Bulletin*, **35**, 859-866 (2010).

*265.* Shuller, L.C.; Ewing, R.C.; and Becker, U. Quantum-mechanical evaluation of Np-incorporation into studtite. *American Mineralogist*, **95**, 1151-1160 (2010).

*266.* Zhang, J.M.; Lian, J.; Zhang, F.X.; Wang, J.W.; Fuentes, A.F.; and Ewing, R.C. Instrinsic structural disorder and radiation response of nanocrystalline $Gd_2(Ti_{0.65}Zr_{0.35})_2O_7$ pyrochlore. *Journal of Physical Chemistry*, **114**, 11810-11815 (2010).

*267.* Zhang, J.M.; Lang, M.; Ewing, R.C.; Devanathan, R.; Weber, W.J.; and Toulemonde, M. Nanoscale phase transitions under extreme conditions with an ion track. *Journal of Materials Research*, **25**, 1344-1351 (2010).

*268.* Zhang, J.M.; Livshits, T.S.; Lizin, A.A.; Hu, Q.N.; and Ewing, R.C. Irradiation of synthetic garnet by heavy ions and alpha-decay of Cm-244. *Journal of Nuclear Materials*, **407**, 137-142 (2010).

*269.* Zhang, J.M.; Hu, Q.N.; Livshits, T.S.; Yudintsev, S.V.; Lian, S.V.; and Ewing, R.C. Irradiation response of synthetic U-containing $REE_2(Sn, Zr)_2O_7$ pyrochlore. *Microscopy and Microanalysis*, **16**, 1626 (2010).

*270.* Knope, K.E. and Cahill, C.L. Homometallic $UO_2^{2+}$ diphosphonates assembled under ambient and hydrothermal conditions. *Dalton Transactions*, **39**, 8319-8324 (2010).

*271.* Knope, K.E. and Cahill, C.L. Room temperature assembly of a uranyl carboxyphosphonate: Synthesis, characterization and $[UO_2]^{2+}$ hydrolysis. *Inorganic Chemistry Communications*, **13**, 1040-1042 (2010).

*272.* Rowland, C.E. and Cahill, C.L. Hydrothermal synthesis of uranyl squarates and squarate-oxalates: Hydrolysis trends and *in situ* oxalate formation. *Inorganic Chemistry,* **49**, 6716-6724 (2010).

*273.* Deifel, N.P. and Cahill, C.L. Supramolecular chemistry with uranyl tetrahalide ($[UO_2X_4]^{2-}$) anions. *Comptes Rendus Chimie*, **13**, 747-754 (2010).

*274.* Diwu, J.; Wang, S.; Liao, Z.; Burns, P.C.; and Albrecht-Schmitt, T.E. Cerium(VI), neptunium(IV), and plutonium(IV) 1,2-phenylenediphosphonates: Correlations and differences between early transuranium elements and their proposed surrogates. *Inorganic Chemistry,* **49**, 10074-10080 (2010).

*275.* Burns, P.C.; Ikeda, Y.; and Czerwinski, K. Advances in actinide solid-state and coordination chemistry. *MRS Bulletin,* **35**, 868-876 (2010).

*276.* Wang, S.; Alekseev, E.V.; Casey, W.H.; Diwu, J.; Phillips, B.L.; Depmeier, W.; and Albrecht-Schmitt, T.E. NDTB-1: A supertetrahedral cationic framework that removes $TcO_4^-$ from solution. *Angewandte Chem. International Edition,* **49**, 1057-1060 (2010).

*277.* Ferriss, E.D.A.; Ewing, R.C.; and Becker, U. Simulation of thermodynamic mixing properties of actinide-containing zircon solid solutions. *American Mineralogist*, **95**, 229-241 (2010).

*278.* Lang, M.; Zhang, F.; Zhang, J.; Wang, J.; Lian, J.; Weber, W.J.; Schuster, B.; Trautmann, C.; Neumann, R.; and Ewing, R.C. Review of $A_2B_2O_7$ pyrochlore response to irradiation and pressure. *Nuclear Instruments and Methods in Physics Research B*, **268**, 2951-2959 (2010).

*279.* Wang, S.; Alekseev, E.V.; Stritzinger, J.T.; Depmeier, W.; and Albrecht-Schmitt, T.E. How are centrosymmetric and noncentrosymmetric structures achieved in uranyl borates? *Inorganic Chemistry*, ***49***, 2948-2953 (2010).

*280.* Wang, S.; Alekseev, E.V.; Ling, J.; Liu, G.; Depmeier, W.; and Albrecht-Schmitt, T.E. Polarity and chirality in uranyl borates: Insights into understanding the vitrification of nuclear waste and the development of nonlinear optical materials. *Chemistry of Materials*, **22**, 2155-2163 (2010).

*281.* Wang, S.; Alekseev, E.V.; Ling, J.; Skanthakumar, S.; Soderholm, L.; Depmeier, W.; and Albrecht-Schmitt, T.E. Neptunium diverges sharply from uranium and plutonium in crystalline borate matrixes: Insights into the complex behavior of the early actinides relevant to nuclear waste storage. *Angewandte Chem. International Edition,* **49**, 1263-1266 (2010).

*282.* Knope, K.E. and Cahill, C.L. Synthesis and characterization of 1-, 2-, and 3-dimensional bimetallic $UO_2^{2+}$/$Zn^{2+}$ phosphonoacetates. *European Journal of Inorganic Chemistry*, **8**, 1177-1185 (2010).

*283.* Rowland, C.E. and Cahill, C.L. Hydrothermal synthesis of disulfide-containing uranyl compounds: In situ ligand synthesis versus direct assembly. *Crystal Growth and Design*, **10**, 1390-1398 (2010).

*284.* Rowland, C.E. and Cahill, C.L. Capturing hydrolysis products in the solid state: Effects of pH on uranyl squarates under ambient conditions. *Inorganic Chemistry*, **49**, 8668-8673 (2010).

*285.* Livshits, T.S.; Lizin, A.A.; Zhang, J.M.; Ewing R.C. Amorphization of rare earth aluminate garnets by ionic irradiation and decay of $^{244}Cm$ admixture. *Geology of Ore Deposits*, **52**, 267-278 (2010).

*286.* Knope, K.E. and Cahill, C.L. Uranyl triazolate formation via an in situ Huisgen 1,3-dipolar cycloaddition reaction. *CrystEngComm*, **13**, 153-157 (2011).

*287.* Rowland, C.E.; Cahill, C.L.; and Post, J.E. The structure of braitschite, a calcium rare earth borate. *American Mineralogist*, **96**, 197-201 (2011).

*288.* Wang, S.; Alekseev, E. V.; Depmeier, W.; and Albrecht-Schmitt, T. E. Surprising coordination for plutonium in the first plutonium (III) borate. *Inorganic Chemistry*, **50**, 2079-2081 (2011).

*289.* Diwu, J.; Good, J. J.; DiStefano, V. H.; and Albrecht-Schmitt, T. E. Self-assembly of hexanuclear clusters of 4*f* and 5*f* elements with cation specificity. *European Journal of Inorganic Chemistry*, **9**, 1374-1377 (2011).

*290.* Alsobrook, A. N.; Hauser, B. G.; Hupp, J. T.; Alekseev, E. V.; Depmeier, W.; and Albrecht-Schmitt, T. E. From layered structures to cubic frameworks: Expanding the structural diversity of uranyl carboxyphosphonates via the incorporation of cobalt. *Crystal Growth and Design*, **11**, 1385-1393 (2011).

*291.* Wang, S.; Villa, E. M.; Diwu, J.; Alekseev, E. V.; Depmeier, W.; Albrecht-Schmitt, T. E. Role of anions and reaction conditions in the preparation of uranium (VI), neptunium (VI), and plutonium (VI) borates. *Inorganic Chemistry*, **50**, 2527-2533 (2011).

*292.* Alsobrook, A. N.; Hauser, B. G.; Hupp, J. T.; Alekseev, E. V.; Depmeier, W.; and Albrecht-Schmitt, T. E. Uranyl carboxyphosphonates that incorporate Cd(II). *Journal of Solid State Chemistry*, **184**, 1195-1200 (2011).

*293.* Adelani, P.O.; Oliver, A.G.; and Albrecht-Schmitt, T.E. Hydrothermal synthesis and structural characterization of organically templated uranyl diphosphonates. *Crystal Growth and Design*, **11**, 1966-1973 (2011).

*294.* Lu, F.; Zhang, J.; Huang, M.; Namavar, F.; Ewing, R.C.; and Lian, J. Phase transformation of nano-sized $ZrO_2$ upon thermal annealing and intense radiation. *Journal of Physical Chemistry C*, **115**, 7193-7201 (2011).

*295.* Ohlin, C.A.; Harley, S.J.; McAlpin, J.G.; Hocking, R.K.; Mercado, B.Q.; Johnson, R.; Villa, E.M.; Fidler, M.K.; Olmstead, M.M.; Spiccia, L.; Britt, R.D.; and Casey, W.H. Rates of water exchange for two cobalt(II) heteropoly-oxotungstate compounds in aqueous solution. *Chemistry - A European Journal*, **17**, 4408-4417 (2011). Chosen as VIP Article.

*296.* Deifel, N.P. and Cahill, C.L. Combining coordination and supramolecular chemistry for the formation of uranyl-organic hybrid materials. *Chemical Communications*, **47**, 6114-6116 (2011).

*297.* Rowland, C.E.; Cantos, P.M.; Toby, B.H.; Frisch, M.; Deschamps, J.R.; and Cahill, C.L. Controlling disulfide bond formation and crystal growth from 2-mercaptobenzoic acid. *Crystal Growth and Design*, **11**, 1370-1374 (2011).

*298.* Alsobrook, A.N.; Alekseev, E.V.; Depmeier, W.; and Albrecht-Schmitt, T.E. Incorporation of Mn(II) and Fe(II) into uranyl carboxyphosphonates. *Crystal Growth and Design*, **11**, 2358-2367 (2011).

*299.* Diwu, J.; Wang. S.; Good, J.J.; DiStefano, V.H.; and Albrecht-Schmitt, T.E. Deviation between the chemistry of Ce(IV) and Pu(IV) and routes to ordered and disordered heterobimetallic 4*f*/5*f* and 5i/5*f* phosphonates. *Inorganic Chemistry*, **50**, 4842-4850 (2011).

*300.* Wang, S.; Alekseev, E.V.; Depmeier, W.; and Albrecht-Schmitt, T.E. $K(NpO_2)_3(H_2O)Cl_4$: A channel structure assembled two- and three-center cation-cation interactions of neptunyl cations. *Inorganic Chemistry*, **50**, 4692-4694 (2011).

*301.* Wang, S.; Alekseev, E.V.; Diwu, J.; Miller, H.M.; Oliver, A.G.; Liu, G.K; Depmeier, W.; and Albrecht-Schmitt, T.E. Functionalization of borate networks by the incorporation of fluoride: Syntheses, crystal structures; and nonlinear optical properties of novel actinide fluoroborates. *Chemistry of Materials*, **23**, 2931-2939 (2011).

*302.* Xiao, H.Y.; Duan, G.; Zu, X.T.; and Weber, W.J. *Ab initio* molecular dynamics simulation of pressure-induced phase transformation of BeO. *Journal of Materials Science*, **46**, 6408-6415 (2011).

*303.* Vlaisavljevich, B.; Miro, P.; Cramer, C.J.; Gagliardi, L.; Infante, I.; and Liddle, S.T. On the nature of actinide- and lanthanide-metal bonds in heterobimetallic compounds. *Chemistry – A European Journal*, **17**, 8424-8433 (2011).

*304.* Luneville, L.; Simone, D.; and Weber, W.J. Study of the fragmentation of a displacement cascade into subcascades within the binary collision approximation framework. *J. Nuclear Materials*, **415**, 55-60 (2011).

*305.* Moll, S.; Sattonnay, G.; Thome, L.; Jagielski, J.; Decorse, C.; Simon, P.; Monnet, I.; and Weber, W.J. Irradiation damage in $Gd_2Ti_2O_7$ single crystals: Ballistic versus ionization processes. *Physical Review B*, **84**, 064115 (2011).

*306.* Wang, X.J.; Xiao, H.Y.; Zu, X.T.; and Weber, W.J. Study of cerium solubility in $Gd_2Zr_2O_7$ by DFT + U calculations. *J. Nuclear Materials*, **419**, 105-111 (2011).

*307.* Wang, S.; Alekseev, E.V.; Depmeier, W.; and Albrecht-Schmitt, T.E. Recent progress in actinide borate chemistry. *Chemical Communications*, **47**, 10874-10885 (2011). *Invited Highlight*.

*308.* Knope, K.E.; de Lill, D.T.; Rowland, C.E.; Cantos, P.M.; de Bettencourt-Dia, A.; and Cahill, C.L. Uranyl sensitization of samarium (III) luminescence in a two-dimensional coordination polymer. *Inorganic Chemistry*, **51**, 201-206 (2012).

*309.* Liu, G.; Deifel, N.P.; Cahill, C.L.; Zhurov, V.V.; and Pinkerton, A.A. Charge transfer vibronic transitions in uranyl tetrachloride compounds. *J. Physical Chemistry A*, **116**, 855-864 (2012).

*310.* Wang, X.J.; Xiao, H.Y.; Zu, X.T.; and Weber, W.J. A DFT + U study of cerium solubility in $La_2Zr_2O_7$. *J. Nuclear Materials*, **424**, 69-74 (2012).

*311*. Englert, M.; Krall, L.; and Ewing, R.C. Is nuclear fission a sustainable source of energy? *Materials Research Society Bulletin*, **37**, 417-424 (2012).

*312*. Hanken, B.E.; Shvareva, T.Y.; Gronbech-Jensen, N.; Stanek, C.R.; Asta, M.; and Navrotsky, A. Energetics of cation mixing in urania-ceria solid solutions with stoichiometric oxygen concentrations. *Physical Chemistry Chemical Physics*, **14**, 5680-5685 (2012).

*313.* Gil, A.; Karhanek, D.; Miro, P.; Antonio, M. R.; Nyman, M.; and Bo, C. A journey inside the $U_{28}$ nanocapsule. *Chemistry - A European Journal*, **18**, 8340-8346, 2012. DOI: 10.1002/chem201200801.

*314.* Lu, F.Y.; Wang, J.W.; Lang, M.; Namavar, F.; Trautmann, C.; Zhang, J.M.; Ewing, R.C.; and Lian, J. Amorphization of nanocrystalline monoclinic $ZrO_2$ by swift heavy ion irradiation. *Physical Chemistry Chemical Physics*, **14**, 12295-12300 (2012). DOI: 10.1039/c2cp41553d.

*315.* Panasci, A.F.; Ohlin, C.A.; Harley, S.J.; and Casey, W.H. Rates of water exchange on the $[Fe_4(OH)_2(hpdta)_2(H_2O)_4]^0$ molecule and its implication for geochemistry. *Inorganic Chemistry*, **51**, 6731-6738 (2012).

*316.* Kogawa, M.; Watson, E.B.; Ewing, R.C.; and Utsunomiya, S. Lead in zircon at the atomic scale. *American Mineralogist*, **97**, 1094-1102 (2012).

*317.* Polinski, M.J.; Grant, D.J.; Wang, S.; Alekseev, E.V.; Cross, J.N.; Villa, E.M.; Depmeier, W.; Gagliardi, L.; and Albrecht-Schmitt, T.E. Differentiating between trivalent lanthanides and actinides. *Journal of the American Chemical Society*, **134**, 10682-10692 (2012).

*318.* Diwu, J.; Grant, D.J.; Wang, S.; Gagliardi, L.; and Albrecht-Schmitt, T.E. Periodic trends in lanthanide and actinide phosphonates: Discontinuity between plutonium and americium. *Inorganic Chemistry*, **51**, 6906-6915 (2012).

*319.* Miro, P.; Ling, J.; Qiu, J.; Burns, P.C.; Gagliardi, L.; and Cramer, C.J. An experimental and computational study of wheel-shaped $\{(W_5O_{21})_3[(U^{VI}O_2)_2(O_2)_3]\}^{30-}$ polyoxometalate. *Inorganic Chemistry,* **51**, 8784-8790 (2012).

*320.* Andrews, M.B. and Cahill, C.L. Uranyl bearing hybrid materials: Synthesis, speciation, and solid state structures. *Chemical Reviews*, **113**, 1121-1136 (2013). DOI: 10.1021/cr300202a.

*321.* Vlaisavljevich, B.; Miro, P.; Ma, D.; Sigmon, G.E.; Burns, P.C.; Cramer, C.J.; and Gagliardi, L. Synthesis and characterization of the first 2D neptunyl structure stabilized by side-on cation-cation interactions. *Chemistry - A European Journal,* **19**, 2937-2941 (2013).

*322.* Skomurski, F.N.; Wang, J.W.; Ewing, R.C.; and Becker U. Charge distribution and oxygen diffusion in hypertoichiometric uranium dioxide $UO_{2+x}$ ($x \leq 0.25$)*. Journal of Nuclear Materials*, **434**, 422-433 (2013).

*323.* Pomogaev, V.; Tiwari, S.P.; Rai, N.; Goff, G.S.; Runde, W.; Schneider, W.F.; and Maginn, E.J. Development and application of effective pairwise potentials for $UO_2^{n+}$, $NpO_2^{n+}$, $PuO_2^{n+}$, and $AmO_2^{n+}$ (n = 1, 2) ions with water. *Physical Chemistry Chemical Physics*, **15**, 15954-15963 (2013).

*324.* Maerzke, K.; Goff, G.S.; Runde, W.H.; Schneider, W.F.; and Maginn, E.J. Structure and dymanics of uranyl (VI) and plutonyl (VI) cations in ionic liquid / water mixtures via molecular dynamics simulations. *Journal of Physical Chemistry B*, **117**, 10852-10868 (2013).

*325.* Spencer, E.C.; Zhao, J.; Ross, N.L.; Andrews, M.B.; Surbella, R.G.; and Cahill, C.L. The influence of pressure on the photoluminescence properties of a terbium-adipate framework. *J. Solid State Chemistry*, **202**(0), 99-104 (2013).

*326.* Lu, F.; Dong, Z.; Zhang, J.; White, T.; Ewing, R.C.; and Lian, J. Tailoring the radiation tolerance of vanadate-phosphate fluorapatites by chemical composition control. *RCS Advances*, **3**, 15178-15184 (2013).

*327.* Polinski, M.J.; Cross, J.N.; Villa, E.M.; Lin, J.; Alekseev, E.V.; Depmeier, W.; and Albrecht-Schmitt, T.E. Synthesis of divalent europium borate via in situ reductive techniques. *Inorganic Chemistry*, **52**, 8099-8105 (2013).

*328.* Cross, J.N.; Duncan, P.M.; Villa, E.M.; Polinski, M.J.; Babo, J.-M.; Alekseev, E.V.; Booth, C.H.; and Albrecht-Schmitt, T.E. From yellow to black: Dramatic changes between Ce(IV) and Pu(IV) molybdates. *J. American Chemical Society*, **135**, 2769-2775 (2013). DOI: 10.1021/ja311910h.

*329.* Hulvey, Z.; Lawler, K.V.; Qao, Z.W.; Zhou, J.; Fairen-Jimenez, D.; Snurr, R.Q.; Ushakov, S.V.; Navrotsky, A.; Brown, C.M.; and Forster, P.M. Noble gas adsorption in copper trimesate, HKUST-1: An experimental and computational study. *J. Physical Chemistry C*, **117**, 20116-20126 (2013). DOI: 10.1021/jp408034u.

*330.* Pike, R.D.; Dziura, T.M.; deButts, J.C.; Murray, C.A.; Kerr, A.T.; and Cahill, C.L. Copper(I) cyanide networks with 1-phenylpiperazine. *J. Chemical Crystallography*, **44**, 42-50 (2014). Kerr and Cahill supported by the EFRC. Collaborators at William and Mary Supported by NSF. Cahill and Kerr supported their effort by running PXRD experiments, preparing figures and interpreting results. DOI: 10.1007/s10870-013-0482-2.

*331.* Li, D.; Simotwo, S.; Nyman, M.; and Liu, T. Evolution of actinyl peroxide clusters U28 in dilute electrolyte solution: Exploring the transition from simple ions to macroionic assemblies. *Chemistry - A European Journal*, **20**, 1683-1690 (January 2014). DOI: 10.1002/chem.201303266.

*332.* Nelson, A.-G.D.; Rak, Z.; Albrecht-Schmitt, T.E.; Becker, U.; and Ewing, R.C. Three new silver uranyl diphosphonates: Structures and properties. *Inorganic Chemistry*, **53**, 2787-2796 (2014).

*333.* Kerr, A.T.; Kumalah, S.A.; Holman, K.T.; Butcher, R.J.; and Cahill, C.L. Uranyl coordination polymers incorporating n5-cyclopentadienyliron-functionalized n6-phthalate metalloligands: Syntheses, structures, and photophysical properties. *J. Inorganic and Organometallic Polymers*, **24**, 128-136 (2014). DOI: 10.1007/s10904-013-9980-0.

*334.* Henline, K.M.; Wang, C.; Pike, R.D.; Ahern, J.C.; Sousa, B.; Patterson, H.H.; Kerr, A.T.; and Cahill C.L. Structure, dynamics, and photophysics in the copper (I) iodide-tetrahyrothiophene system. *Crystal Growth and Design*, **14**, 1449-1458 (2014). DOI: 10.1021/cg500005p.

*335.* Zhang, Y.; Varga, T.; Ishimaru, M.; Edmondson, P.D.; Xue, H.; Liu P.; Moll, S.; Namavar, F.; Hardiman, C.; Shannon, S.; and Weber, W.J. Competing effects of electronic and nuclear energy loss on microstructural evolution in ionic-covalent materials. *Nuclear Instrumentation and Methods in Physics Research*, **B 327**, 33-43 (2014).

*336.* Xin, G.; Sun, H.T.; Fard, F.R.; Sun, X.; Koratkar, N.; Borca-Tasciuc, T.; and Lian, J. Large-area free standing grapheme paper for superior thermal management. *Advanced Materials*, **26**, 4521-4526 (2014). DOI: 10.1002/adma.201400951.

*337.* Panasci, A.; Harley, S. J.; Zavarin, M.; and Casey, W. H. Kinetic studies of the $[NpO_2(CO_3)_3]^{4-}$ ion at alkaline conditions using $^{13}C$ NMR. *Inorganic Chemistry*, **53**, 4202-4208 (2014). DOI: 10.1021/ic500314v.

*338.* Guo, Z.; Lee, D.; Liu, Y.; Sun, F.; Gau, H.; Burns, P.C., Huang, L.; and Luo, T. Tuning the thermal conductivity of solar cell polymers through side chain engineering. *Physical Chemistry Chemical Physics*, **16**, 7764-7771 (2014).

*339.* Tiferet, E.; Gil, A.; Bo, C.; Shvareva, T.Y.; Nyman, M.; Navrotsky, A. The energy landscape of uranyl peroxide species. *Chemistry – A European Journal*, **20**, 3646-3651 (2014). DOI: 10.1002/chem.201304076. Cover Feature.

*340.* Yu, N.; Klepov, V.V.; Villa, E.M.; Bosbach, D.; Suleimanov, E.V.; Depmeier, W.; Albrecht-Schmitt, T.E.; and Alekseev, E.V. Topologically identical, but geometrically isomeric layers in hydrous α-, β-$Rb[UO_2(AsO_3OH)(AsO_2(OH)_2)]\cdot H_2O$ and anhydrous $Rb[UO_2(AsO_3OH)(AsO_2(OH)_2)]$. *J. Solid State Chemistry*, **215**, 152-159 (2014). DOI: 10.1016/j.jssc.2014.03.017.

*341.* Rodriguez, M.D.; Li, W.X.; Trautmann, C.; Bierschenk, T.; Afra, B.; Schauries, D.; Ewing, R.C.; Mudie, S.T.; and Kluth, P. SAXS and TEM investigation of ion tracks in neodymium-doped yttrium aluminum garnet. *Nuclear Instruments and Methods in Physics Research B*, **326**, 150-153 (2014).

*342.* Spencer, E.C.; Ross, N.L.; Surbella, R.G.; and Cahill, C.L. The influence of pressure on the structure of a 2D uranium (VI) carboxyphosphonate compound. *Journal of Solid State Chemistry*, **218**, 1-5 (Oct 2014). DOI: 10.1016/j.jssc.2014.05.026.

*343.* Zhang, F.X.; Lang, M.; Tracy, C.; Ewing, R.C.; Gregg, D.J.; Lumpkin G.R. Incorporation of uranium in pyrochlore oxides and pressure-induced phase transitions. *Journal of Solid State Chemistry*, **219**, 49-54 (2014). DOI: 10.1016/j.jssc.2014.07.011.

*344.* Navrotsky, A. Progress and new directions in calorimetry: A 2014 perspective. *Journal of American Ceramic Society*, **97**, 3349-3359 (2014). DOI: 10.1111/jace.13278.

*345.* Navrotsky, A. Taking the measure of molten uranium oxide. *Science*, **346**, 916-917 (2014). DOI: 10.1126/science.aaa0163. Navrotsky gives a perspective on molten uranium dioxide structure and dynamics – L.B. Skinner et al, *Science*, **346**, 984-987.

*346.* Miro, P.; Vlaisavljevich, B.; Dzubak, A.L.; Hu, S.; Burns, P.C; Cramer, C. J.; Spezia, R.; and Gagliardi, L. Uranyl-peroxide nanocapsules in aqueous solution: Force field development and first applications, *Journal of Physical Chemistry C*, **118**, 24730-24740 (2014). DOI: 10.1021/jp504147s.

*347.* Guo, X.; Ushakov, S.V.; Labs, S.; Curtius, H.; Bosbach, D., and Navrotsky, A. Energetics of metastudtite and implications for nuclear waste alternative. *Proceedings of the National Academy of Sciences*, **111**, 17737-17742 (2014). DOI: 10.1073/pnas.1421144111.

*348.* Yudintsev, S.V.; Lizin, A.A.; Livshits, T.S.; Stafanovsky, S.V.; Tomilin, S.V., and Ewing, R.C. Ion-beam irradiation and 244Cm-doping investigations of the radiation response of actinide-bearing crystalline waste forms. *Journal of Materials Research* (2015). DOI: 10.1557/jmr.2015.23.

*349.* Sahu, S.; Unruh, D.; Forbes, T.Z.; and Navortsky, A. Energetics of formation and hydration of a porous metal organic nanotube. *Chemistry of Materials*, **26**, 5105-5112 (2014). DOI: 10.1021/cm5024053.

*350.* Deditius, A.P.; Smith, F.N.; Utsunomiya, S.; Ewing, R.C. Role of vein-phases in nanoscale sequestration of U, Nb, Ti and Pb during the alteration of pyrochlore. *Geochimica et Cosmochimica Acta*, **150**, 226-252 (2015). DOI: 10.1016/j.gca.2014.11.024.

*351.* Jackson, M.N., Jr.; Kamunde-Devonish, M.K., Hammann, B.A.; Wills, L.A.; Fullmer, L.B., Hayes, S.E.; Cheong, P.H.-Y.; Casey, W.H.; Nyman, M.D.; and Johnson, D.W. An overview of current approaches to the characterization of aqueous inorganic clusters. *Dalton Transactions*, **44**, 16982-17006 (2015).

*352.* Ramshaw, B.J.; Shekhter, A.; McDonald, R.D.; Betts, J.B.; Mitchell, J.N.; Tobash, P.H.; Mielke, C.H.; Bauer, E.D.; and Migliori, A. Avoided valence transition in a plutonium superconductor. *Proceedings of the National Academy of Sciences*, **112**, 3285-3289 (2015). DOI: 10.1073/pnas.1421174112.

*353.* Wiss, T.; Hiernaut, J.-P.; Roudil, D.; Colle, J.-Y.; Maugeri, E.; Talip, Z.; Janssen, A.; Rondinella, V.; Konings, R.J.M.; Matzke, H.-J.; and Weber, W. Evolution of spent nuclear fuel in dry storage conditions for millennia and beyond. *Journal of Nuclear materials*, **451**, 198-206 (2014). DOI: 10.1016/j.jnucmat.2014.03.055.

*354.* Liu, B.; Aidhy, D.S. ; Zhang, Y.; and Weber, W. Theoretical investigation of thermodynamic stability and mobility of the oxygen vacancy in $ThO_2$-$UO_2$ solid solutions. *Phys Chem Chem Phys*, **16**, 25461-25467 (2014). DOI: 10.1039/c4cp03660c.

*355.* Rittman, D.R.; Tracy, C.L.; Cusick, A.B.; Abere, M.J.; Torralva, B.; Ewing, R.C., and Yalisove, S.M. Ultrafast laser and swift heavy ion irradiation: Response to $Gd_2O_3$ and $ZrO_2$

to intense electronic excitation. *Applied Physics Letters*, **106**, 171914 (2015). DOI: 10.1063/1.4919720.

*356.* Guo, X.; Szenknect, S.; Mesbah, A.; Labs, S.; Clavier, N.; Poinssot, C.; Ushakov, S.V.; Durtius, H.; Bosbach, D.; Ewing, R.C.; Burns, P.C.; Dacheux, N., and Navrotsky, A. Thermodynamics of formation of coffinite, $USiO_4$. *Proceedings of the National Academy of Sciences*, **112**, 6551-6555 (2015) DOI: 10.1073/pnas.1507441112.

*357.* Mesbah, A.; Szenknect, S.; Clavier, N.; Lozano-Rodriguez, J.; Poinssot, C.; Den Auwer, C.; Ewing, R.C.; and Dacheux, N. Coffinite, $USiO_4$, is abundant in nature: So why is it so difficult to synthesize? *Inorganic Chemistry*, **54**, 6687 – 6696 (2015) DOI: 10.2012/ic502808n.

*358.* Pellemoine, F.; Avilov, M.; Bender, M.; Ewing, R.C.; Fernandes, S.; Lang, M.; Li, W.X.; Mittig, W.; Schein, M.; Severin, D.; Tomut, M.; Trautmann, C.; and Zhang, F.X. Study on structural recovery of graphit*e irradiated with swift heavy ions at high temperature. Nuclear Instruments and Methods B*, **235**, 522-524 (2015). DOI:10.1016/j.nimb.2015.09.007.

*359.* Szenknect, S.; Mesbah, A.; Cordara, T.; Clavier, N.; Brau, H.P.; Le Goff, X.r; Poinssot, C.; Ewing, R.C.; and Dacheux, N. First experimental determination of the solubility constant of coffinite. *Geochimica et Cosmochimica Acta*, **181**, 36-53 (2016). DOI: 10.1016/j.gca.2016.02.010.

*360.* Guo, X.; Tiferet, E.; Qi, L.; Solomon, J. M.; Lanzirotti, A.; Newville, M.; Engelhard, M. H.; Kukkadapu, R. K.; Wu, D.; Ilton, E. S.; Asta, M.; Sutton, S. R.; Xu, H.; and Navrotsky, A. U(V) in metal uranates: A combined experimental and theoretical study of $MgUO_4$, $CrUO_4$, and $FeUO_4$. *Dalton Transactions*, **45**, 4622-4632 (2016). DOI: 10.1039/C6DT00066E.

*361.* Long, G.; Grandjean, F.; Guo, X.; Navrotsky, A.; and Kukkadapu, R. Mössbauer spectral properties of yttrium iron garnet, $Y_3Fe_5O_{12}$, and its isovalent and non-isovlaent yttrium substituted solid solutions. *Inorganic Chemistry*, **55**, 3413-3418 (2016). DOI: 10.1021/acs.inorgchem.5b02769.

*362.* Miro, P.; Vlaisavljevich, B.; Gil, A.; Burns, P.C.; Nyman, M.; and Bo, C. Self-assembly of uranyl-peroxide nanocapsules in basic peroxidic environments. *Chemistry – A European Journal*, **22**, 8571-8578 (2016). DOI: 10.1002/chem.201600390.

*363.* Zietlow, P.; Beirau, T.; Mihailova, B.; Groat, L.A.; Chudy, T.; Shelyug, A.; Navrotsky, A.; Ewing, R.C.; Schluter, J.; Skoda, R.; Bismayer, U. Thermal annealing of natural, radiation-damaged pyrochlore. *Zeitschrift fur Kristallographie – Crystalline Materials*, **232**, 25-38 (2017). DOI: 10.1515/zkri-2016-1965.

*364.* Yoon, S.J.; Guo, Z.; Claro, P.C. dos Santos; S., Elena, V.; Huang, L. *ACS Nano*, **10**, 7208-7215 (2016). DOI: 10.1021/acsnano.6b03700.

*365.* Guo, X.; Szenknect, S.; Mesbah, A.; Clavier, N.; Poinssot, C.; Wu, D.; Xu, H.; Dacheux, N.; Ewing, R.C.; and Navrotsky, A. Energetics of a uranothroite ($Th_{1-x}U_xSiO_4$) solid solution. *Chemistry of Materials*, **28**, 7117-7124 (2016). DOI: 10.1021/acs.chemmater.6b03346.

*366.* Sachan, R.; Cooper, V.R.; Liu, B.; Aidhy, D.S.; Voas, B.V.; Lang, M.; Ou, X.; Trautmann, C.; Zhang, Y.; Chisholm, M.F.; and Weber, W.J. Forging fast ion conducting nanochannels with swift heavy ions: The correlated role of local electronic and atomic structure. *Journal of Physical Chemistry C*, **121**, 975-981 (2017). DOI: 10.1021/acs.jpcc.6b12522.

*367.* Guo, X.; Navrotsky, A.; Kukkadapu, R. K.; Engelhard, M. H.; Lanzirotti, A.; Newville, M.; Ilton, E. S.; Sutton, S. R.; and Xu, H. Structure and thermodynamics of uranium-containing iron garnets. *Geochimica et Cosmochimica Acta*, **189**, 269-281 (2016). DOI: 10.1016/j.gca.2016.05.043.

*368.* Hirsch, A.; Kegler, P.; Alencar, I.; Ruiz-Fuertes, J.; Shelyug, A.; Peters, L.; Schreinemachers, C.; Neumann, A.; Neumeier, S.; Liermann, H.-P.; Navrotsky, A.; and Roth, G. Structural, vibrational, and thermochemical properties of the monazite-type solid solution $La_{1-x}Pr_xPO_4$. *Journal of Solid State Chemistry*, **245**, 82-88 (2017). DOI: 10.1016/j.jssc.2016.09.032.

*369.* Neumeier, S.; Kegler, P.; Arinicheva, Y.; Shelyug, A.; Kowalski, P. M.; Schreinemachers, C.; Navrotsky, A.; and Bosbach, D. Thermochemistry of $La_{1-x}Ln_xPO_4$-monazites (Ln = Gd, Eu). *Journal of Chemical Thermodynamics*, **105**, 396-403 (2017). DOI: 10.1016/j.jct.2016.11.003.

*370.* Finkeldei, S.; Kegler, P.; Kowalski, P.; Schreinemachers, C.; Brandt, F.; Bukaemskiv, A.; Vinograd, V.; Beridze, G.; Shelyug, A.; Navrotsky, A.; and Bosbach, D. Composition dependent order-disorder transition in $Nd_xZr_{1-x}O_{2-0.5x}$ pyrochlores: A combined structural, calorimetric and *ab initio* modeling study. *Acta Materialia*, **125**, 166-176 (2017). DOI: 10.1016/j.actamat.2016.11.059.

*371.* Li, D.; Pigga, J.M.; Liu, G.; and Liu, T. Tuning the surface hydrophobicity of keplerate $\{Mo_{72}Fe_{30}\}$ porous molecular capsules by surface ligand-replacement process", *Journal of Cluster Science*, **28**,745-755 (2017). DOI: 10.1007/s10876-016-1105-9.

*372.* Gao, Y.; Eghtesadi, S.A.; and Liu, T. Solution behaviors of polyoxometalates driven by Counterion-macro ion interaction. *Advances in Inorganic Chemistry*, **69**, 29-65 (2017). DOI: 10.1016/bs.adioch.2016.12.006.

*373.* Li, D.; Liu, Z.; Song, J.; Li, H.; Zhang, B.; Yin, P.; Zheng, Z.N.; Roberts, J.E.; Tsige, M.; Hill, C.L.; and Liu, T. Cation translocation around single polyoxometalate-organic hybrid clusters regulated by electrostatic and cation-π interactions. *Angewante Chem. International Edition*, **56**, 3294-3298 (2017). DOI: 10.1002/ange.201612008.

*374.* Nyman, M. Small-angle X-ray scattering to determine solution speciation of metal-oxo clusters. *Coordination Chemistry Reviews*, 352, 461-472 (2017). DOI: 10.1016/j.ccr.2016.11.014.

*375.* Carvajal-Nunez, U.; Saleh, T.A.; White, J.T.; Maiorov, B.; and Nelson, A.T.

Determination of elastic properties of polycrystalline $U_3Si_2$ using resonant ultrasound spectroscopy. *Journal of Nuclear Materials*, **498**, 438-444 (2018). DOI: 10.1016/j.jnucmat.2017.11.008.

*376.* Beirau, T.; Nix, W.D.; Pollmann, H.; and Ewing, R.C. Radiation-induced effects on the mechanical properties of natural $ZrSiO_4$: Double cascade-overlap damage accumulation. *Physics and Chemistry of Minerals*, **45**, 435-442 (2018). DOI: 10.1007/s00269-017-0931-0.

*377.* Shamblin, J.; Heres, M.; Zhou, H.; Sangoro, J.; Lang, M.; Neuefeind, J.; Alonso, J.A.; and Johnston, S. Experimental evidence for bipolaron condensation as a mechanism for the metal-insulator transition in rare-earth nickelates. *Nature Communications*, **9**, 86 (2018). DOI: 10.1038/s41467-017-02561-6.

*378.* Heuser, J.M.; Palomares, R.I.; Bauer, J.D.; Lozano Rodriguez, M.J.; Cooper, J.; Lang, M.; Scheinost, A.C.; Schlenze, H.; Winkler, B.; Bosbach, D.; Neumeier, S.; and Deissmann, G. Structural characterization of $(Sm,Tb)PO_4$ solid solutions and pressure-induced phase transitions. Journal of the European Ceramic Society, 38, 4070-4081 (2018). DOI: 10.1016/j.jeurceramsoc.2018.04.030.

*379.* Li, W.X.; Shen, Y.; Zhou Y.; Chen, C-H.; Ewing, R.C. *In situ* TEM observation of alpha-particle induced annealing of radiation damage in Durango apatite. *Scientific Reports*, **7** (2017). DOI: 10.1038/s41598-017-14379-9.

*380.* Wang, C.; Yang, T.; Tracy, C.L.; Xiao, J.; Liu, S.; Fang, Y.; Yan, Z.; Ge, W.; Xue, J.; Zhang, J.; Wang, J.; Huang, W.; Ewing, R.C.; Wang, Y. Role of the X and n factors in ion-irradiation induced phase transformations of $M_{n+1}AX_n$ phases. *Acta Materialia*, **144**, 432-446 (2018). DOI: 10.1016/j.actamat.2017.11.008.

*381.* Chu, Y.; Chen, J.; Haso, F.; Gao, Y.; Szymanowski, J.E.S.; Burns, P.C.; Liu, T. Expanding the Schulze–Hardy rule and the Hofmeister Series to nanometer-scaled hydrophilic macroions. *Chemistry – A European Journal*, **24**, 5479-5483 (2018). DOI: 10.1002/chem.201706101.

*382.* Beirau, T.; Nix, W.D.; Ewing, R.C.; Pollmann, H.; Salje, E.K.H. Radiation-damage-induced transitions in zircon: Percolation theory applied to hardness and elastic moduli as a function of density. *Applied Physics Letter*, **112**, 201901 (2018). DOI: 10.1063/1.5030626.

*383.* Hickam, S.; Aksenov, S.M.; Dembowski, M.; Perry, S.N.; Traustason, H.; Russell, M.; and Burns, P.C. Complexity of uranyl peroxide cluster speciation from alkali-directed oxidative dissolution of uranium dixoide. *Inorganic Chemistry*, **57**, 9296-9305 (2018). DOI: 10.1021/acs.inorgchem.8b01299.

*384.* Cureton, W.F.; Palomares, R.I.; Walters, J.; Tracy, C.L.; Chen, C.H.; Ewing, R.C.; Baldinozzi, G.; Lian, J.; Trautmann, C.; and Lang, M. Grain size effects on irradiated $CeO_2$, $ThO_2$, and $UO_2$. *Acta Materialia*, **160**, 47-56 (2018). DOI: 10.1016/j.actamat.2018.08.040.

*385*. Liu, Z.; Liu, T.; and Tsige, M. Unique symmetry-breaking phenomenon during the self-assembly of macroions elucidated by simulation. *Scientific Reports*, **8**, 13076 (2018). DOI: 10.1038/s41598-018-31533-z.

*386*. Fuentes, A.F.; Montemayor, S.M.; Maczka, M.; Lang, M.; Ewing, R.C.; Amador, U. A critical review of existing criteria for the prediction of pyrochlore formation and stability. *Inorganic Chemistry*, **57**, 12093-12105 (2018). DOI: 10.1021/acs.inorgchem.8b01665.

*387*. Grote, R.; Zhao, M.; Shuller-Nickles, L.; Amoroso, J.; Gong, W.; Lilova, K.; Navrotsky, A.; Tang, M.; and Brinkman, K.S. Compositional control of tunnel features in hollandite-based ceramics: Structure and stability of $(Ba,Cs)_{1.33}(Zn,Ti)_8O_{16}$. *Journal of Materials Science*, **54**, 1112-1125 (2019). DOI: 10.1007/s10853-018-2904-1.

*388*. Deyneko, D.V.; Nikiforov, I.V.; Lazoryak, B.I.; Spassky, D.A.; Leonidov, I.I.; Stefanovich, S.Y.; Petrova, D.A.; Aksenov, S.M.; and Burns, P.C. $Ca_8MgSm_{1-x}(PO_4)_7$:$xEu^{3+}$, promising red phosphors for WLED application. *Journal of Alloys and Compounds*, **776**, 897-903 (2018). DOI: 10.1016/j.jallcom.2018.10.317.

*389*. Villa, E.M.; Cross, J.N.; and Albrecht-Schmitt, T.E. New uranyl open framework and sheet compounds formed via in-situ protonation of piperazine by phosphorous acid. *Minerals*, **8**, 497 (2018). DOI: 10.3390/min8110497.

*390*. Ling, J.; Zhang, H.; Qiu, J.; Stoffer, M.; Burgess, D.; and Burns, P.C. Pyrophosphate and methylenediphosphonate incorporated uranyl peroxide cage clusters. *Crystal Growth and Design*, **18**, 7720-7729 (2018). DOI: 10.1021/acs.cgd.8b01638.

*391*. Zhao, M.; Xu, Y.; Shuller –Nickels, L.; Amoroso, J.; Frenkel, A.I.; Li, Y.; Gong, W.; Lilova, K.; Navrotsky, A.; Brinkman, K. Compositional control of radionuclide retention in hollandite-based ceramic waste forms for Cs-immobilization. *Journal of the American Ceramic Society*, **102**, 4314-4324 (2018). DOI: 10.1111/jace.16258.

*392*. Zhang, L.; Dembowski, M.; Arteaga, A.; Hickam, S.; Martin, N.P.; Zakharov, Lev, N.; Nyman, M.; and Burns, P.C. Energetic trends in monomer building blocks for uranyl peroxide clusters. *Inorganic Chemistry*, **58**, 439-445 (2018). DOI: 10.1021/acs.inorgchem.8b02661.

*393*. Sigmon, G.E. and Hixon, A.E. Extension of the plutonium oxide nancluster family to include {Pu16} and {Pu22}. *Chemistry – A European Journal*, **25**, 2463-2466 (2019). DOI: 10.1002/chem.201805605.

*394*. Wang, C.; Yang, T.; Tracy, C.L.; Lu, C.; Zhang, H.; Hu, Y.J.; Wang, L.; Qi, L.; Gu, L.; Huang, Q.; Zhang, J.; Wang, J.; Xue, J.; Ewing, R.C.; and Wang, Y. Disorder in $M_{n+1}AX_n$

phases at the atomic scale. *Nature Communications*, **10**, 622 (2019). DOI: 10.1038/s41467-019-08588-1.

*395.* Arteaga, A.; Zhang, L.; Hickam, S.; Dembowski, M.; Burns, P.C.; and Nyman, M. Uranyl peroxide capsule self-assembly in slow motion. *Chemistry – A European Journal*, 25, 6087-6091 (2019). DOI: 10.1002/chem.201806227.

*396.* Kornyakov, I.V.; Gurzhiy, V.V.; Szymanowski, J.E.S.; Zhang, L.; Perry, S.N.; Krivovichev, S.V.; and Burns, P.C. A novel family of Np(VI) oxysalts: Crystal structures, calorimetry, thermal behaviour and comparison with U(VI) compounds. *Crystal Growth and Design*, 19, 2811-2819 (2019). DOI: 10.1021/acs.cgd.9b00043.

*397.* Ennaceur, S.M. and Migliori, A. Toward an understanding of aging in plutonium from direct measurements of stored energy. *Philophical Magaine Letters*, **98**, 502-510 (2019). DOI: 10.1080/09500839.2019.1583392.

*398.* Lobeck, H.L.; Isner, J.K.; and Burns, P.C. Transformation of uranyl peroxide studtite, $[(UO_2)(O_2)(H_2O)_2](H_2O)_2$, to soluble nanoscale cage clusters. *Inorganic Chemistry*, 58, 6781-6789 (2019). DOI: 10.1021/acs.inorgchem.9b00230.

*399.* Batrice, R.J.; Wacker, J.N., Glass, E.N.; Julani, S.Z.; Tong, Y.Y.J.; Nyman, M.; and Knope K.E. Template-free cyclic hexavanadate: Synthesis, characterization, solid-state structure, and solution-state dynamics. *Polyhedron*, **169**, 266-277 (2019). DOI: 10.1016/j.poly.2019.05.014.

*400*. Palomares, R.I.; McDonnell, M.T.; Lang, Y.; Yao, T.; Szymanowski, J.E.S.; Neuefeind, J.; Sigmon, G.E.; Lian, J.; Tucker, M.G.; Wirth, B.D.; and Lang, M. Oxygen point defect accumulation in single-phase $UO_{2+x}$. *Physical Review Materials*, **3**, 053611 (2019). DOI: 10.1103/PhysRevMaterials.3.053611.

*401*. Reissner, C.E.; Bismayer, U.; Kern, D.; Reissner, M.; Park, S.; Zhang, J.; Ewing, R.C.; Shelyug, A.; Navrotsky, A.; Paulmann, C.; Skoda, R.; Groat, L.A.; Pollmann, H.; and Beirau, T. Mechanical and structural properties of radiation-damaged allanite-(Ce) and the effects of thermal annealing. *Physics and Chemistry of Materials*, 1-13 (2019). DOI: 10.1007/s00269-019-01051-z.

*402*. Li, H.; Shen, Y.; Yang, P.; Szymanowski, J.E.S.; Chen, J.; Gao, Y.; Burns, P.C.; Kortz, U.; and Liu, T. Isotope and hydrogen bond effects on the self-assembly of macroions in dilute solution. *Chemistry – A European Journal*, online (2019). DOI: 10.1002/chem.201902444.

**Book Chapter Titles and Proceedings:**

*403.* Albrecht-Schmitt, T.E.; Burns, P.C.; and Krivovichev, S.V. *Hydrothermal synthesis and crystal structures of actinide compounds. The Chemistry of the Actinide and Transactinide Elements* (2010).

*404.* Lu, F.Y.; Nyman, M.; Shen, Y.Q.; Dong, Z.L.; Wang, K.; Zhang, F.X.; Ewing, R.C.; and Lian, J. Ion beam irradiation-induced amorphization in nano-sized $K_xLn_YTa_2O_{7-v}$ tantalate pyrochlore. MRS Proceedings, 1298 (2010).

*405.* Diwu, J. and Albrecht-Schmitt, T.E. Structural chemistry of transuranium phosphonates in metal phosphonates. A. Clearfield ed., RSC (2011).

*406.* Ewing, R.C. and Weber, W.J. Chapter 15: Nuclear waste management and disposal, in *Fundamentals of Materials for Energy and Environmental Sustainability,* edited by D.S. Ginley and D. Cahen (Cambridge University Press, New York) pp. 178-193. (2012).

*407.* Utsunomiya, S.; Kogawa, M.; Kamiishi, E.; and Ewing, R.C. Chapter 8: Scanning transmission electron microscopy and related techniques for research on actinide and radionuclide nanomaterials. In: Actinide Nanoparticle Research. Editors - Stepan N. Kalmykov and Melissa A. Denecke (Springer-Verlag Berlin Heidelberg), 33-62 (2012).

*408.* McGrail, B.T.; Jouffret, L.J.; Villa, E.M.; and Burns, P.C. In-situ Raman spectroscopy studies of room-temperature and hydrothermal reactions. Actinides and Nuclear Energy Materials, MRS Proceedings, **1444**, 281-288 (2012).

*409.* Burns, P.C. and Sigmon, G.E. Uranium – Cradle to Grave. Chapter 2 in *Uranium: Cradle to Grave*. GAC-MAC Volume (ed. P.C. Burns and G.E. Sigmon). (2013).

*410.* Navrotsky, A.; Shvareva, T.; and Guo, X. Thermodynamics of Uranium Minerals and Related Materials. Chapter 5 in *Uranium: Cradle to Grave*. GAC-MAC Volume (ed. P.C. Burns and G.E. Sigmon). (2013).

*411.* Fein, J.B. and Powell, B. Uranium Adsorption: Speciation at Mineral:Water and Bacterial Cell:Water Interfaces. Chapter 6 in: *Uranium: Cradle to Grave*. GAC-MAC Volume (ed. P.C. Burns and G.E. Sigmon). (2013).

*412.* Weber, W.J. and Ewing, R.C. Ceramic waste forms for uranium and transuranium elements. Chapter 10 in *Uranium: Cradle to Grave*. GAC-MAC Volume (ed. P.C. Burns and G.E. Sigmon). (2013).

*413.* Polinski, M.J.; Yang, Y.; and Albrecht-Schmitt, T.E. Borates as potential radiation damage-resistant materials. Chapter 12 in *Uranium: Cradle to Grave*. GAC-MAC Volume (ed. P.C. Burns and G.E. Sigmon). (2013).

*414.* Weber, W.J. Radiation and thermal ageing of nuclear waste glass. *Procedia Materials Science*, **7**, 237-246 (2014). DOI: 10.1016/j.mspro.2014.10.031.

*415*. Hickam, Sarah and Burns, P.C. Chapter 4: Oxo clusters of 5*f* elements. Recent Development in Clusters of Rare Earths and Actinides: Chemistry and Materials. Editor – Zhiping Zheng. Series: Structure and Bonding, Volume 173, Pages 121-153. DOI: 10.1007/430_2016_8. (2016).